Doctoral Dissertation

Characteristics of interfacial reaction between Sn–Cu solder alloys with trace elements and Cu substrates

BANG JUNG HWAN

July 2019

Graduate School of Engineering,

Osaka University

Supervisor

Prof. Hiroshi Nishikawa, Ph. D.

Department of Manufacturing Process, Joining and Welding Research Institute

Osaka University

Doctoral Committee

Prof. Hiroshi Nishikawa, Ph. D

Department of Manufacturing Process, Joining and Welding Research Institute

Osaka University

Prof. Soshu Kirihara, Ph. D.

Division of Sustainable Energy and Environmental Engineering, Graduate School of Engineering

Osaka University

Assoc. Prof. Hiroaki Muta, Ph. D.

Division of Sustainable Energy and Environmental Engineering, Graduate School of Engineering

Osaka University

Contents

List of Tables

List of Figures

Chapter 1

Chapter 2

Chapter 3

Chapter 4

Chapter 5

Chapter 6

Chapter 1

Research background

1.1 Electronic packaging

Electronic packaging refers to the method of hardware configuration to either electronic components or finished electronic devices. In the fields of semiconductor and electronic packaging, wire bonding and tape automated bonding (TAB) technologies were traditional mainstays of chip bonding technology. However, these technologies had disadvantages of having a low chip integration density and reliability problems such as delay in electrical signal transmission and a high heat generation rate. To overcome these disadvantages, flip-chip technology was developed and has attracted extensive research interest worldwide for its advantages of processing high-speed signals using solder bumps and providing a large number of I/O pins. In line with this research trend, ball grid array (BGA) packages make up a great proportion of market share. Given their high specific relative to solder, which provides interconnections, studies have revolved around solder, such as solder bonding properties, interfacial reactions with the underlying metal layer, and the deformation behavior, thermomechanical properties, and thermal fatigue mechanism of solder joints.

Electronic packaging involves two major functions, one at the IC or device level and the other at the system-level [1]. The hierarchy of electronic packaging is illustrated in **Figure 1.1**. The electronic packaging is constructed by various interconnection methods ranging from first-level (chip or single chip-level package) to second-level (printed circuit boards; PCBs) and third-level (motherboard) packages. At first-level, three bonding technologies of wire-boding, tape automated bonding (TAB), and flip-chip bonding are used. Generally, two bonding technologies are used at the second level of reflow and flow soldering, using solder materials. Soldering is a metallurgical joining method that uses a solder with melting point below 450 ℃ [2]. In the electronic packaging technology, solder plays a crucial role in the interconnection of the silicon die (or chip). Recent developments in electronic packaging tend to achieve a higher level of integration by utilizing new materials and processes [3]. Because assembly and packaging has become more importance and is often a limiting factor for cost and performance of electronic systems [4].

1.2 Solder alloys for electronic packaging

Until now, in electronic materials, solder materials have been used for the interconnection between chips and substrates. Solders also have acted as joining materials, electrical and mechanical interconnection in electronic packaging. Among solder materials, eutectic Pb-Sn solder is widely used in electronic packaging to solder semiconductor chips and electronic components onto substrates; however, Pb-free soldering materials with Sn as the main element containing Ag, Cu, or Bi have been proposed for research and review in order to replace Pb, following international environmental regulations such as the Restriction of Hazardous Substances (RoHS) [5]. The leading two alternatives to Sn-Pb solder were Sn-Ag-Cu eutectic and Sn-Cu eutectic, both considered acceptable by academia and industry. In the general electronics industry, eutectic Sn-Pb solder was successfully replaced with SAC solders. In terms of wettability and operation temperature, the SAC305 solders perform well. However, SAC305 exhibits poor drop and shock performance due to large Ag_3Sn intermetallic compounds (IMC) existing in the matrix [6]. Additionally, cost is another important factor that limits the SAC solder application. As a result, the electronics industry has been looking for less expensive alternatives to SAC305. Unfortunately, while there are numerous alternatives to SAC305, reliability studies on these alternatives have been minimal.

In general, the substrate materials in electronic packaging are Cu and Ni-based metals. This means that the IMC formed at the joint are either Cu-solder system or Ni-solder system, as shown in **Figure 1.2**. In previous studies, the reactions and IMC formation of Cu-Sn IMC [7] and Ni-Sn IMC [8,9] were reported. When Cu-solder system, the reactions between Sn and Cu induce the formation of Cu_6Sn_5 and Cu_3Sn IMC [10]. Both IMCs are orthorhombic structures and Cu_3Sn has a long period superlattice with 80 atoms per unit cell [11–13]. Kirkendall voids are also reported; these induce failure of the joint in electronic packages when they form at the joint interface [14]. Moreover, because of the rapid diffusion of Cu, thicker layers of IMC form at the interface and the growth of the IMC layers can occur during multiple reflow or isothermal aging processes [15–17]. These IMC can affect the reliability of the joints [18]. The rapid growth of IMC can cause degradation of the mechanical properties and reliability of the joints because they decrease the fracture toughness [19] and increase the likelihood of brittle fracture [20]. It has been reported that the properties of these IMC, such as their composition, thickness, morphology, modulus, and hardness, affect joint reliability [18,21,22].

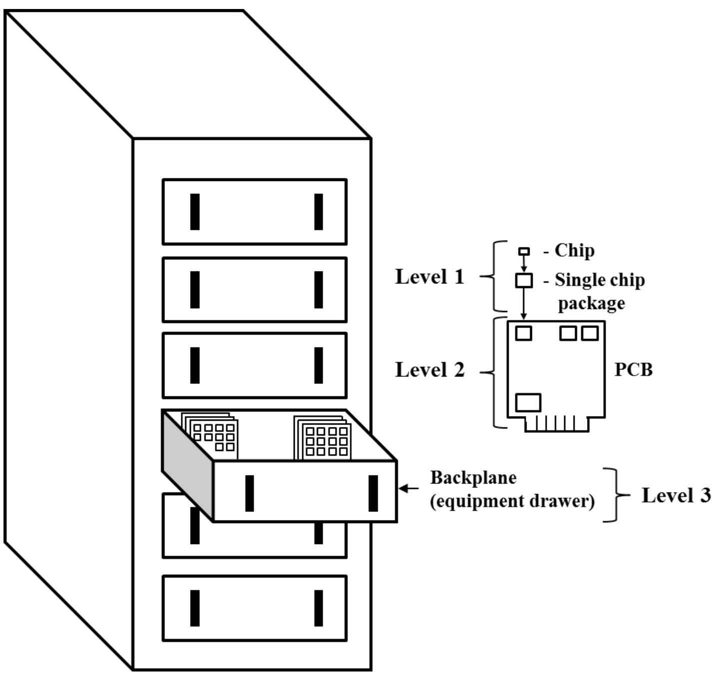

Figure 1.1 Hierarchy of electronic packaging in computer.

(a)

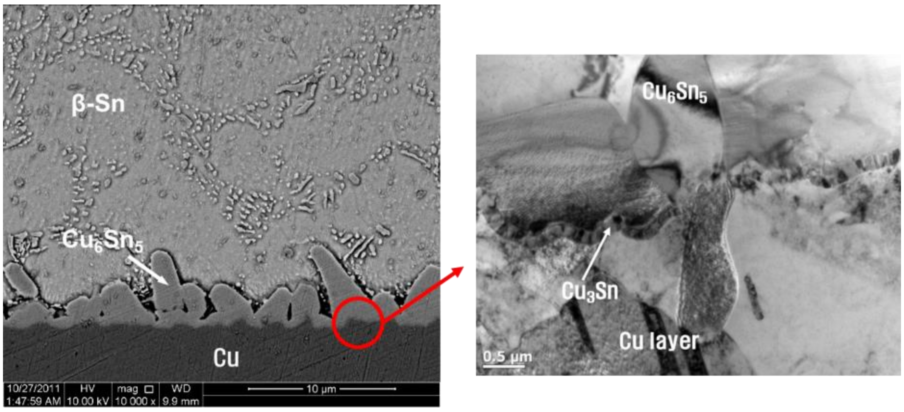

(b)

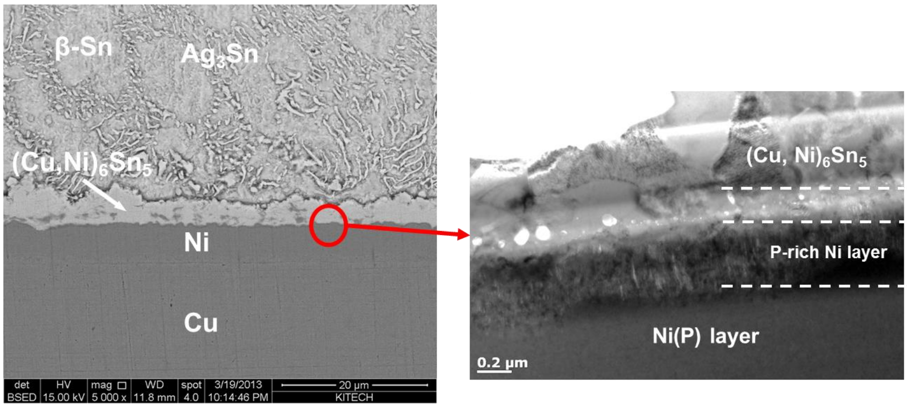

Figure 1.2 Interfacial IMC between SAC and (a)Cu substrate, (b)Ni substrate.

When Ni-solder system, ENIG was proposed to form a diffusion barrier layer on Cu [23]. However, the reliability degradation occurs at the joint interface, because P-rich layers such as Ni_3P and Ni–Sn-P are reported to form during the bonding process [24,25]. The galvanic corrosion in the ENIG called “black pad” is also caused by the immersion Au solution [26]. Thus, ENEPIG was recently proposed and researched as a barrier for Cu or Ni to prevent the formation of P-rich layers or black pad [26–28]. Meanwhile, methods using various binary substrates such as Cu–Zn [29,30] and Cu–Mn [31] for suppressing IMC growth have also been reported. The effects of various surface-finishing materials on the properties and reliabilities of joints have been reviewed and reported [32–35].

In previous studies, the effects of IMC thickness and growth at interfaces or joints on the mechanical [36–38] and electrical reliabilities [38,39] of the joints were observed. Thicker IMCs and faster IMC growth can degrade the mechanical and electrical properties of joints in electronic packaging. Therefore, it is critical to suppress the growth of IMCs at such joints.

1.3 Lead-free solders in automotive electronics

Since 2002, because of environmental concerns, the European Union (EU) has been implementing and enforcing regulatory legislation prohibiting the use of toxic substances, including Pb, in electronic products [40]. For example, eutectic Tin-lead solder used in typical electronic products has been successfully substituted with SAC305 lead-free solder. However, because of the new restrictions on the use of Pb, such as the end-of-life vehicles (ELV) Directive, which prescribes that lead-bearing solder may not be used in automotive electronic components as of January 1, 2016, lead-free soldering has become a significant issue in the field of automotive electronic components [41,42]. As is well known, the performance of SAC solder is superior in terms of its wettability and operating temperature. However, owing to the presence of a Ag_3Sn intermetallic compound (IMC) with high brittleness in the matrix, SAC solder has poor thermal reliability, which is a serious threat because solder joints are continuously exposed to thermal shock [43]. Basically, automotive electronic components require a higher level of reliability because the environment they are used in is more severe than that of typical electronic components. In particular, the electric control units (ECUs) in vehicles are exposed to more severe thermal shocks and thermal vibration conditions. For example, ECUs around the transmission and engine are subject to vibrations of 3 Grms to 20 Grms, and their operating temperatures are approximately 130 ℃ [44]. General Motors Global Research and Delphi Delco Electronic Systems described the automotive environment for electronics and actuators as shown in **Table 1.1**. In particular, the temperature range in the underhood is -40 to 125 ℃. Therefore, Some Pb-free solders have been suggested to replace SAC solder, like Sn-3.5Ag, Sn-Au, Sn-Sb, Sn-Cu, and Sn-Zn solders. However, these have all had problems under actual operating conditions. For example, Sn-Au alloy has a high cost for raw materials due to usage of Au metal. Zn and Al-based alloys exhibit poor wettability due to their strong susceptibility to oxidation [45,46]. Bi-based alloy has limited uses because of poor mechanical properties and a low melting temperature [47]. Cost is another important factor in the adoption of solders for practical electronic applications [48,49]. Sn-Cu solder has a low cost, relative high melting temperature and moderate mechanical properties. However, disadvantages of the Sn-0.7Cu solder are a relative low wettability and reliability.

1.4 Issues on solder joints reliability in automotive electronics

The Sn-Ag-Cu system is used as a Pb-free solder alloy composition in automotive electronics, as in the electrical and electronics industry. However, this composition exhibits lower ductility compared to the conventional Sn-Pb solder composition and forms highly brittle joints due to the rapid growth of Ag_3Sn, making it unsuitable for automotive solder application exposed to continuous vibration [50]. Therefore, there is an urgent demand for alloy development that addresses the complex destructive conditions applied on automotive electronics solder joints by simultaneously improving high-temperature reliability, thermal cycling and high vibration characteristics. Recent studies have actively investigated solder alloys doped with a trace of multiple elements [51–56]. Particularly, it is known that doping alloying elements is only effective when an amount within a specific range is introduced. In other words, doping alloying elements more than necessary forms precipitates with Sn in the solder, which enlarge through the subsequent aging process and promote brittle fracture [57–60]. Therefore, it is preferable to add minor doping elements only in small quantities to the extent of their solubility limit in the Sn base, or to disperse them in the matrix without dissolving them in the base metal, resulting in dispersion strengthening [61–63]. In addition, as it is difficult to improve high-temperature reliability, thermal cycling and high vibration characteristics simultaneously by adding only one alloying element, a combination of alloying elements must be added. In this case, it is important to note that the solubility limit of each element may change. In specific compositions of alloying elements, very unusual mechanical properties of decreased hardness and increased ductility are observed; such properties may serve as an effective factor for thermal cycling, high vibration and other characteristics [64].

Meanwhile, the type of pad finish is another key factor in determining the reliability of solder joints [65]. Since a thick Au finish or a pad finish containing Au significantly increases the brittleness of the solder joint, it is desirable to restrict its usage. Therefore, the OSP finish, low in production cost and free of Au, is recommended as a pad finish for application to automotive electronics. However, when an OSP/Cu pad is used, special measures are required to suppress the Kirkendall void [66–69].

1.5 Effect of trace elements on properties of solder

Many control methods have been proposed to suppress IMC growth at solder joints in electronic packaging. Tsao added TiO_2 particles to a Pb-free solder alloy and reduced the diffusion coefficient [70]. Methods for suppressing IMC growth by adding minor elements such as In [71] and Zn [72,73], Cr [74,75], AlSi [76] to Pb-free solder alloys have been proposed. Jee et al. [77,78] reported the effect of Zn on suppressing IMC growth and improving the reliability of solder joints. The effects of impurities and minor alloying elements in Pb-free solders on interfacial reactions and IMC growth were reviewed [79–81]. The influence of nanoparticles reinforcing Pb-free solders were also examined [82]. Various Pb-free solders containing minor elements and particles are shown in **Table 1.2** [81]. In this study, the joint properties were evaluated after the addition of trace elements to improve the performance of the Sn-Cu solder.

1.6 Characteristics of Sn-Cu alloy system with Cr and Al additions

Sn-Cu eutectic alloys exhibit two intermetallic compounds, Cu_6Sn_5 and Cu_3Sn, as shown in **Figure 1.3**, at typical soldering temperatures of 300 ℃ or below [83–85]. Through a preliminary investigation, elements possibly inducing precipitation or dispersion strengthening without considerably affecting the liquidus and solidus when added to the Sn-Cu eutectic composition were considered.

Table 1.1 The automotive environment [44].

Temperature	Driver interior	-40℃ to + 85℃
	Underhood	-40℃ to + 125℃
	On-engine	-40℃ to + 150℃
	In the exhaust and Combustion areas	-40℃ to + 200-600℃
Mechanical Shock	During assembly (drop test)	3000g
	On the vehicle	50-500g
Mechanical Vibration		15g, 100Hz to 2kHz
Electromagnetic Impulses		100 to 200V/m
Exposure to	Common	Humidity, salt spray
	In some applications	Fuel, oil, brake fluid, transmission fluid, ethylene glycol, exhaust gases

Table 1.2 Various Pb-free solders added minor elements and particles [81].

Solder (weight per cent)	Melting temperature, T_M (°C)	Solidus temperature, T_S (°C)	Liquidus temperature, T_L(°C)
60Sn-40Pb	183	183	187
Sn-3.5Ag (SA)	223	221	221
Sn-3.8Ag-0.7Cu (SAC)	217	217	217
Sn-3.9Ag-0.1Cu (SAC)	220.40	217.31	222.71
Sn-3.0Ag-0.5Cu	217.64	217.64	217.64
Sn.3.5Ag-0.5Cu (SAC)	221.58	–	216.92
Sn-3.8Ag-0.7Cu (SAC)	217.73	–	–
Sn-1.1Ag-0.45Cu-0.25Mn	–	217.39	227.63
Sn-1.07Ag-0.58Cu-0.037Ce	–	217.65	226.14
Sn-3.8Ag-0.7Cu-0.5Zn	216.23	212.06	–
Sn-3.8Ag-0.7Cu-1Zn	216.65	212.61	-
Sn-3.8Ag-0.7Cu-1.5Zn	216.86	213.32	–
Sn-3.0Ag-0.5Cu-0.25Al_2O_3	222.3	–	–
Sn-3.0Ag-0.5Cu-0.5Al_2O_3	222.7	–	–
Sn-3.0Ag-0.5Cu-1Al_2O_3	223.0	–	–
Sn-3.8Ag-0.7Cu-2Bi	213.08	–	–
Sn-3.8Ag-0.7Cu-4Bi	206.48	–	–
Sn-3.0Ag-0.5Cu 0.25Ti	220.95	–	216.73
Sn-3.0Ag-0.5Cu-0.5Ti	220.86	–	216.75
Sn-3.0Ag-0.5Cu-1Ti	219.47	–	216.59
Sn-3.5Ag-0.7Cu-0.5TiO_2	224.1	217.7	–
Sn-3.0Ag-0.5Cu-0.5ZrO_2	–	217.08	221.63
Sn-3.0Ag-0.5Cu-1ZrO_2	–	217.12	221.65
Sn-3.0Ag-0.5Cu-3ZrO_2	–	217.25	221.95
Sn-3.0Ag-0.5Cu-0.5$SrTiO_3$	217.7	–	–

In this study, the improvement of the mechanical properties due to the increased melting temperature and modified microstructure of the alloy with the addition of trace elements such as Cr and Al(Si) compounds was expected.

While Cr has a density similar to that of Sn, it has a high melting point and is known to provide high oxidation resistance in Fe, Zn and Ni-based alloys [86,87]. Moreover, a study has reported that the addition of Cr to the SnBi solder in the range of 0.1-0.2 wt.% noticeably inhibits the growth of intermetallic compounds [88]. Based on the Cr-Sn binary phase diagrams reported in previous studies, there is no Cr solubility in Sn at room temperature as shown in **Figure 1.4** [89,90].

In the case of Cr-doped alloys, several methods for producing master alloys have been proposed [91,92]. However, the conditions for producing the master alloy differ with the amount of base alloy and additives. Nevertheless, the common point between these methods is that the material is melted in an induction furnace in an inert gas atmosphere and homogenized at a constant temperature.

It has been reported that the addition of Al improves the wettability and increases ductility and toughness, enhancing the drop property [93–95]. Si is reported to have the effect of suppressing the voids generated between Cu and Cu_3Sn when alloyed to Sn base solder [96]. The method of alloying Al(Si) does not significantly differ from that of Cr [97]. However, the process conditions must be set in consideration of the melting point and the oxidation properties of the doping elements. **Figure 1.5** is a Sn-Cu-Al binary diagram [98]. The eutectic temperature is approximately 226.8 °C and is calculated as 229.2 °C, 229.4 °C and 230.1 °C according to 0.01 wt.%, 0.03 wt.% and 0.05 wt.% of Al(Si), respectively.

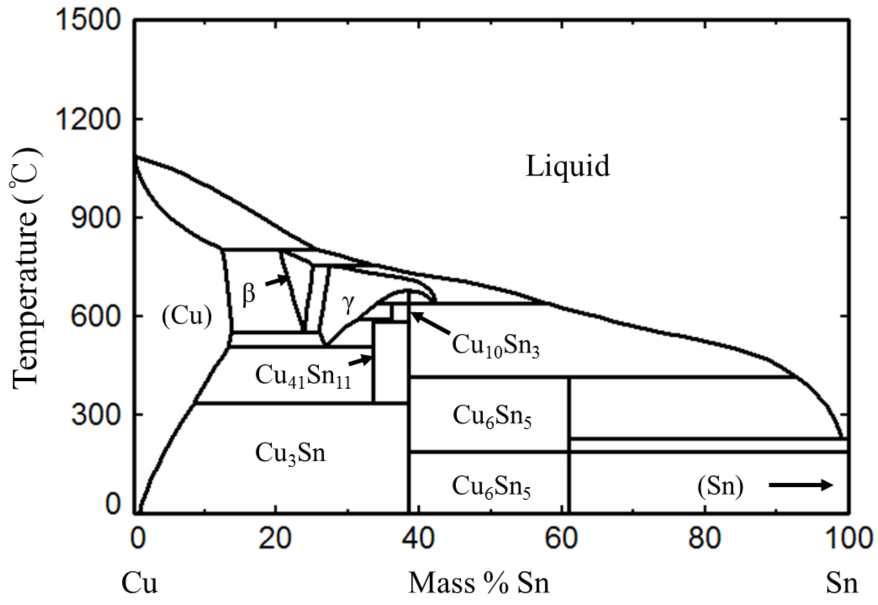

Figure 1.3 Phase diagram of Sn-Cu system [84,85].

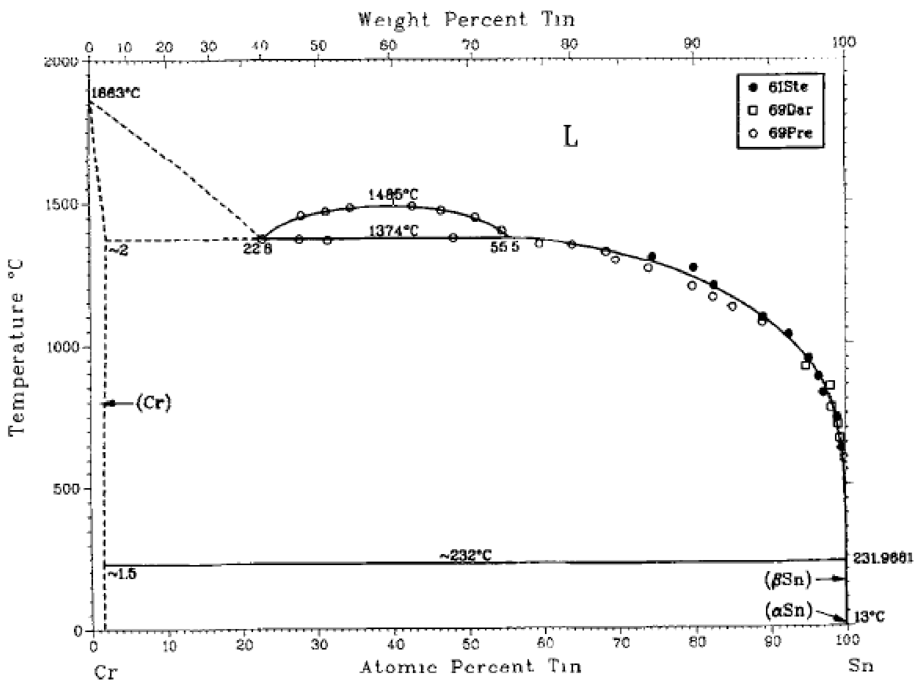

Figure 1.4 Cr solubility by Thermo-Calc in the Sn–Cr system [89].

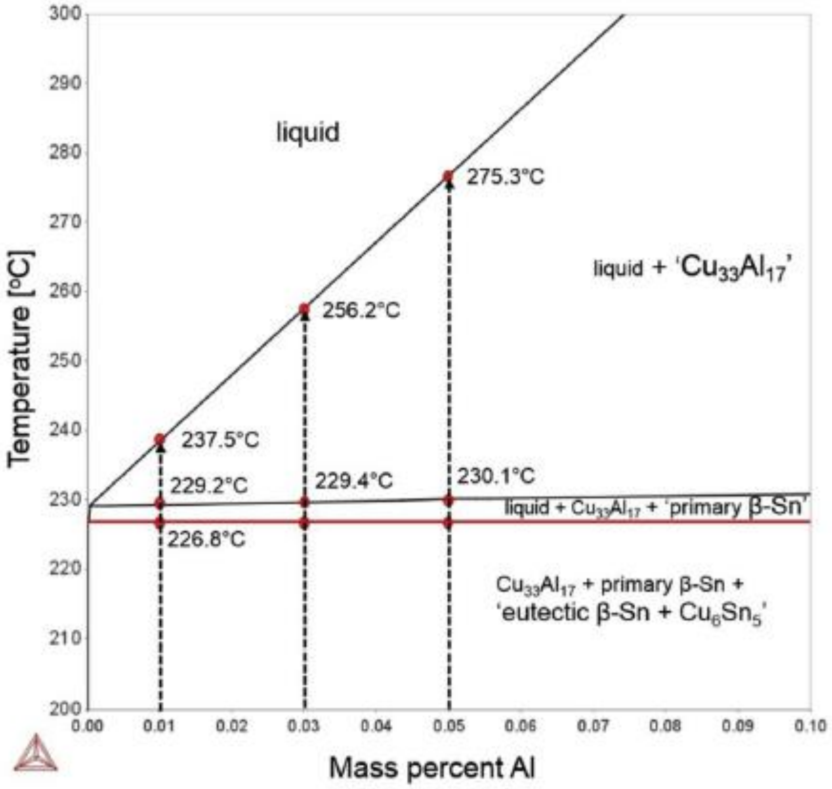

Figure 1.5 Ternary phase diagram of Sn-Cu-Al [98].

1.7 Research purpose

As described, there are many issues in electronic packaging. Interfacial reactions and intermetallic compounds (IMCs) can affect the properties and reliability of joints between solder and substrate. The immoderate growth of IMCs can degrade the joint properties and reliability. Therefore, it is important to control and suppress interfacial reactions and IMC growth. In this dissertation, new approaches are suggested to improve the interfacial characteristics of solder joint in electronic packaging for automotive.

Chapter 1, described the research back ground of my study.

Chapter 2, proposed a method of producing master alloys by adding a small amount of Cr and Al(Si) to the Sn-Cu eutectic solder. The master alloy was fabricated in a solder ball shape to produce bonding samples. This chapter also evaluated the basic properties of the alloy containing trace alloying elements and discussed the results.

Chapter 3, discussed the doping effects of Al(Si) on the Sn-Cu eutectic solder, focusing on the interfacial intermetallic compound behavior. This chapter also discussed the interfacial intermetallic compound's formation, growth and mechanical properties regarding the Al(Si) doped solder on the Cu substrate under various thermal stresses after fabricating the test coupon through reflow.

Chapter 4, discussed the doping effects of Cr on the Sn-Cu eutectic solder, focusing on the interfacial intermetallic compound behavior. This chapter also discussed the formation and growth behavior of the interfacial intermetallic compound regarding the Cr doped solder on the Cu substrate under various thermal stresses after fabricating the test coupon through reflow.

Chapter 5, discussed the calculation of the activation energy using the intermetallic compound growth results in the SC-Cr/Cu joint. In addition, after the activation energy calculation, the acceleration factor was calculated based on the intermetallic compound growth behavior under thermal shock.

Chapter 6, the shear strength of SC-Cr/Cu joint was evaluated after thermal treatment. In addition, after the shear tests, fracture behavior of interface was analyzed.

In Chapter 7, an overall summary and conclusion of this dissertation are given.

1.8 Bibliography

[1] Tummala, R. "*Fundamentals of microsystems packaging*" McGraw Hill, New York, (2001) 16–18.

[2] ISO 857-2:2005(en) Welding and allied processes – Vocabulary – Part 2: Soldering and brazing processes and related terms.

[3] Ivan SZENDIUCH "*Development in Electronic Packaging –Moving to 3D System Configuration*" RADIOENGINEERING, 20 (2011) 214–220.

[4] R. Plieninger , M. Dittes, K. Pressel "Modern IC Packaging Trends and their Reliability Implications" *Microelectronics Reliability*, 46 (2006) 1868–1873.

[5] Automotive Industry Interpretation Guide for ELV Annex II (2016/774/EU)

[6] Wislei R. Osório, Leandro C. Peixoto, Leonardo R. Garcia, Amauri Garcia, José E. Spinelli "The Effects of Microstructure and Ag3Sn and Cu6Sn5 Intermetallics on the Electrochemical Behavior of Sn-Ag and Sn-Cu Solder Alloys" Journal of ELECTROCHEMICAL SCIENCE, 7 (2012) 6436–6452.

[7] Tu, K. "Interdiffusion and reaction in bimetallic Cu-Sn thin films" *Acta Metallurgica*, 21 (1973) 347–354.

[8] Kim, P., Jang, J., Lee, T. and Tu, K. "Interfacial reaction and wetting behavior in eutectic SnPb solder on Ni/Ti thin films and Ni foils" *Journal of Applied Physics*, 86 (1999) 6746–6751.

[9] Sohn, Y., Yu, J., Kang, S., Choi, W. and Shih, D. "Study of the reaction mechanism between electroless Ni–P and Sn and its effect on the crystallization of Ni–P" *Journal of materials research*, 18 (2003) 4–7.

[10] Tu, K. and Thompson, R. "Kinetics of interfacial reaction in bimetallic Cu-Sn thin films" *Acta Metallurgica*, 30 (1982) 947–952.

[11] Y. Watanabe, Y. Fujinaga, and H. Iwasaki "Lattice modulation in the long-period superstructure of Cu_3Sn" Acta Cryst. B, 39 (1983) 306–311.

[12] A. PAUL, C. GHOSH, W.J. BOETTINGER "Diffusion Parameters and Growth Mechanism of Phases in the Cu-Sn System" The Minerals, Metals & Materials Society and ASM International 2010.

[13] N. Ssunders and A.P. Miodownik "The Cu-Sn (Copper-Tin) System" Bulletin of Alloy Phase Diagrams, 11 (1990).

[14] Zeng, K., Stierman, R., Chiu, T.-C., Edwards, D., Ano, K. and Tu, K. "Kirkendall void formation in eutectic SnPb solder joints on bare Cu and its effect on joint reliability" *Journal of applied physics*, 97 (2005) 4508.

[15] Lim, G.-T., Kim, B.-J., Lee, K., Kim, J., Joo, Y.-C. and Park, Y.-B. "Temperature effect on intermetallic compound growth kinetics of Cu pillar/Sn bumps" *Journal of electronic materials*, 38 (2009) 2228–2233.

[16] Jeong, S. W., Kim, J. H. and Lee, H. M. "Effect of cooling rate on growth of the intermetallic compound and fracture mode of near-eutectic Sn-Ag-Cu/Cu pad: Before and after aging" *Journal of Electronic Materials*, 33 (2004) 1530–1544.

[17] Zhong, W., Chan, Y., Alam, M., Wu, B. and Guan, J. "Effect of multiple reflow processes on the reliability of ball grid array (BGA) solder joints" *Journal of alloys and compounds*, 414 (2006) 123–130.

[18] Yoon, J.-W., Kim, S.-W. and Jung, S.-B. "IMC morphology, interfacial reaction and joint reliability of Pb-free Sn–Ag–Cu solder on electrolytic Ni BGA substrate" *Journal of Alloys and Compounds*, 392 (2005) 247–252.

[19] Pratt, R. E., Stromswold, E. and Quesnel, D. J. "Effect of solid-state intermetallic growth on the fracture toughness of Cu/63Sn-37Pb solder joints" *Components, Packaging, and Manufacturing Technology, Part A, IEEE Transactions on*, 19 (1996) 134–141.

[20] Song, F. and Lee, S. R. "Investigation of IMC thickness effect on the lead-free solder ball attachment strength: comparison between ball shear test and cold bump pull test results" *Electronic Components and Technology Conference, 2006. Proceedings. 56th*, (2006) 1196–1203.

[21] So, A. C. and Chan, Y. C. "Reliability studies of surface mount solder joints-effect of Cu-Sn intermetallic compounds" *Components, Packaging, and Manufacturing Technology, Part B: Advanced Packaging, IEEE Transactions on*, 19 (1996) 661–668.

[22] Chen, Z., He, M., Balakrisnan, B. and Chum, C. C. "Elasticity modulus, hardness and fracture toughness of Ni_3Sn_4 intermetallic thin films" *Materials Science and Engineering: A*, 423 (2006) 107–110.

[23] Yoon, J. W. and Jung, S. B. (2005). "Interfacial reactions between Sn-0.4Cu solder and Cu substrate with or without ENIG plating layer during reflow reaction." *Journal of Alloys and Compounds*, 396, pp. 122-127.

[24] Zeng, K. J., Stierman, R., Abbott, D. and Murtuza, M. (2006). "The root cause of black pad failure of solder joints with electroless Ni/immersion gold plating." *Jom*, 58, pp. 75-79.

[25] Alam, M., Chan, Y. and Hung, K. (2002). "Reliability study of the electroless Ni–P layer against solder alloy." *Microelectronics Reliability*, 42, pp. 1065-1073.

[26] Tseng, C.-F., Lee, T.-K., Ramakrishna, G., Liu, K.-C. and Duh, J.-G. (2011). "Suppressing Ni_3Sn_4 formation in the Sn–Ag–Cu solder joints with Ni–P/Pd/Au surface finish." *Materials Letters*, 65, pp. 3216-3218.

[27] Yoon, J. W., Noh, B. I. and Jung, S. B. (2011). "Comparative Study of ENIG and ENEPIG as Surface Finishes for a Sn-Ag-Cu Solder Joint." *Journal of Electronic Materials*, 40, pp. 1950-1955.

[28] Kim, Y. M., Park, J. Y. and Kim, Y. H. (2012). "Effect of Pd Thickness on the Interfacial Reaction and Shear Strength in Solder Joints Between Sn-3.0Ag-0.5Cu Solder and Electroless Nickel/Electroless Palladium/Immersion Gold (ENEPIG) Surface Finish." *Journal of Electronic Materials*, 41, pp. 763-773.

[29] Chen, W.-Y., Yu, C.-Y. and Duh, J.-G. (2012). "Suppressing the growth of interfacial Cu–Sn intermetallic compounds in the Sn–3.0Ag–0.5Cu–0.1Ni/Cu–15Zn solder joint during thermal aging." *Journal of Materials Science*, 47, pp. 4012-4018.

[30] Kim, Y. M., Harr, K.-M. and Kim, Y.-H. (2010). "Mechanism of the delayed growth of intermetallic compound at the interface between Sn−4.0Ag−0.5Cu and Cu−Zn substrate." *Electronic Materials Letters*, 6, pp. 151-154.

[31] Tseng, C.-F., Wang, K.-J. and Duh, J.-G. (2010). "Interfacial reactions of Sn-3.0Ag-0.5Cu solder with Cu-Mn UBM during aging." *Journal of electronic materials*, 39, pp. 2522-2527.

[32] Bradley, E. and Banerji, K. (1996). "Effect of PCB finish on the reliability and wettability of ball grid array packages." *IEEE Transactions on Components, Packaging, and Manufacturing Technology: Part B*, 19, pp. 320-330.

[33] Sundelin, J. J., Nurmi, S. T., Lepistö, T. K. and Ristolainen, E. O. (2005). "Effect of PCB surface finish on creep properties of lead-free solder joints." *Soldering & surface mount technology*, 17, pp. 3-9.

[34] Nurmi, S. T., Sundelin, J. J., Ristolainen, E. O. and Lepistö, T. K. (2005). "The effect of PCB surface finish on lead-free solder joints." *Soldering & surface mount technology*, 17, pp. 13-23.

[35] Tu, P., Chan, Y. C. and Lai, J. "Effect of intermetallic compounds on the thermal fatigue of surface mount solder joints" *Components, Packaging, and Manufacturing Technology, Part B: Advanced Packaging, IEEE Transactions on*, 20 (1997) 87–93.

[36] Chan, Y., Tu, P., So, A. C. and Lai, J. "Effect of intermetallic compounds on the shear fatigue of Cu/63Sn-37Pb solder joints" *Components, Packaging, and Manufacturing Technology, Part B: Advanced Packaging, IEEE Transactions on*, 20 (1997) 463–469.

[37] Kang, S., Choi, W., Yim, M. and Shih, D. "Studies of the mechanical and electrical properties of lead-free solder joints" *Journal of electronic materials*, 31 (2002) 1292–1303.

[38] Yoon, J.-W., Kim, S.-W., Koo, J.-M., Kim, D.-G. and Jung, S.-B. "Reliability investigation and interfacial reaction of ball-grid-array packages using the lead-free Sn–Cu solder" *Journal of electronic materials*, 33 (2004) 1190–1199.

[39] K.N. Tu (Ed.). "Solder Joint Technology: Materials, Properties, and Reliability" Springer, New York, (2007) 386.

[40] K. Zeng, K.N. Tu, "Six cases of reliability study of Pb-free solder joints in electronic packaging technology" Mater. Sci. Eng. R. 49 (2005) 55–105.

[41] Q.K. Zhang, W.M. Long, Z.F. Zhang "Growth behavior of intermetallic compounds at Sn–Ag/Cu joint interfaces revealed by 3D imaging" J. Alloys Compd. 646 (2015) 405–411.

[42] T. Hurtony, A.S.L. Almasy, A. Len, B. Kugler, A. Bonyar, P. Gordon "Characterization of the microstructure of tin-silver lead free solder" J. Alloys Compd. 672 (2016) 13–19.

[43] R.W. Johnson, J.L. Evans, P. Jacobsen, J.R. Thompson, M. Christopher "The changing automotive environment: high-temperature electronics" IEEE Trans. Electron. Pack. Manuf. 27 (2004) 164–176.

[44] R. W. Johnson, J. L. Evans, P. Jacobsen, J. R. Thompson, M. Christopher "The changing automotive environment: high-temperature electronics" IEEE Trans. Electron. Pack Manu. 27(3) (2004) 164.

[45] X. Chen, M. Li, X. Ren, D. Mao "Effects of alloying elements on the characteristics of Sn-Zn lead-free solder" 6th International Conference on Electronics Packaging Technology (2005).

[46] K. L. Lin, P. C. Liu, J. M. Song "Wetting interaction between Pb-free Sn-Zn series solders and Cu, Ag substrates" Electronic Compound and Technology Conference (2003).

[47] J. Wang, L. Wen, J. Zhou, M. Chung "Mechanical properties and joint reliability improvement of Sn-Bi alloy" 13th Electronics Packaging Technology Conference (2011).

[48] Yang, M.; Ji, H.; Wang, S.; Ko, Y.-H.; Lee, C.-W.; Wu, J.; Li, M. "Effects of Ag content on the interfacial reactions between liquid Sn–Ag–Cu solders and Cu substrates during soldering" *J. Alloy. Compd.*, *679 (*2016) 18–25.

[49] Ko, H.; Lee, J.D.; Yoon, T.; Lee, C.W.; Kim, T.S. "Controlling interfacial reactions and intermetallic compound growth at the interface of a lead-free solder joint with layer-by-layer transferred grapheme" *ACS Appl. Mater. Interfaces*, *8* (2016) 5679–5686.

[50] Lihua Qi, Jihua Huang, Xingke Zhao, Hua Zhang "Effect of thermal-shearing cycling on Ag3Sn microstructural coarsening in SnAgCu solder" Journal of Alloys and Compounds, 469 (2009) 102–107.

[51] CHANG S Y, JAIN C C, CHUANG T H, FENG L P, TSAO L C. "Effect of addition of TiO2 nanoparticles on the microstructure,microhardness and interfacial reactions of Sn3.5AgXCu solder" J. Materials & Design, 32 (2011) 4720−4727.

[52] TSAO L C, CHANG S Y, LEE C I, SUN W H, HUANG C H. "Effects of nano-Al2O3 additions on microstructure development and hardness of Sn3.5Ag0.5Cu solder" J. Materials & Design, 31 (2010) 4831−4835.

[53] GAIN A K, FOUZDER T, CHAN Y C, YUNG W K C. "Microstructure, kinetic analysis and hardness of Sn−Ag−Cu−1wt% nano-ZrO2 composite solder on OSP-Cu pads" Journal of Alloys and Compounds, 509 (2011) 3319−3325.

[54] LIN F, BI W, JU G, WANG W, WEI X. "Evolution of Ag3Sn at Sn−3.0Ag−0.3Cu−0.05Cr/Cu joint interfaces during thermal aging" Journal of Alloys and Compounds, 509 (2011) 6666−6672.

[55] LEE Y H, LEE H T. "Shear strength and interfacial microstructure of Sn−Ag−xNi/Cu single shear lap solder joints" Materials Science and Engineering A, 444 (2007) 75−83.

[56] LAW C M T, WU C M L, YU D Q, WANG L, LAI J K L. "Microstructure, solderability, and growth of intermetallic compounds of Sn−Ag−Cu−RE lead-free solder alloys" Journal of Electronic Materials, 35 (2006) 89−93.

[57] Y. Tang, Q.W. Guo, S.M. Luo, Z.H. Li, G.Y. Li, C.J. Hou, Z.Y. Zhong, J.J. Zhuang "Formation and growth of interfacial intermetallics in Sn-0.3Ag-0.7Cu xCeO_2/Cu solder joints during the reflow process" Journal of Alloys and Compounds, 778 (2019) 741–755.

[58] Wenbo Zhu, Weiwei Zhang, Wei Zhou, Ping Wu "Improved microstructure and mechanical properties for SnBi solderalloy by addition of Cr powders" Journal of Alloys and Compounds, 789 (2019) 805–813.

[59] Lei Sun, Ming-he Chen, Liang Zhang "Microstructure evolution and grain orientation of IMC in Cu-Sn TLP bonding solder joints" Journal of Alloys and Compounds, 789 (2019) 805–813.

[60] Li Yanga, Lu Zhu, Yaocheng Zhang, Shiyuan Zhou, Guoqiang Wang, Sai Shen, Xiaolong Shi "Microstructure, IMCs layer and reliability of Sn-58Bi solder joint reinforced by Mo nanoparticles during thermal cycling" Materials Characterization, 148 (2019) 280–291.

[61] Chi-Yang Yu, Joseph Lee, Wen-Lin Chen, Jenq-Gong Duh "Enhancement of the impact toughness in Sn–Ag–Cu/Cu solder joints via modifying the microstructure of solder alloy" Materials Letters, 119 (2014) 20–23.

[62] A.B. El Basaty, A.M. Deghady, E.A. Eid "Influence of small addition of antimony (Sb) on thermal behavior, microstructural and tensile properties of Sn-9.0Zn-0.5Al Pb-free solder alloy" Materials Science & Engineering, A 701 (2017) 245–253.

[63] Liang Zhang, K.N. Tu "Structure and properties of lead-free solders bearing micro and nano particles" Materials Science and Engineering, R 82 (2014) 1–32.

[64] A-Mi Yu, Chang-Woo Lee, Mok-Soon Kim, Jong-Hyun Lee "The Effect of the Addition of In on the Reaction and Mechanical Properties of Sn-1.0Ag-0.5Cu Solder Alloy" METALS AND MATERIALS International, 13 (2007) 517–520.

[65] Jeong-Won Yoon, Bo-In Noh, Bong-Kyun Kim, Chang-Chae Shur, Seung-Boo Jung "Wettability and interfacial reactions of Sn–Ag–Cu/Cu and Sn–Ag–Ni/Cu solder joints" Journal of Alloys and Compounds, 486 (2009) 142–147.

[66] Glenn Ross, Vesa Vuorinen, Mervi Paulasto-Krockel "Void formation and its impact on CueSn intermetallic compound formation" Journal of Alloys and Compounds, 677 (2016) 127–138.

[67] Chun Yu, Dongye Wang, Jieshi Chen, JijinXu, Junmei Chen, Hao Lu "Study of Cu6Sn5 and Cu3Sn growth behaviors by considering trace Zn" Materials Letters, 121 (2014) 166–169.

[68] Yousra Bettahi, Caroline Richard "Evolution of microstructure of Lead free cu/Sn solders and copper oxide phase precipitation in Cu3Sn intermetallic during thermal cycling" Microelectronics Reliability, 92 (2019) 20–26.

[69] D.K. Mu, S.D. McDonald, J. Read, H. Huang, K. Nogita "Critical properties of Cu6Sn5 in electronic devices: Recent progress and a review" Current Opinion in Solid State and Materials Science, 20 (2016) 55–76.

[70] Tsao, L. C. (2011). "Suppressing effect of 0.5wt.% nano-TiO_2 addition into Sn–3.5Ag–0.5Cu solder alloy on the intermetallic growth with Cu substrate during isothermal aging." *Journal of Alloys and Compounds*, 509, pp. 8441–8448.

[71] Sharif, A. and Chan, Y. (2005). "Effect of indium addition in Sn-rich solder on the dissolution of Cu metallization." *Journal of alloys and compounds*, 390, pp. 67–73.

[72] Kotadia, H., Mokhtari, O., Clode, M., Green, M. and Mannan, S. (2012). "Intermetallic compound growth suppression at high temperature in SAC solders with Zn addition on Cu and Ni–P substrates." *Journal of Alloys and Compounds*, 511, pp. 176–188.

[73] Cho, M. G., Kang, S. K., Shih, D.-Y. and Lee, H. M. (2007). "Effects of Minor Additions of Zn on Interfacial Reactions of Sn–Ag–Cu and Sn-Cu Solders with Various Cu Substrates during Thermal Aging." *Journal of Electronic Materials*, 36, pp. 1501–1509.

[74] J. Koo, J. Chang, Y.W. Lee, S.J. Hong, K.S. Kim, H.M. Lee "New Sn–0.7Cu-based solder alloys with minor alloying additions of Pd, Cr and Ca" Journal of Alloys and Compounds, 608 (2014) 126–132.

[75] J. Hu, A. Hu, M. Li, D. Mao "Depressing effect of 0.1 wt.% Cr addition into Sn–9Zn solder alloy on the intermetallic growth with Cu substrate during isothermal aging" Materials Characterization, 61 (2010) 355–361.

[76] WON SIK HONG, CHULMIN OH, MI-SONG KIM, YOUNG WOO LEE, HUI JOONG KIM, SUNG JAE HONG, and JEONG TAK MOON "Al and Si Alloying Effect on Solder Joint Reliability in Sn-0.5Cu for Automotive Electronics" Journal of E. MATERIALS, 45 (2016) 6250–6162.

[77] Jee, Y., Ko, Y. and Yu, J. "Effect of Zn on the intermetallics formation and reliability of Sn-3.5Ag solder on a Cu pad" *Journal of materials research*, 22 (2007) 1879–1887.

[78] Jee, Y., Yu, J. and Ko, Y. "Effects of Zn addition on the drop reliability of Sn–3.5Ag–xZn/Ni (P) solder joints" *Journal of Materials Research*, 22 (2007) 2776–2784.

[79] Laurila, T., Vuorinen, V. and Paulasto-Kröckel, M. "Impurity and alloying effects on interfacial reaction layers in Pb-free soldering" *Materials Science and Engineering: R: Reports*, 68 (2010) 1–38.

[80] Sun, L. and Zhang, L. "Properties and Microstructures of Sn–Ag–Cu–X Lead-Free Solder Joints in Electronic Packaging" *Advances in Materials Science and Engineering,* (2015) 16.

[81] Noor, E. E. M. and Singh, A. "Review on the effect of alloying element and nanoparticle additions on the properties of Sn–Ag–Cu solder alloys" *Soldering & Surface Mount Technology,* 26 (2014) 147–161.

[82] Efzan Mhd Noor, E., Singh, A. and Tze Chuan, Y. "A review: influence of nano particles reinforced on solder alloy" *Soldering & Surface Mount Technology*, 25 (2013) 229–241.

[83] N, Mookam, P. Tunthawiroon, and K. Kanlayasiri "Effects of copper content in Sn-based solder on the intermetallic phase formation and growth during soldering" ICMM, 361(2018) 012008.

[84] C. Yu, H. Lu, and S. Li "Effect of Zn addition on the formation and growth of intermetallic compound at Sn–3.5 wt% Ag/Cu interface" J. of Alloys and Compd. 460 (2008) 594–598.

[85] Y. Wang, D.T. Chu, and K.N. Tu "Porous Cu3Sn formation in Cu-Sn IMC-based microjoints" IEEE 66th Electronic Components and Technology Conference, (2016) 439–446.

[86] S.W. Park, T. Sugahara, K.S. Kim, K. Suganuma "Enhanced ductility and oxidation resistance of Zn through the addition of minor elements for use in wide-gap semiconductor die-bonding materials"

Journal of Alloys and Compounds 542 (2012) 236–240.

[87] I. Wolf, H.J. Grabke "A STUDY ON THE SOLUBILITY AND DISTRIBUTION OF CARBON IN OXIDES" Solid State Communications, 54 (1985) 5–10.

[88] Wenbo Zhu, Weiwei Zhang, Wei Zhou a, Ping Wu "Improved microstructure and mechanical properties for SnBi solder alloy by addition of Cr powders" Journal of Alloys and Compounds 789 (2019) 805–813.

[89] Rosa Jerlerud Perez, Bo Sundman "THERMODYNAMIC ASSESSMENT OF THE CR-SN BINARY SYSTEM" Calphad, 25 (2001) 59-66.

[90] M. Venkatreman, J.P. Neumann "The Cr-Sn (Chromium-Tin) System" Polonides of the Transition Metals and of Copper and Gold, Silver, Isotopenpraxis, 20 (1984) 454-458.

[91] Xi Chen, Anmin Hu, Ming Li, Dali Mao "Study on the properties of Sn–9Zn–xCr lead-free solder" Journal of Alloys and Compounds 460 (2008) 478–484.

[92] Jin Hu, Anmin Hu, Ming Li, Dali Mao "Depressing effect of 0.1 wt.% Cr addition into Sn–9Zn solder alloy on the intermetallic growth with Cu substrate during isothermal aging" Materials characterization, 61 (2010) 355–361.

[93] Mohd Faizul Mohd Sabri, Dhafer Abdulameer Shnawah, Irfan Anjum Badruddin, Suhana Binti Mohd Said "Effects of aging on Sn–1Ag–0.5Cu solder alloys containing 0.1 wt.% and 0.5 wt.% Al" Journal of Alloys and Compounds 582 (2014) 437–446.

[94] Md Ershadul Alam, Manoj Gupta "Development of Extremely Ductile Lead-Free Sn-Al Solders for Futuristic Electronic Packaging Applications" Electron. Mater. Letter, 10 (2014) 515-524.

[95] J.F. Li, P.A. Agyakwa, C.M. Johnson "Effect of trace Al on growth rates of intermetallic compound layers between Sn-based solders and Cu substrate" Journal of Alloys and Compounds, 545 (2012) 70–79.

[96] I.E. ANDERSON, J.L. HARRINGA "Suppression of Void Coalescence in Thermal Aging of Tin-Silver-Copper-X Solder Joints" Journal of ELECTRONIC MATERIALS, 35 (2006) 94–106

[97] K. Maslinda, M.S. Nurulakmal, A.S. Anasyida, R.Sivakumar "Effect of Aluminium and Silicon Addition to the Microstructure of Low-Ag SAC Solder Alloy" ResearchGate, (2015)

[98] Jahyun Koo, Changsoo Lee, Sung Jea Hong, Keun-Soo Kim, Hyuck Mo Lee "Microstructural discovery of Al addition on Sne0.5Cu-based Pb-free solder design" Journal of Alloys and Compounds, 650 (2015) 106–115.

Chapter 2

Fabrication of trace element addition solder alloys

2.1 Introduction

As mentioned in *Chapter 1*, in lead-free solder alloys, various elements are added to the Sn base solder to control the properties of the alloy [1-9]. The additive elements should be easy to obtain and inexpensive, and should not deteriorate the basic properties of the alloy when added.

This chapter proposes that Cr and Al(Si), which can be more easily supplied than noble metals, are added in small amounts to the Sn-Cu solder to obtain the effect of dispersion hardening or precipitation hardening [10,11]. After fabricating the Sn-Cu solder alloy to which Cr and Al(Si) were added, we analyzed the components and confirmed that Cr and Al(Si) showed the desired alloy composition. A solder ball was additionally fabricated to fabricate the reflow samples. We then measured the melting point and hardness to evaluate the basic properties of the fabricated solder alloy.

2.2 Experimental procedures

2.2.1 Fabrication of Sn-Cu-Cr alloy

Pure Sn (99.9 %), Cu (99.9 %), and Cr (99.9 %) were used to prepare a parent alloy, and the amount of Cr was controlled at 0.2 wt.%. Because these three elements have different densities and specific gravities, problems may occur during the casting process. Thus, more precise compositional control is required. First, to prepare a Sn-Cu alloy, pure Sn and Cu were dissolved at 500 ℃ in a vacuum furnace filled with argon gas, and further cooled in air. The Sn-Cu alloy and Cr were then dissolved together. The alloy was heated to 1,100 ℃ and mixed thoroughly for 20 min. The alloy was then cooled to 600 ℃, and then subsequently air cooled to 50 ℃, the heat treatment profile of which is shown in **Figure 2.1**. After the alloying procedure, the molten solder in the crucible was homogenized at 600 ℃ for 1 h. The chemical composition of the prepared alloy was analyzed using Inductively Coupled Plasma Spectrometer (ICP) and the results are shown in **Table 2.1**.

2.2.2 Fabrication of Sn-Cu-Al(Si) alloy

Pure Sn (99.9 %), Cu (99.9 %) and 0.01–0.05 wt.% Al(Si) alloy were used as raw materials. The Al contents was controlled in the range of the ppm level. Pure Al has poor machinability to weight and alloy during the casting process. Here, the commercial Al alloy 4047 (MKE Co., Ltd) was selected to easily alloy minor Al(Si) contents due to its high machinability. In addition, it decreases the alloying cost and reliability issue together with eliminating the use of Ag. First, pure Sn and Cu were melted at 500 ℃ to produce Sn-0.7Cu alloy in a vacuum furnace charged with argon gas, and cooled in air. Then, Sn-0.7Cu alloy and Al(Si) alloy were melted together. The profile of the heat treatment is shown in **Figure 2.1**. The alloy was heated to 900 ℃ and melted completely and mixed for 20 min. Then, the alloy was furnace-cooled down to 600 ℃ and air-cooled down to 50 ℃ sequentially. After the alloying procedure, the molten solders in the crucible were homogenized at 600 ℃ for 1 h. Four systematic solder alloys were produced: the Sn-0.7Cu reference alloy, together with Sn-0.7Cu-0.01Al(Si), Sn-0.7Cu-0.03Al(Si) and Sn-0.7Cu-0.05Al(Si). The chemical compositions of the produced alloys were analyzed using Inductively Coupled Plasma Spectrometer (ICP) and the results are shown in **Table 2.1**.

Table 2.1 Composition of solder alloy with minor Cr and Al(Si).

Solder alloy	Cu (wt. %)	Cr (wt. %)	Al (wt. %)	Si (wt. %)
Sn-Cu-0.2Cr	0.6640	0.1750	-	-
Sn-Cu-0.01Al(Si)	0.6527	-	0.0140	0.0014
Sn-Cu-0.03Al(Si)	0.6620	-	0.0307	0.0030
Sn-Cu-0.05Al(Si)	0.6857	-	0.0473	0.0056

Table 2.2 Results of wetting balance test.

Solder alloy	Wetting time(sec)	Wetting force(mN)
Sn-Cu	2.71	5.81
Sn-Cu-0.2Cr	2.82	5.13
Sn-Cu-0.01Al(Si)	2.81	5.26
Sn-Cu-0.03Al(Si)	2.55	5.58
Sn-Cu-0.05Al(Si)	2.54	4.63

2.2.3 Sample preparation for evaluation of basic properties

The master alloys were made by induction heating in a high-vacuum argon atmosphere. Then, solder balls with diameters of 300 μm were fabricated. The test modules were fabricated by reflow process with the solder balls. As shown in **Figure 2.2**, the sample was prepared by extruding alloys with punching. To measure the melting temperatures of the three solder materials, differential scanning calorimetry (DSC, Perkin-Elmer, Inc, TA Q10) analysis was performed. Approximately 8 mg samples of the three solder alloys were used for the DSC analysis. The measurement was carried out in three steps. First, the sample temperature was stabilized at 50 °C, and then it was increased up to 300 °C at a rate of 10 °C/min. Finally, the temperature was cooled down to 100 °C at a rate of 10 °C/min to check the heat flow and analyze the endothermic and exothermic reactions. The hardness of the trace elements added alloys was measured using a vicker’s hardness tester (Mitutoyo, Inc, HM-210A).

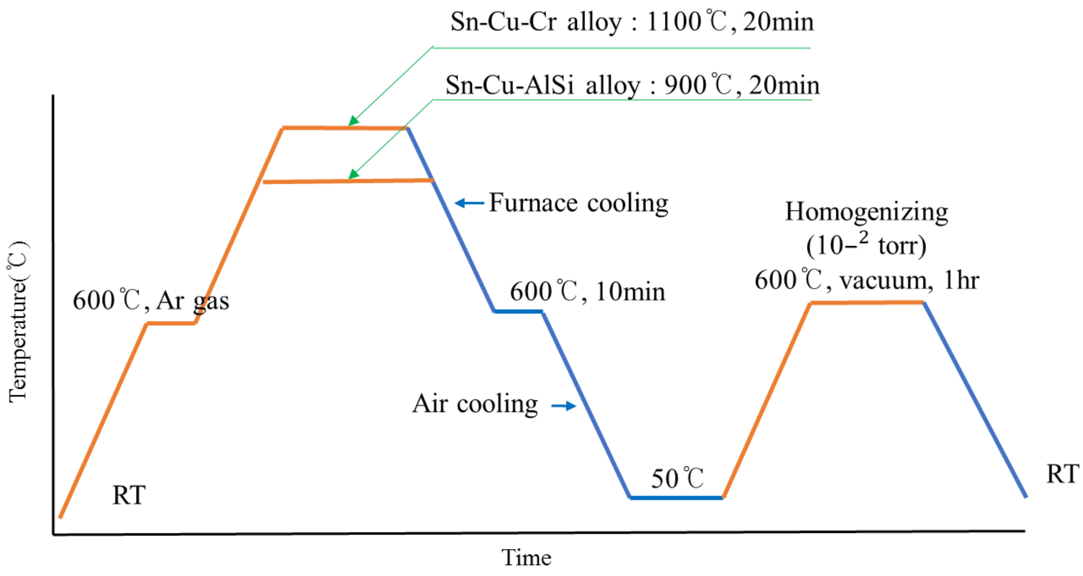

Figure 2.1 Temperature profile of Sn-based solder with added Cr and Al(Si).

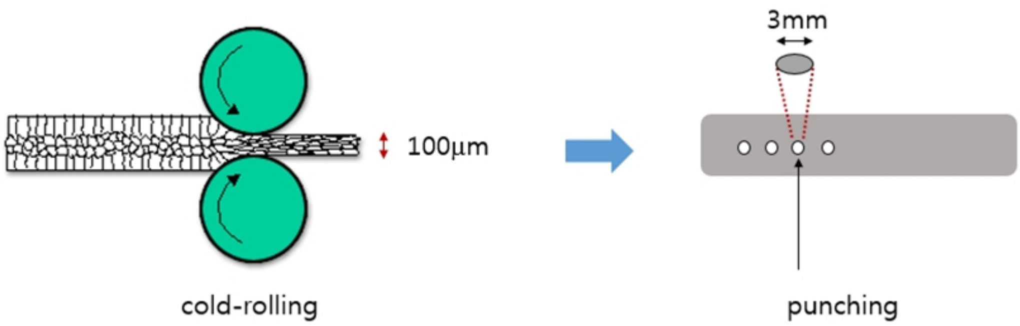

Figure 2.2 Schematic diagram of cold-rolling and punching.

2.3 Results and discussion

2.3.1 Melting behavior

As is well known, the melting point of Sn-Cu eutectic composition is 227 °C [12,13] and SAC305 is 217 °C [14,15]. The addition of Cr and Al(Si) to Sn-Cu resulted in 3 to 4 °C increase in melting temperature due to reduction of under-cooling. DSC curves for each alloy are shown in **Figure 2.3** and **Figure 2.4**.

2.3.2 Wetting Characteristics

To quantitatively evaluate wettability, the wetting force and wetting time of the alloys were measured using the wetting balance method. The 0.2 wt.% of Cr-added solder showed slightly lower wettability than the Sn-Cu solder. Similar wettability was seen with 0.01 wt.% and 0.03 wt.% of Al(Si) doping, and rather decreased at 0.05 wt.% **(Table 2.2)**. In addition, the 0.05 wt.% of Al(Si) composition caused a problem of deteriorating the fluidity of the alloy and of increasing oxidation properties in the remelting process for the fabrication of solder balls. Therefore, this study evaluated the compositions of 0.01 wt.% and 0.03 wt.%, excluding 0.05 wt.%.

The spreadability evaluation of the solder through the contact angle measurement can be expressed by the following formula [16]. (JIS Z 3197 Standard):

$$\mathrm{S} = \frac{D-H}{D} \times 100 \quad \cdots\cdots \quad (2.1)$$

where S is the rate of solder spreading, H is the height of spread solder, and D is the diameter when the solder used is assumed to be a sphere. $1.2407V^{1/3}$ is thus applied, where V is the mass/specific gravity. **Figure 2.5** is a result of measuring the wetting angle of Sn-Cu-Cr and Sn-Cu-Al(Si) using a contact angle tester. As a result, Sn-Cu-Cr and Sn-Cu-Al(Si) were 81 % and 83 %, respectively, exhibiting slightly higher spreadability in the Al(Si) added solder.

2.3.3 Microstructure and hardness

After solidification, the solder matrix is composed of β-Sn dendrites, eutectic areas, and some large precipitated IMC [17,18]. **Figure 2.6 and 2.7** shows the typical microstructures of the as-solidified Sn-Cu alloys. Initial microstructures are composed of β-Sn regions surrounded by eutectic networks with spherical Cu_6Sn_5 IMC particles. However, with the increasing Cr and Al(Si) content, refined eutectic β-Sn + Cu-Sn IMC networks were observed **(Figure 2.6, 2.7)**. Although the trace element content was very small, the Cr and Al(Si) effectively disturbed the formation of the eutectic β-Sn + Cu-Sn IMC networks. Because of the small amount of additions, Cr and Al(Si) could not be observed the IMC particles or precipitation using SEM. Therefore, observations of Cr and Al(Si) using STEM are described in Chapters 3 and 4, respectively.

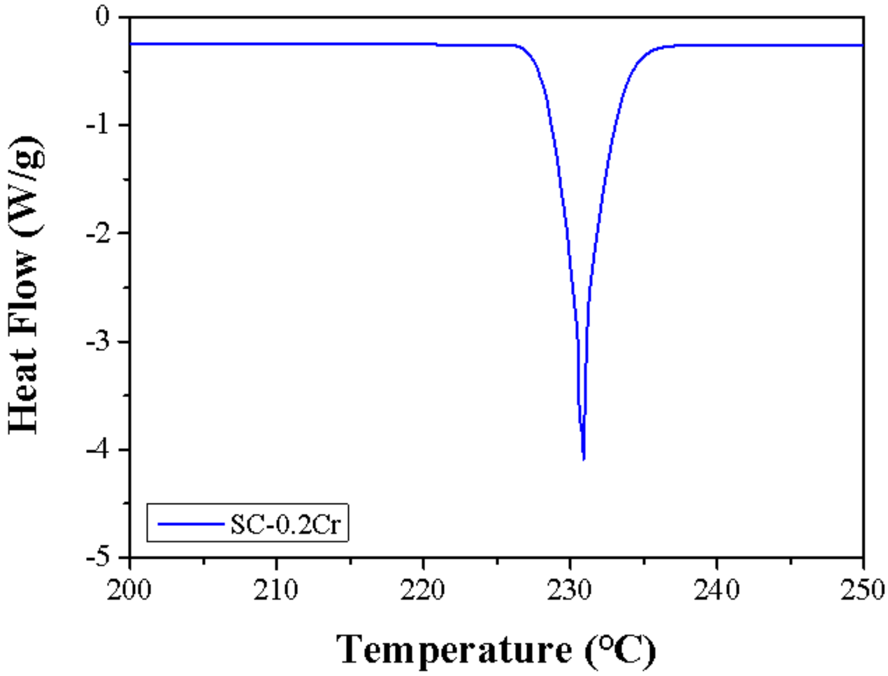

Figure 2.3 DSC curve of Sn-Cu-0.2Cr solder.

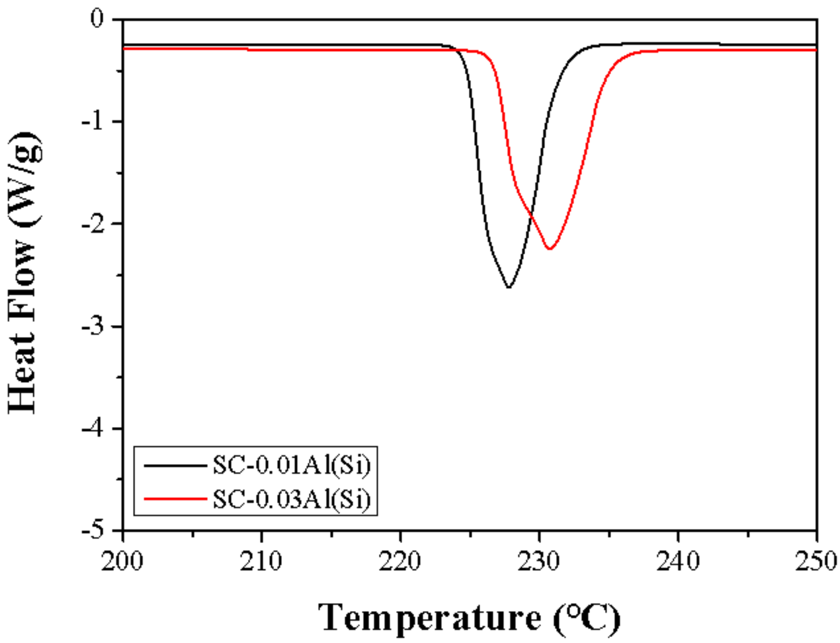

Figure 2.4 DSC curve of Sn-Cu-0.01Al(Si) and Sn-Cu-0.03Al(Si) solder.

(a) (b)

Figure 2.5 Images of contact angle after spread: (a) Sn-Cu-0.2Cr (b) Sn-Cu-0.03Al(Si).

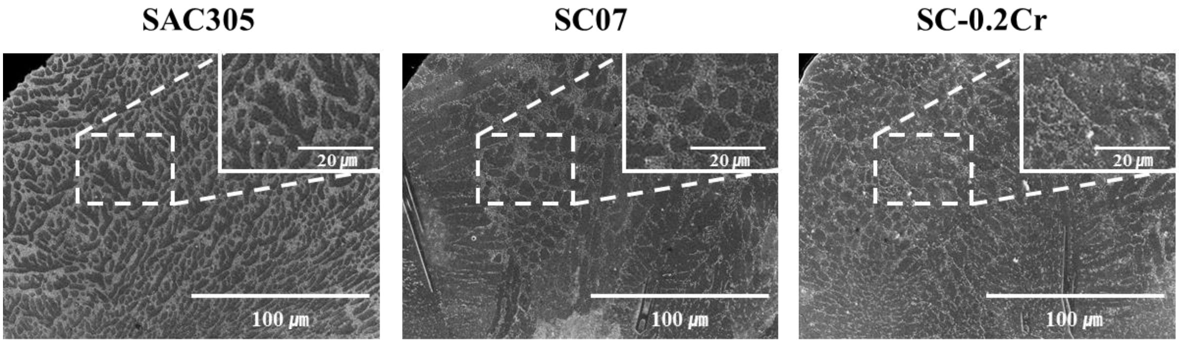

Figure 2.6 Microstructure of SAC305, Sn-0.7Cu and Sn-Cu-0.2Cr.

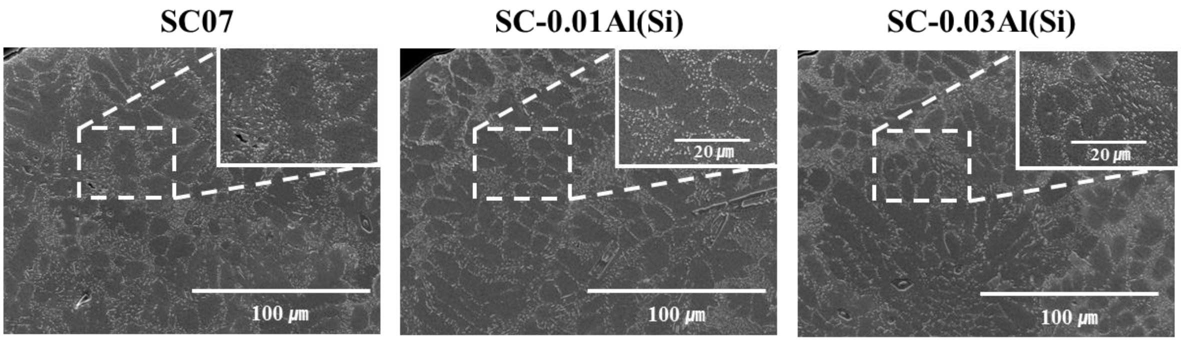

Figure 2.7 Microstructure of Sn-Cu, Sn-Cu-0.01Al(Si) and Sn-Cu-0.03Al(Si).

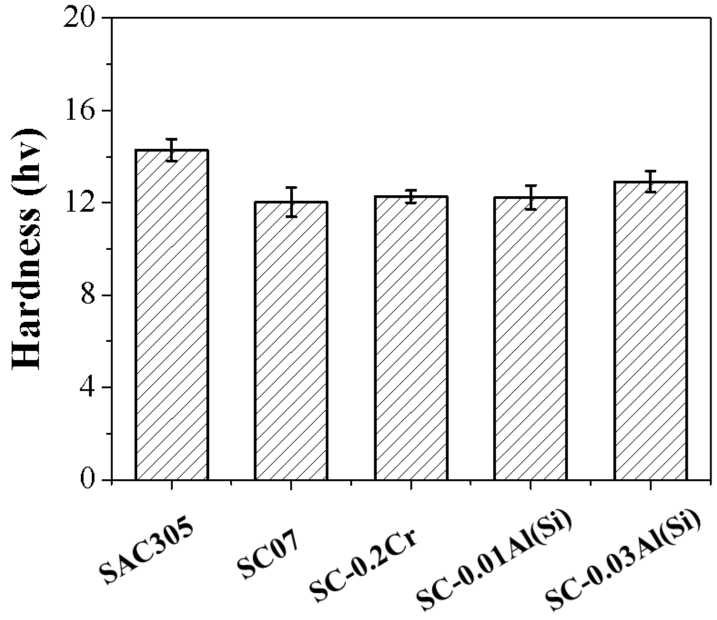

Figure 2.8 Hardness of SAC305, Sn-07Cu, Sn-Cu-0.2Cr, Sn-Cu-0.01Al(Si) and Sn-Cu-0.03Al(Si).

In case of SAC305, during soldering, Cu and Ag are dissolved in solder matrix, and due to the great difference in solubility, they precipitate during cooling in the form of Ag_3Sn and Cu_6Sn_5 IMC, dispersing in solder matrix to form eutectic areas, as shown in **Figure 2.6 and 2.7**. Because these IMC is much harder than the solder matrix, these dispersed IMC could act as second-phase particles to pin the dislocation and block the crack propagation generated in shear test process, therefore enhancing the joint strength. It is known that more IMC exist in SAC305 solder than that in SC07 and SC-Cr solders. Correspondingly, **Figure 2.8** shows the SAC305 solder exhibited higher hardness and strength than the other two solders in the case of a low shear speed.

2.4 Conclusion

In order to improve the properties of the Sn-Cu eutectic solder, alloys containing Cr and Al(Si) were prepared. The alloys were produced using a vacuum induction furnace; the content of Cr was 0.2 wt.% and the content of Al(Si) was 0.01 wt.% to 0.05 wt.%. The alloys were then fabricated in the form of solder balls for reflow samples. The melting point of the alloy doped with Cr and Al(Si) was approximately 230 °C, approximately 3 °C higher than that of the Sn-Cu eutectic alloy. The wettability evaluation using the wetting balance method showed similar wetting characteristics to the Sn-Cu eutectic alloy. In the spreadability evaluation using the contact angle test, Al(Si) was slightly higher than Cr. For the microstructure of the solder, the β-Sn + Cu-Sn IMC networks were observed to be effectively dispersed after the addition of Cr and Al(Si). Hardness was similar to the Sn-Cu eutectic and lower than SAC305. SAC305 showed the highest initial hardness as Ag_3Sn was finely dispersed.

2.5 Bibliography

[1] Gain, A.K.; Zhang, L. "Microstructure, thermal analysis and damping properties of Ag and Ni nano-particles doped Sn–8Zn–3Bi solder on OSP-Cu substrate" J. Alloy. Compd. 617 (2014) 779–786.

[2] Zhang, S.; Yang, M.; Wu, Y.; Du, J.; Lin, T.; Peng, H.; Huang, M.; Paik, K.W. "A study on the optimization of anisotropic conductive films for Sn-3Ag-0.5Cu-Based flex-on-board application at a 250 ℃ bonding temperature" IEEE Trans. Comp. Pack. Manuf. 8 (2018) 1–9.

[3] Fouzder, T.; Li, Q.; Chan, Y.; Chan, D. "Interfacial microstructure and hardness of nickel (Ni) nanoparticle-doped tin-silver-copper (Sn-Ag-Cu) solders on immersion silver (Ag)-plated copper (Cu) substrates" J. Mater. Sci. Mater. Electron. 25 (2014) 4012–4023.

[4] Chen, X.; Zhou, J.; Xue, F.; Bai, J.; Yao, Y. "Microstructures and mechanical properties of Sn-0.1Ag-0.7Cu-(Co, Ni, and Nd) lead-free solders" J. Electron. Mater. 44 (2015) 725–732.

[5] Chen, X.; Hu, A.; Li, M.; Mao, D. "Effect of a trace of Cr on intermetallic compound layer for tin–zinc lead-free solder joint during aging" J. Alloy. Compd. 470 (2009) 429–433.

[6] Bi, J.; Hu, A.; Hu, J.; Luo, T.; Li, M.; Mao, D. "Effect of Cr additions on interfacial reaction between the Sn–Zn–Bi solder and Cu/electroplated Ni substrates" Microelectron. Reliab. 51 (2011) 636–641.

[7] Zhang, L.; Tu, K.N. "Structure and properties of lead-free solders bearing micro and nano particles" Mater. Sci. Eng. R Rep. 82 (2014) 1–32.

[8] Yakymovych, A.; Plevachuk, Y.; Švec, P., Sr.; Švec, P.; Janičkovič, D.; Šebo, P.; Janičkovič, D.; Šebo, P.; Beronská, N.; Roshanghias, A.; etc. "Morphology and shear strength of lead-free solder joints with $Sn_{3.0}Ag_{0.5}Cu$ solder paste reinforced with ceramic nanoparticles" J. Electron. Mater. 45 (2016) 6143–6149.

[9] Xing, W.Q.; Yu, X.Y.; Li, H.; Ma, L.; Zuo, W.; Dong, P.; Wang, W.X.; Ding, M. "Effect of nano Al_2O_3 additions on the interfacial behavior and mechanical properties of eutectic Sn-9Zn solder on low temperature wetting and soldering of 6061 aluminum alloys" J. Alloy. Compd. 695 (2017) 574–582.

[10] J.H. Koo, J.W. Chang, Y.W. Lee, S.J. Hong, K.S. Kim, H.M. Lee, "New Sn–0.7Cu-based solder alloys with minor alloying additions of Pd, Cr and Ca" J. Alloys Compd. 608 (2014) 126–132.

[11] Hong, W.S.; Oh, C.; Kim, M.S.; Lee, Y.W.; Kim, H.J.; Hong, S.J.; Moon, J.T. "Al and Si alloying effect on solder joint reliability in Sn-0.5Cu for automotive electronics" J. Electron. Mater. 45 (2016) 6150–6162.

[12] R.A. GAGLIANO, G. GHOSH, and M.E. FINE, "Nucleation Kinetics of Cu6Sn5 by Reaction of olten Tin with a Copper Substrate" Journal of ELECTRONIC MATERIALS, 31 (2002) 1195–1202.

[13] M.S. Park a, R. Arro´yave "Concurrent nucleation, formation and growth of two intermetallic compounds (Cu6Sn5 and Cu3Sn) during the early stages of lead-free soldering" Acta Materialia 60 (2012) 923–934.

[14] Ali Roshangias, Jan Vrestal, Andriy Yakymovych, Klaus W. Richter, Herbert Ipser "Sn–Ag–Cu nanosolders : Melting behavior and phase diagram prediction in the Sn-rich corner of the ternary system" CALPHAD: Computer Coupling of Phase Diagrams and Thermochemistry, 49 (2015) 101–109.

[15] Hiren R. Kotadia, Philip D. Howes, Samjid H. Mannan "A review: On the development of low melting temperature Pb-free solders" Microelectronics Reliability, 54 (2014) 1253–1273.

[16] Japanese Industrial Standard (JIS) Z 3197:8.3.1.1 "Test methods for soldering fluxes" Japanese Standards Association (JSA), 2012

[17] Yang, M.; Cao, Y.; Joo, S.; Chen, H.; Ma, X.; Li, M. "Cu_6Sn_5 precipitation during Sn-based

solder/Cu joint solidification and its effects on the growth of interfacial intermetallic compounds" Journal of Alloys and Compounds, 582 (2014) 688–695.

[18] Yang, M.; Ko, Y.-H.; Bang, J.; Kim, T.-S.; Lee, C.-W.; Li, M. "Effects of Ag addition on solid–state interfacial reactions between Sn–Ag–Cu solder and Cu substrate" *Mater. Charact.* 124 (2017) 250–259.

Chapter 3
Interfacial reactions and mechanical properties of SC-Al(Si)/Cu solder joint

3.1 Introduction

In this chapter, the eco-friendly Sn-0.7Cu-(0.01, 0.03 wt%)Al(Si) solder composition with a melting point of 230 °C was developed as a highly reliable joint material, and its thermal reliability and the characteristics of the joint were analyzed according to the Al(Si) content. Moreover, the inside of the solder was analyzed and the joint interface response was observed to evaluate the applicability of the developed solder as a high-temperature joint material for automotive electronic components.

3.2 Experimental procedures

3.2.1 Fabrication of solder joint sample

The solder joint samples were fabricated by reflow process with the solder balls. The substrate material of test module was FR4 PCB, and the metal pad was Cu with an organic solderability preservative (OSP) surface finish. **Figure 3.1** shows the schematic illustration of the assembling process for the solder ball mount sample. The thickness of the OSP layer was approximately 0.3 μm. The size of Cu opening pad was approximately 230 μm, and its thickness was about 20 μm. To avoid oxidation during the reflow process, flux was coated on the Cu pad. The reflow process was carried out by using an infrared 9-zone reflow machine. The conditions of reflow process are shown in **Table 3.1.** The peak temperatures of the Sn-0.7Cu and Sn-0.7Cu-Al(Si) solders were 255 and 260.5 °C, respectively. After the reflow process, the test samples were cooled to room temperature in air. **Figure 3.2** shows the schematic graph of the reflow profile for the Sn-0.7Cu-Al(Si) solder. **Figure 3.3** shows the image of actual soldering sample after reflow process.

3.2.2 Multiple reflow processes

Because a solder joint is typically exposed to a multi-reflow process owing to the characteristics of the manufacturing of the electronic component module, the characteristics of the solder joint were evaluated by repeating the reflow process up to 10 times. For the interfacial reaction, the reflow process was performed for 40 s above 227 ℃, the melting temperature of Sn-Cu-Al(Si), with a peak temperature of 260.5 ℃ in a N_2 atmosphere in a reflow oven (1809EXL; Heller, Florham Park, NJ, USA).

3.2.3 Analysis of interfacial reaction and IMC growth

The microstructure of the IMC was observed using scanning electron microscopy (SEM, Hitachi S-4700) and energy dispersive X-ray spectroscopy (EDX, EDAX Genesis XM2 60). For the cross-sectional observations, the reflowed samples were polished with SiC paper and an Al_2O_3 polishing solution and then etched with a solution of 95 % C_2H_5OH−3 % HNO_3−2 % HCl (in vol %). To further observe the thermal stress, the thickness and microstructure of the IMC were measured using cross-sectional images according to the following procedure [1]: (i) an SEM image of each sample was obtained at the appropriate magnification, (ii) the grayscale SEM image was enhanced using Adobe Photoshop to identify the interfaces between the different layers, and (iii) the mean thickness (H_{IMC}) of the individual layers was calculated using the following equation:

$$H_{IMC}=H_{SEM}\times N_{IMC}/N_{SEM} \quad \text{.....................} \quad (3.1)$$

Where H_{SEM} is the actual height of the SEM image, and N_{IMC} and N_{SEM} are the numbers of pixels in the IMC layers and the entire image, respectively. In addition, top-view images of the interface were obtained by deep-etching the samples with a solution of 10% HNO_3–90 % deionized water (vol. %).

Table 3.1 Reflow conditions for each solder.

Solder	Pre-heating Time(s)	Duration time above melting temperature(s)	Peak reflow temperature(°C)
Sn-0.7Cu	73	47	255
Sn-0.7Cu-Al(Si)	73	47	260.5

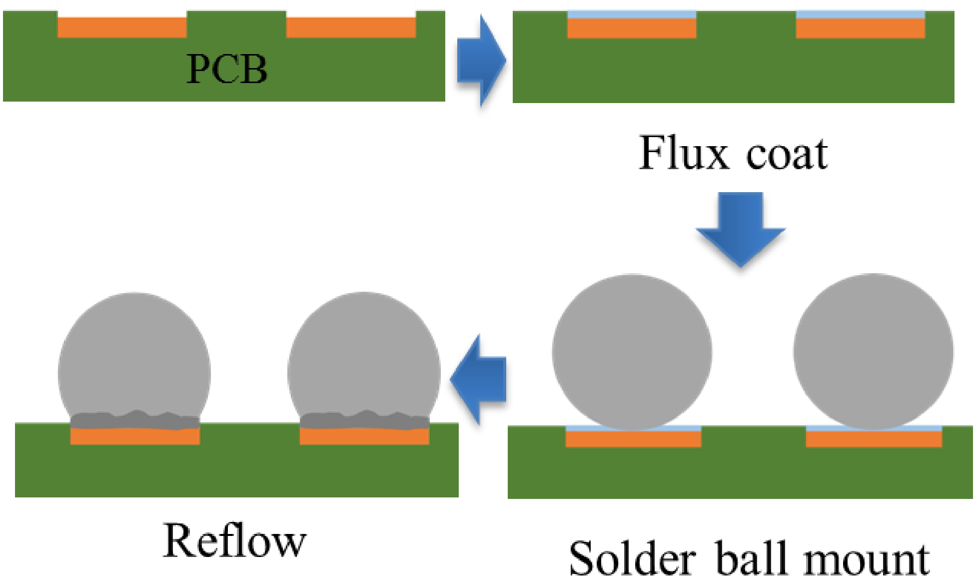

Figure 3.1 Fabrication of ball mount sample.

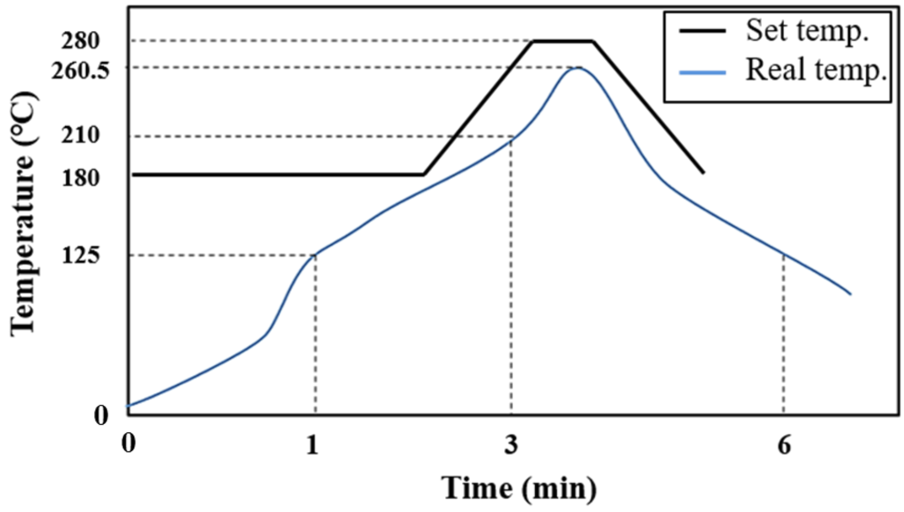

Figure 3.2 Reflow temperature profile for Sn-Cu-Al(Si) solder.

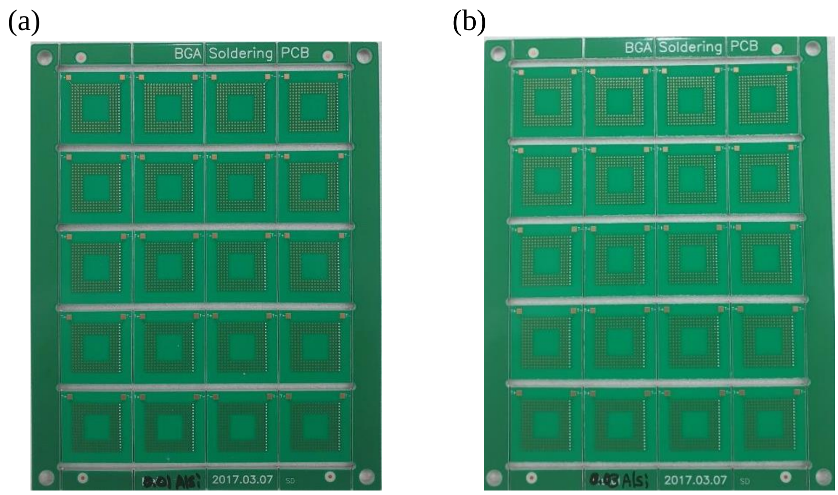

Figure 3.3 Images of actual sample for (a)Sn-Cu-0.01Al(Si) and (b)Sn-Cu-0.03Al(Si) after reflow.

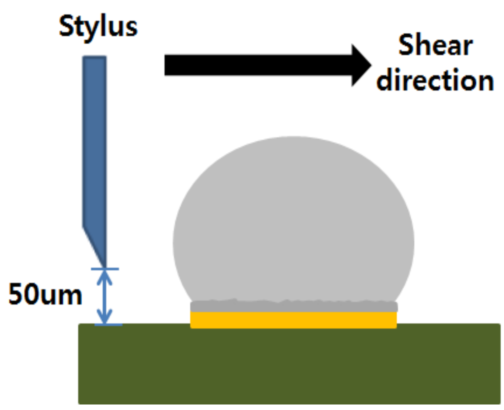

Figure 3.4 Schematic illustration of solder ball shear test.

3.2.4 Evaluation of mechanical properties

To evaluate the mechanical properties of solder joints after thermal storage and multiple reflows, ball shear tests were conducted at shear heights of 50 μm with shear speeds of 0.01, 0.1, and 1 m/s using a bonding tester (PTR-1101, Rhesca Co.). **Figure 3.4** showed Schematic illustration of solder ball shear test. The shear force value was estimated based on the average of 20 trials or more. After shear testing, the fracture surfaces were observed in top and cross-section views using SEM.

3.2.5 Isothermal aging

Electric furnace was used for isothermal aging, and the temperatures was 100 °C, 125 °C, and 150 °C. And then the IMC growth and mechanical properties of the interface was observed after aging and multi-reflow (1809EXL; Heller, Florham Park, NJ, USA).

3.3 Results and discussion

3.3.1 IMC formation and growth under various thermal aging conditions

Figures 3.5 – 3.7 show the IMC growth kinetics of SC-0.01Al(Si) and SC-0.03Al(Si) solders during isothermal aging. Previous studies suggest that adding approximately 1 wt.% of Al to the Sn-base solder inhibits the growth of IMC and increases its mechanical strength [2,3]. With As-reflow, the solders with Al(Si) added showed the reduced total IMC thickness in comparison to SC07/Cu. This difference was most pronounced at temperatures of 100 °C and 125 °C. At 150 °C however, all three systems did not show any large differences. This is attributed to the accelerated interdiffusion of Sn and Cu due to the formation of Cu_6Sn_5 micro grains on the interface, which is further expected to be emphasized at higher temperatures [4,5]. Furthermore, increased aging duration results in the formation of Kirkendall voids at the interface of the Cu substrate and Cu_3Sn [6–10]. The three systems did not show any noticeable differences of this phenomenon. **Figures 3.8 – 3.10** show the changes in the IMC thickness with respect to duration at different aging temperatures.

The initial total IMC thickness at all aging temperatures was 2 to 3 μm. As the aging time increased, the total IMC thickness increased due to the growth of the IMC; the growth rate increased with increasing temperature. There was no large difference in Cu_3Sn thickness between the SC07/Cu and SC-Al(Si)/Cu joint. While Cu_6Sn_5 was slightly thinner in the SC-Al(Si)/Cu joint than the SC07/Cu joint at 100°C and 125°C, at 150℃, no difference was measured. One characteristic is that the Cu_6Sn_5 IMC did not show much growth after aging, whereas the rapid diffusion of Cu greatly accelerated the growth of Cu_3Sn. As a result, under aging, compared to the Cu_6Sn_5, the growth of Cu_3Sn led to the growth of the total IMC, results similar to that observed in the SC-Cr/Cu joint in *Chapter 4*.

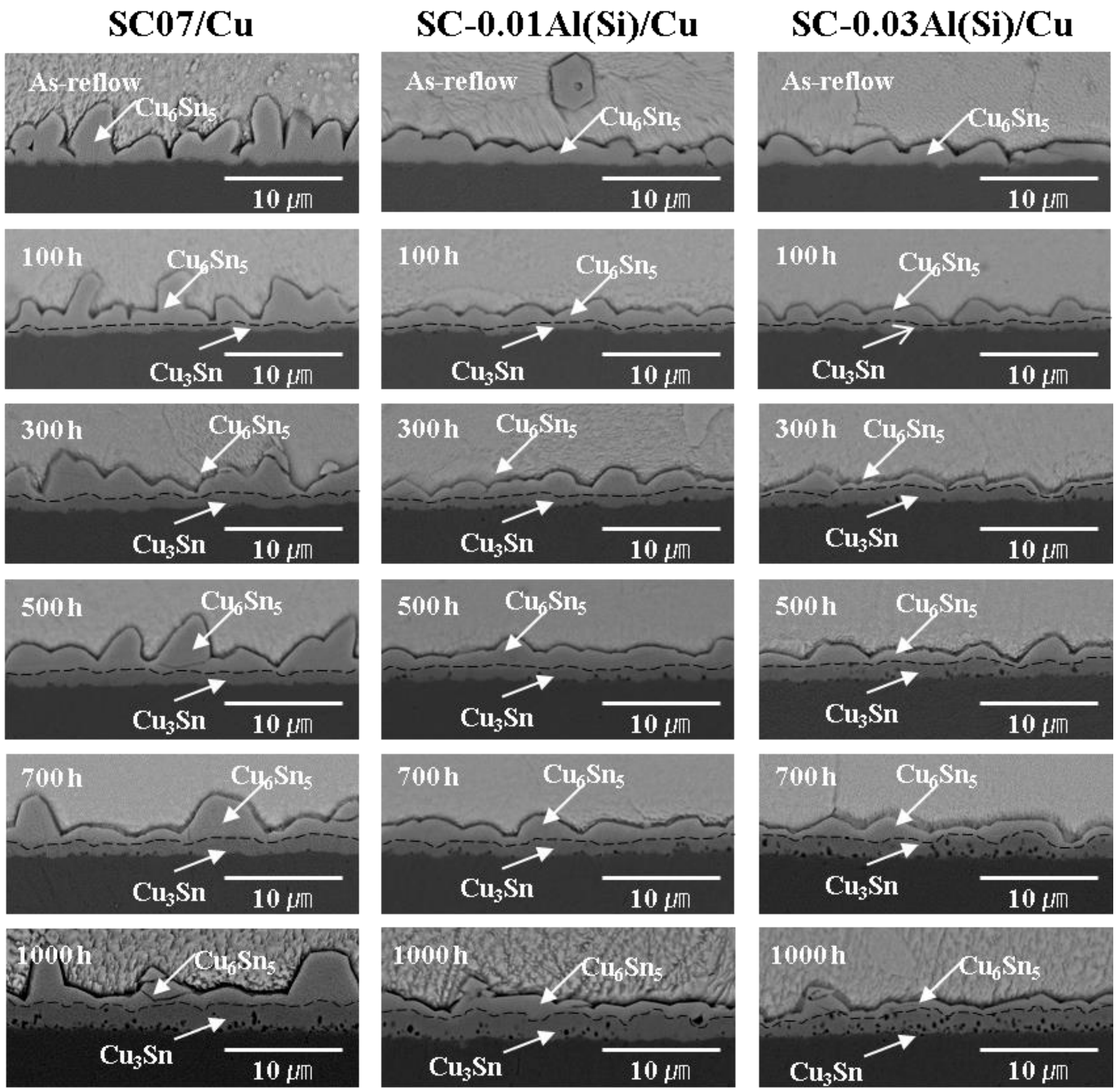

Figure 3.5 Cross-sectional microstructures of solder joints during isothermal aging at 100 °C.

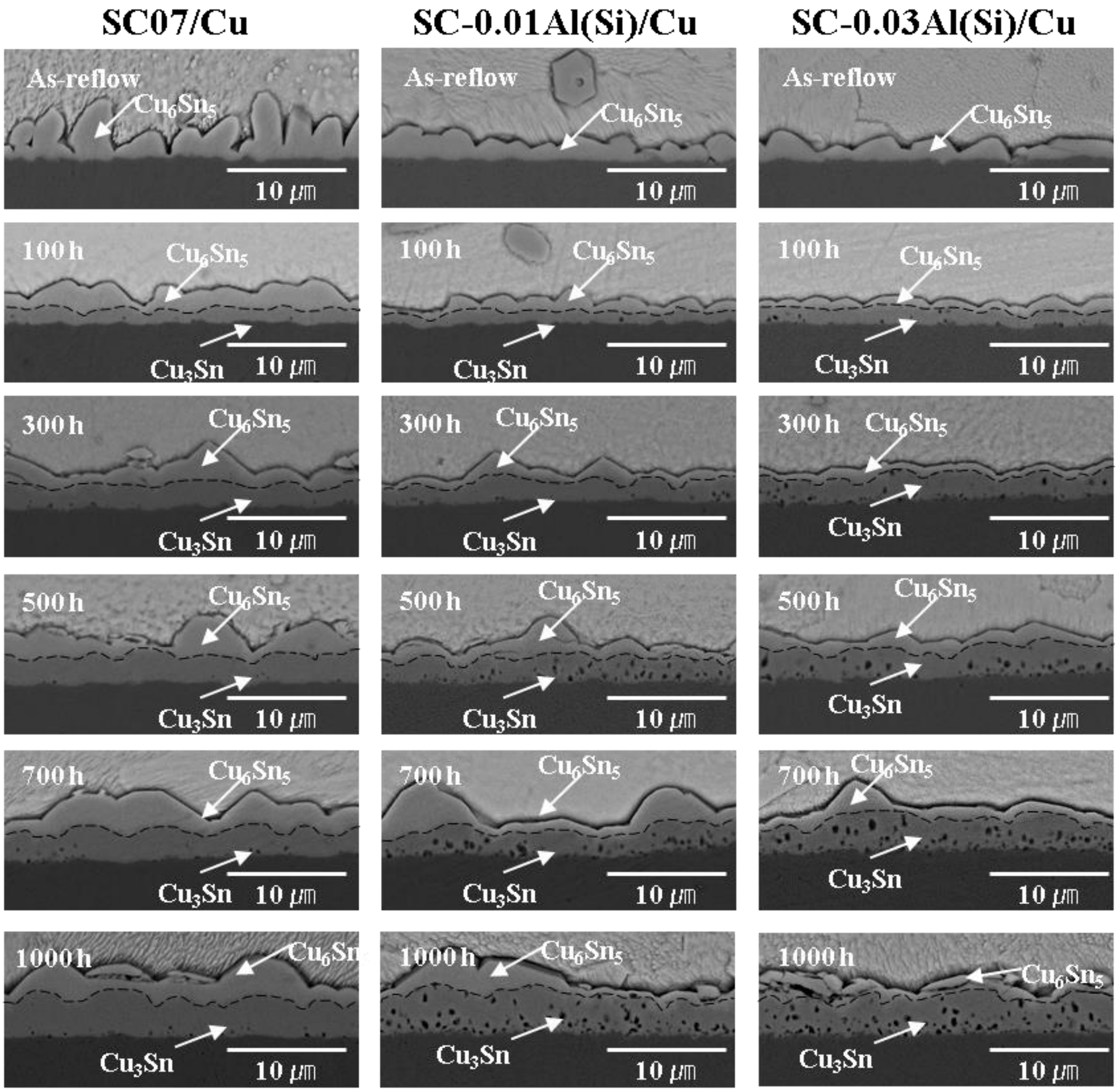

Figure 3.6 Cross-sectional microstructures of solder joints during isothermal aging at 125 °C.

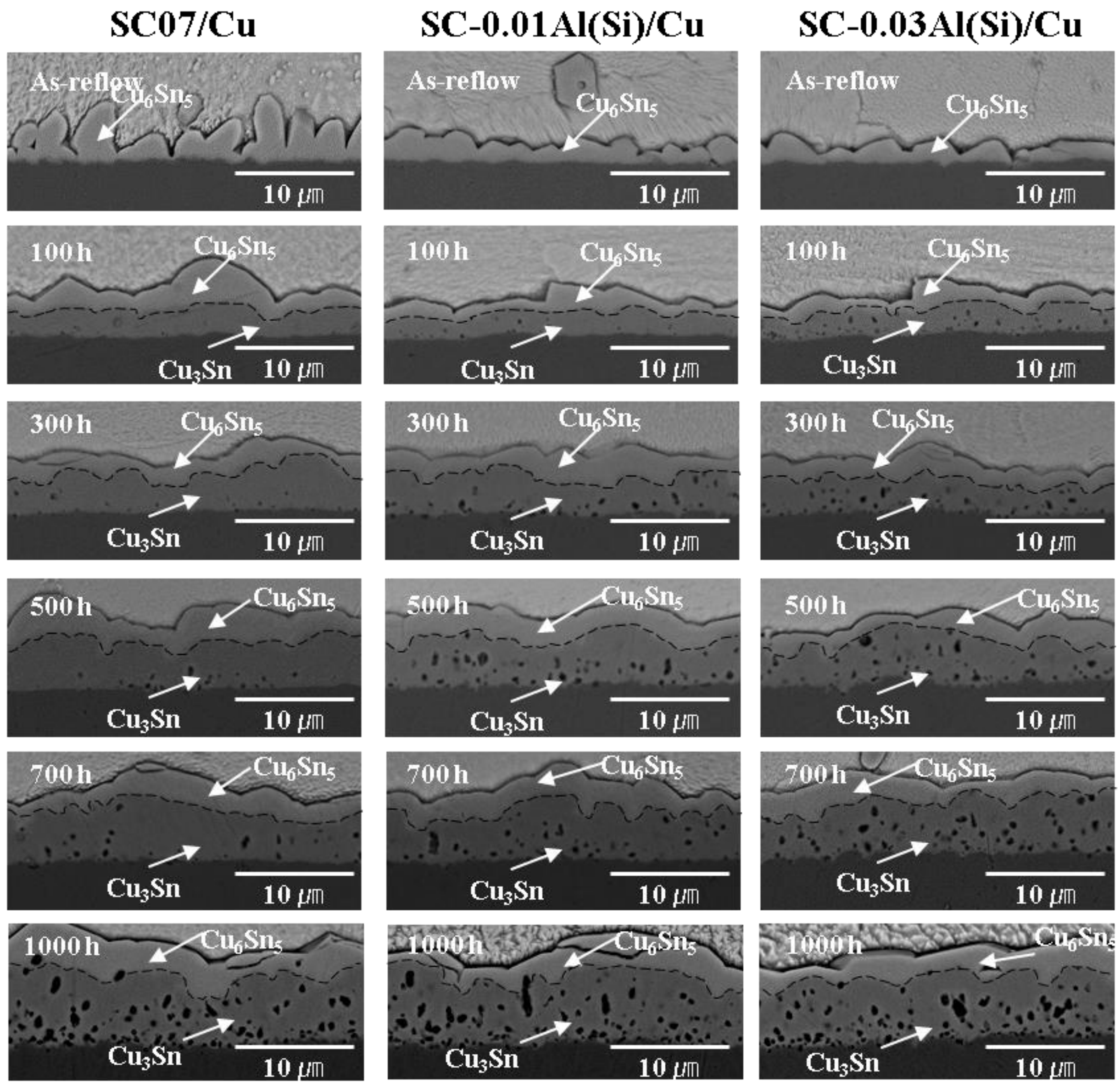

Figure 3.7 Cross-sectional microstructures of solder joints during isothermal aging at 150 °C.

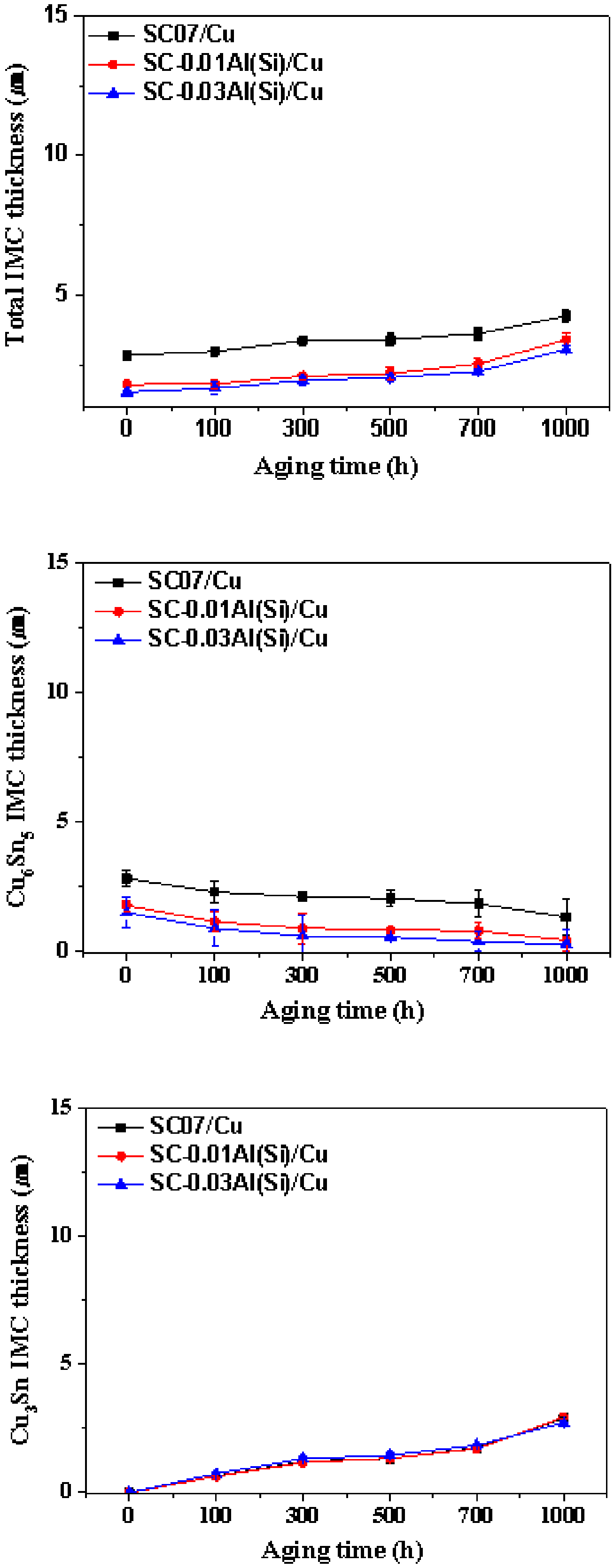

Figure 3.8 IMC thickness of interfacial IMC during isothermal aging at 100 °C.

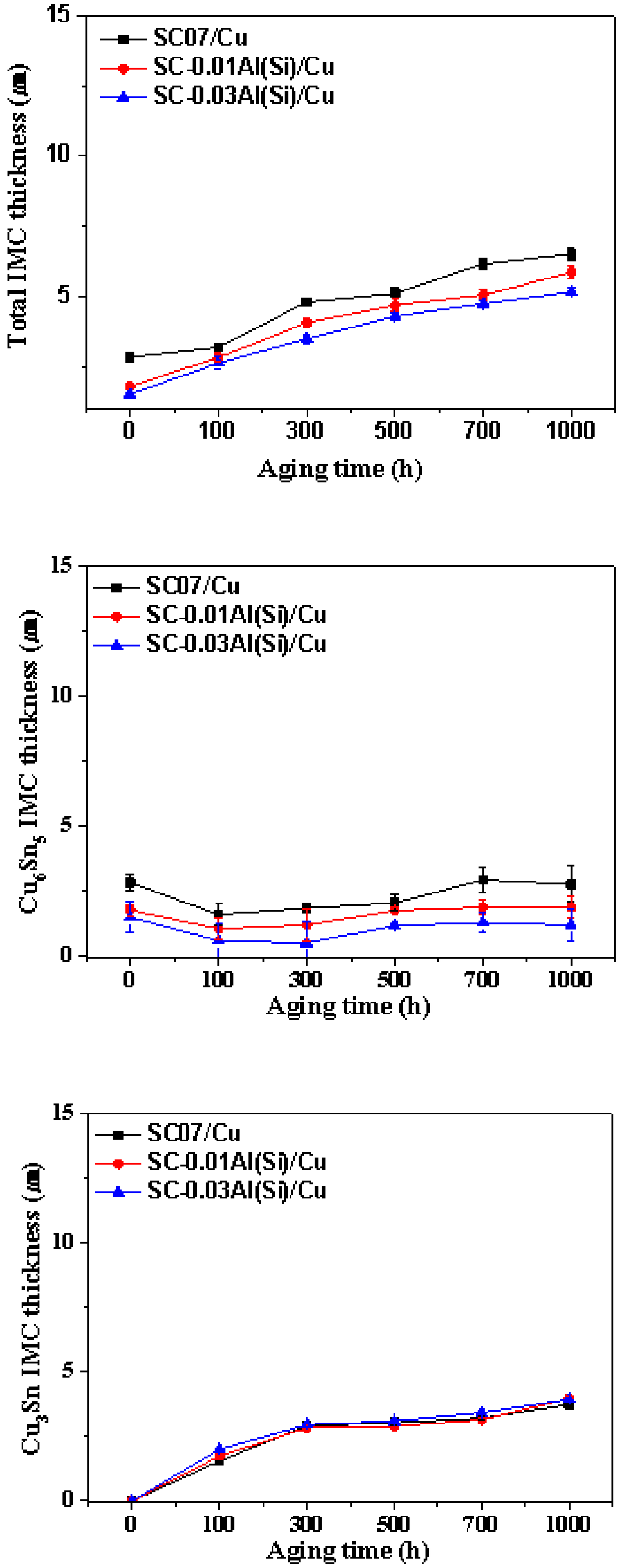

Figure 3.9 IMC thickness of interfacial IMC during isothermal aging at 125 °C.

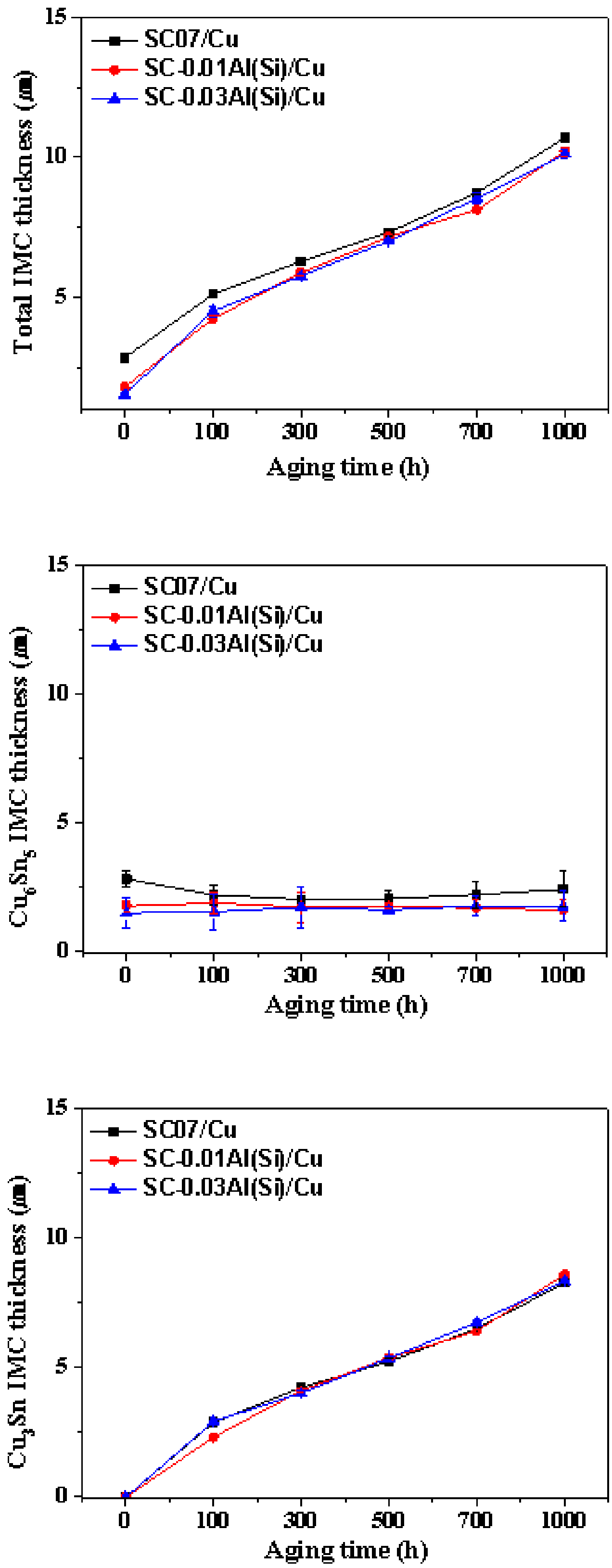

Figure 3.10 IMC thickness of interfacial IMC during isothermal aging at 150 °C.

3.3.2 IMC formation and growth under multi-reflow conditions

Figure 3.11 show the IMC growth kinetics of SC-0.01Al(Si) and SC-0.03Al(Si) solders during multi-reflow. Compared to the SC07/Cu joints, the SC-Al(Si)/Cu joints showed thinner initial IMC thicknesses. The growth rate, which is dependent on the number of reflows, was also shown to be slower. This is in agreement with studies that suggest adding Al to Sn-based solders inhibits the IMC growth in multi-reflow environments [11]. Furthermore, the shape of IMC layer changed from an initial scallop shape to a flat shape. The thickness of Cu_3Sn did not differ among the three systems, suggesting that the total IMC thickness is solely dependent on the growth of Cu_6Sn_5.

Previous studies have demonstrated that diffusion through Cu_6Sn_5 grain boundaries is much faster in liquid solder/solid copper reactions than in solid solder/solid copper reactions [12,13]. Multiple reflow is a liquid/solid reaction and isothermal aging is a solid/solid reaction. Therefore, the IMC growth rates should be compared in different reaction systems. The initial total IMC thickness was thinner in the SC-Al(Si)/Cu joint than the SC07/Cu joint in both reaction systems. In addition, in isothermal aging, the SC-Al(Si)/Cu joint showed a total IMC thickness of approximately 4 μm at approximately 700 hours and 125 °C and at 100 hours and 150 °C. However, in multi-reflow, the thickness grew to 4 μm after only 10 cycles. Ten reflow cycles corresponds to approximately 1 hour. As a result, in all systems, multi-reflow (liquid/solid reaction) showed a much faster diffusion rate than isothermal aging.

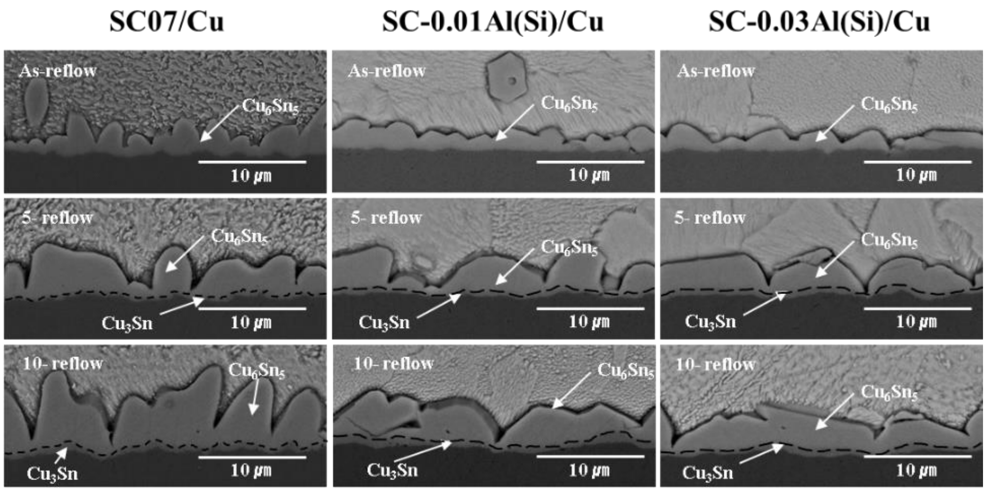

Figure 3.11 Cross-sectional images at the interface during multi-reflow process.

3.3.3 Shear strength of solder joint and fracture mode

Basically, the shear strength of the solder joint is affected by the solder material and the surface properties. Ductile failure occurs when the strength of the solder is lower than the strength of the interface, whereas brittle failure occurs when the strength of the solder is higher than the strength of the interface [14]. To evaluate the effects that the Al(Si) had on the internal structures of the solder and the interface, the shear strength was measured at various shear speeds. **Figures 3.12 – 3.14** show the shear strength with respect to shear speed during aging. Due to the IMC thickness and Kirkendall voids, the shear strength did not vary much among the three systems. With post multi-reflow, however, higher shear strengths were observed at shear speeds greater than 0.1 m/s for SC-0.01Al(Si) and SC-0.03Al(Si) joints in comparison to SC07/Cu. **Figure 3.15** shows the shear strength measurements with respect to shear speeds.

Figure 3.16 shows the results of fracture surface analysis after shear-strength measurements according to multi-reflow. At lower speeds (0.01 m/s), all the joint systems underwent ductile failure in the solder. At speeds of 0.1 m/s or more, an increased number of brittle failures were observed. This is attributed to the brittle nature of the thick IMC layer formed at the interface, which displays lower strengths at higher shear speeds where the shear stress is concentrated at the interface [15].

(a)

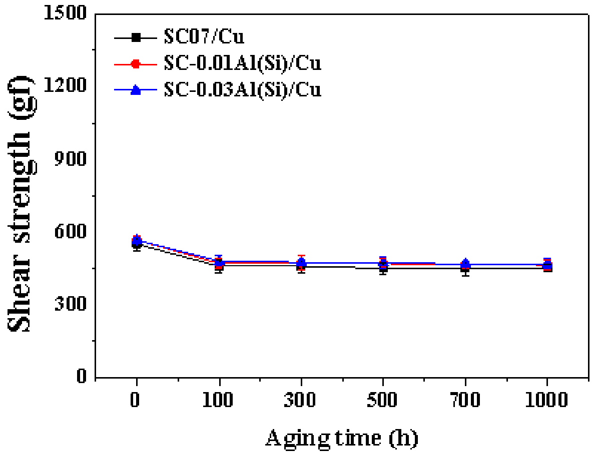

(b)

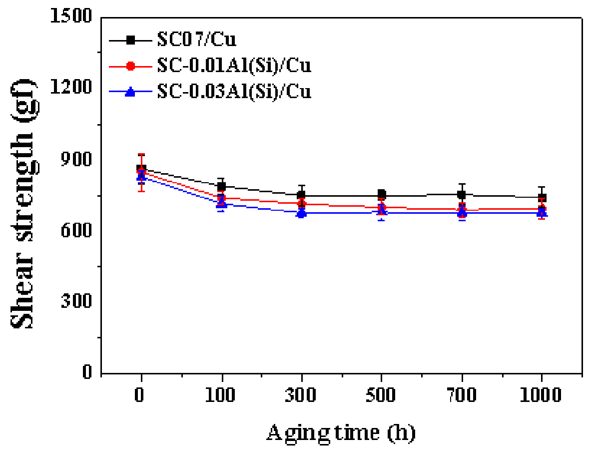

(c)

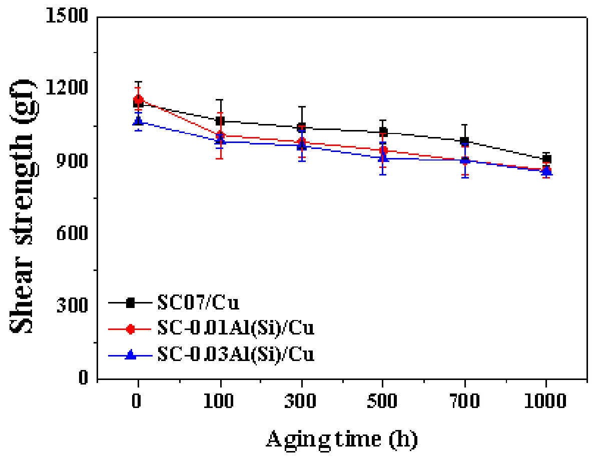

Figure 3.12 Shear strength of solder joints during isothermal aging at 100 ℃ under (a)0.01 m/s, (b)0.1 m/s and (c)1 m/s shear speed.

(a)

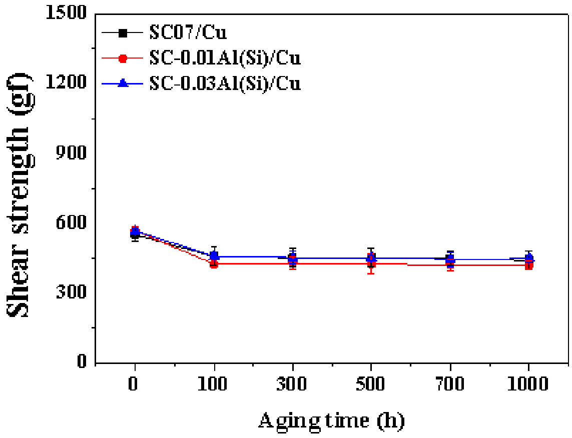

(b)

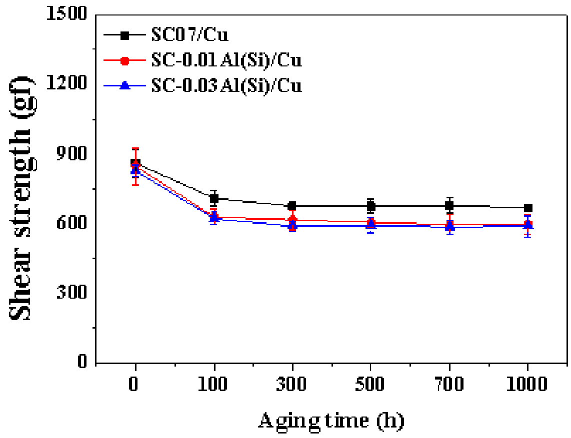

(c)

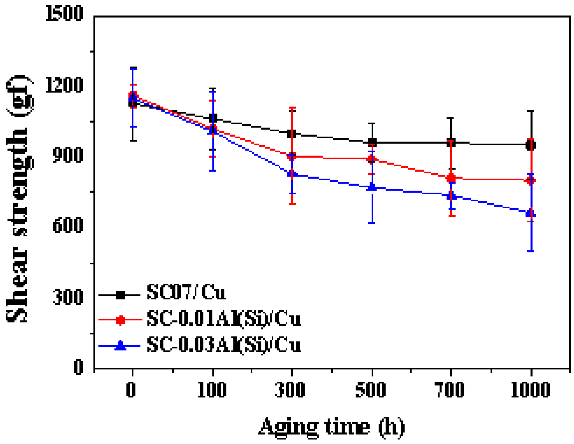

Figure 3.13 Shear strength of solder joints during isothermal aging at 125 ℃ under (a)0.01 m/s, (b)0.1 m/s and (c)1 m/s shear speed.

(a)

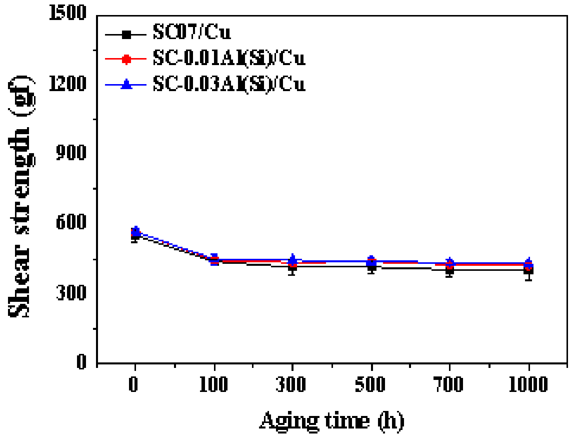

(b)

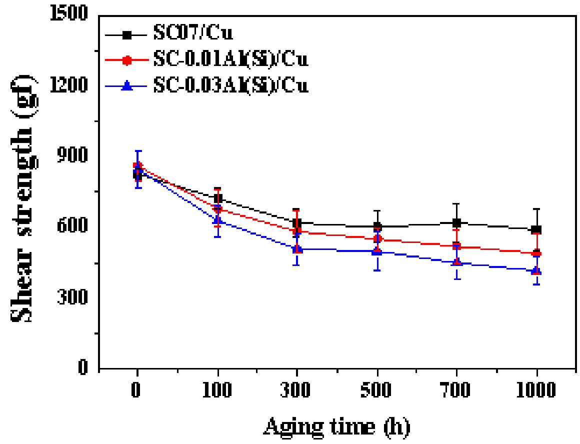

(c)

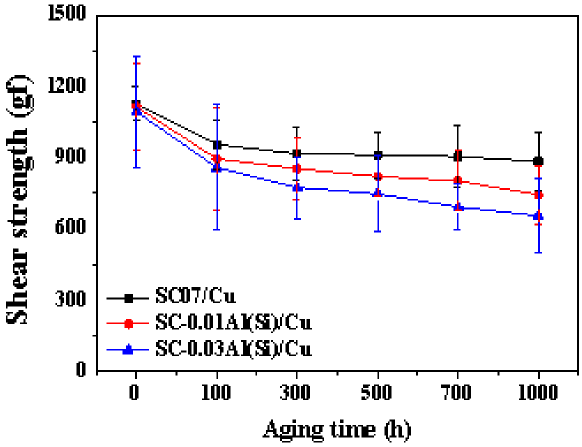

Figure 3.14 Shear strength of solder joints during isothermal aging at 150 ℃ under (a)0.01 m/s, (b)0.1 m/s and (c)1 m/s shear speed.

(a)

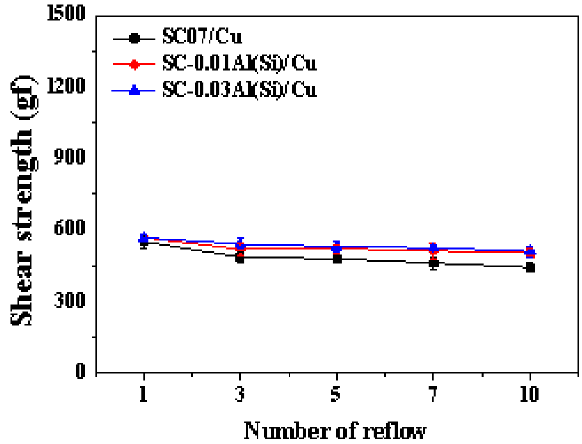

(b)

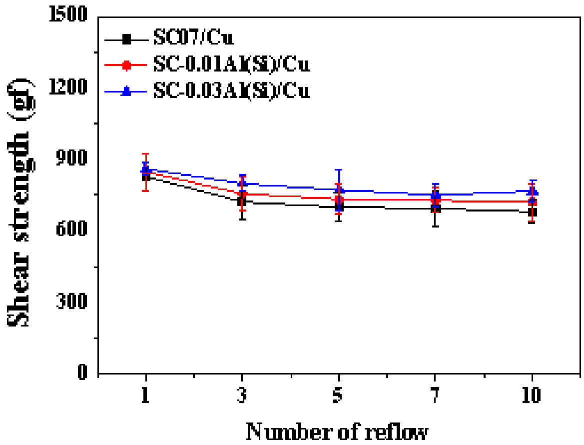

(c)

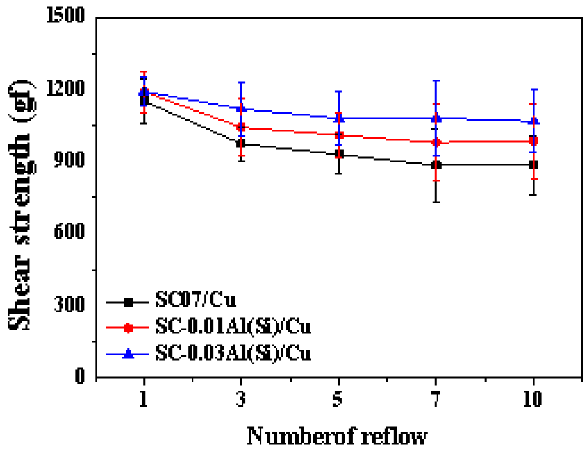

Figure 3.15 Shear strength of solder joints during multi-reflow under (a)0.01 m/s, (b)0.1 m/s and (c)1 m/s shear speed.

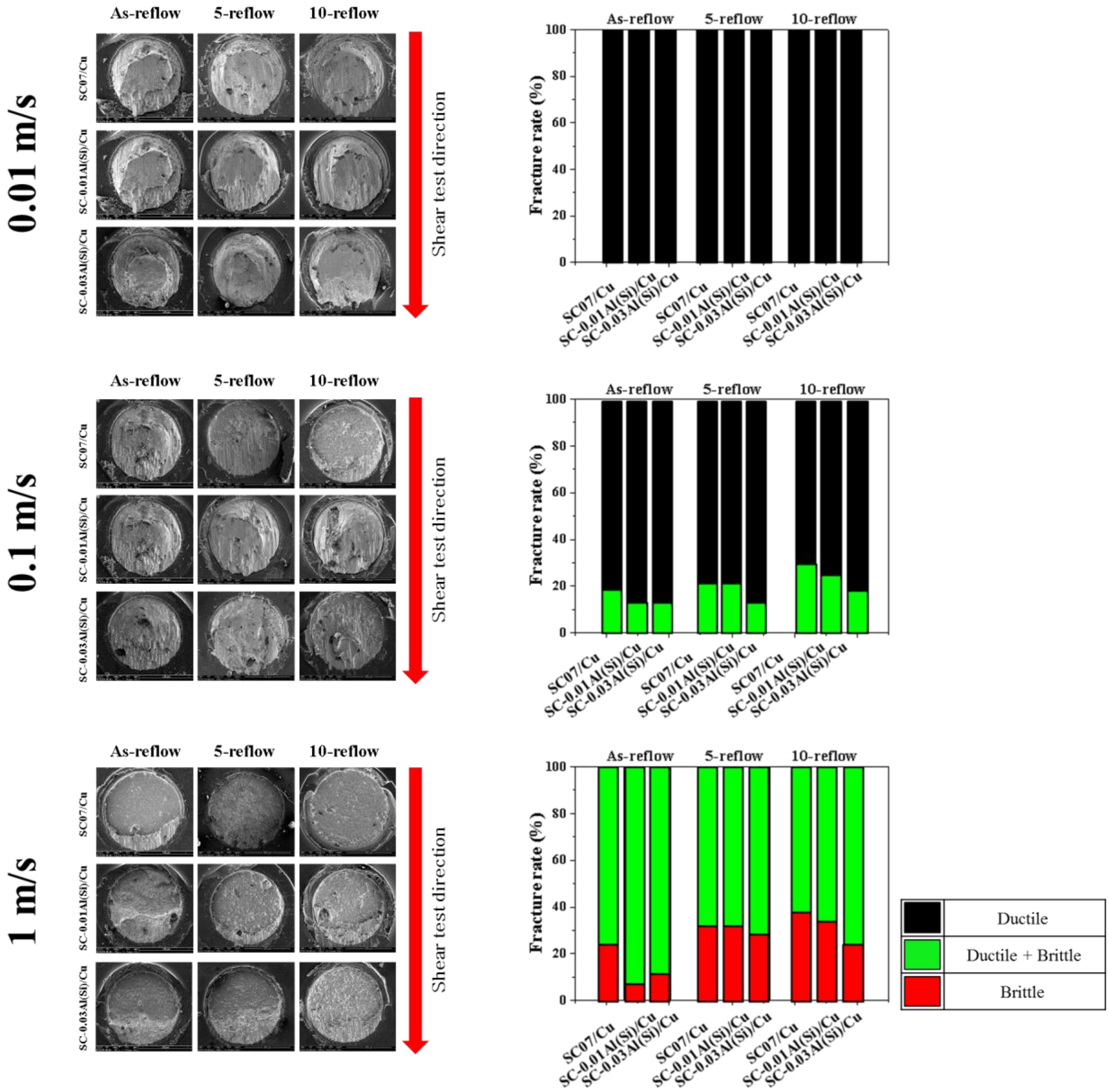

Figure 3.16 Fracture surfaces of the solder joints under various shear speeds during multi-reflow.

3.3.4 Effect of Al(Si) addition on interfacial IMC

Figure 3.17 shows the EMPA mapping results of the As-reflow sample. The joint systems with Al(Si) added show a wider spread of Cu_6Sn_5 particles in comparison to the SC07/Cu system. Furthermore, increased instances of Al(Si) particles were observed within the solder for samples with higher Al(Si) content. Previous studies suggest that adding Al to Sn-Cu binary solders or SAC solders results in the preliminary solidification of $Cu_{33}Al_{17}$ phase, which further aids in the formation of refined β-Sn + Cu_6Sn_5 network [16]. **Figure 3.18** is the SAED pattern image of the IMC within the SC-Al(Si) solder prepared using TEM. Components such as Al_2Cu, Sn-Cu-Al, and Cu_6Sn_5 were observed.

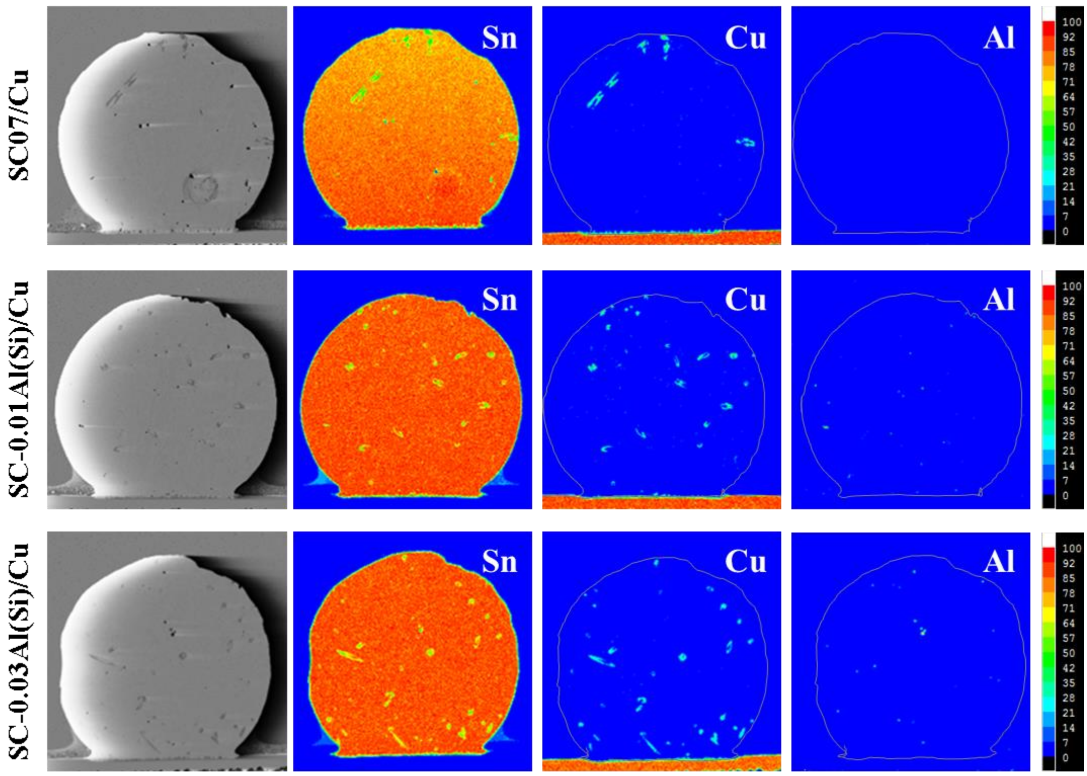

Figure 3.17 EPMA mapping result of SC07, SC-0.01Al(Si) and SC-0.03Al(Si) solder joints.

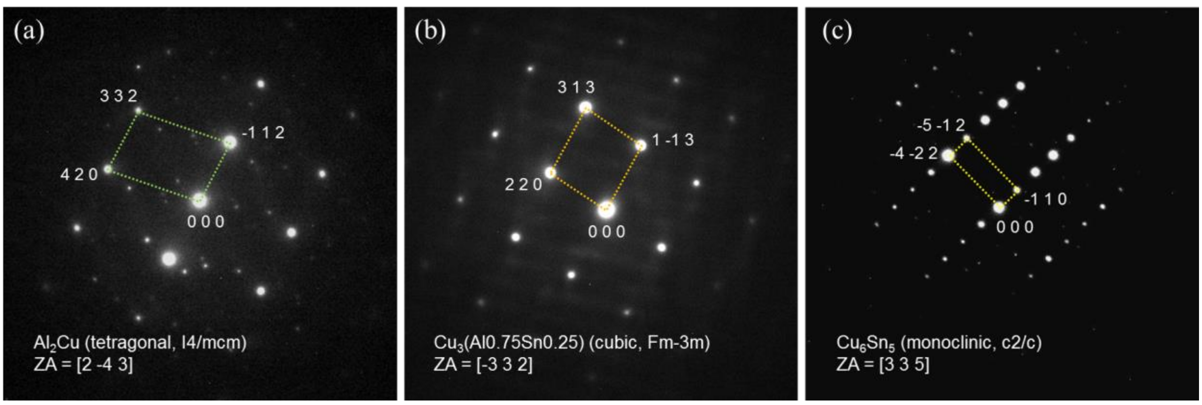

Figure 3.18 Result of SAED pattern analysis for Sn-Cu-Al(Si).

3.4 Conclusion

In this chapter, the IMC growth mechanism and the mechanical properties of SC-Al(Si)/Cu interface were evaluated. Under As-reflow conditions, the SC-Al(Si)/Cu joints showed inhibited IMC growth in comparison to SC07/Cu joints. This is attributed to the delayed formation of Cu_6Sn_5 due to the Cu-Al phase solidification. Thermal aging and multiple reflow techniques were used to treat the solder joint samples. SC-Al(Si)/Cu joints and SC07/Cu joints did not show any significant differences in both the IMC growth speed and Kirkendall void formations during the aging process. With multi-reflow, however, the total IMC growth rates were observed to be slower for SC-Al(Si)/Cu joints. The inhibited IMC growth for SC-Al(Si)/Cu joints resulted in higher shear strength compared to the SC07/Cu joint. In summary, the SC-Al(Si)/Cu joint did not show excellent performance compared to the SC07/Cu joint in isothermal aging, and shear strength greatly decreased as aging time and temperature increased due to the Kirkendall voids. However, an inhibition effect on IMC growth was observed in multi-reflow, resulting in slightly higher shear strength compared to the SC07/Cu joint. As shear speed increased, the difference in strength widened. Through EPMA mapping, compounds such as Cu-Al and Cu-Sn were observed throughout the internal structure of the solder. Additionally, the SAED pattern analysis using TEM showed that there exist other phases in the solder other than Cu_6Sn_5, which were determined to be compounds such as Al_2Cu and Sn-Cu-Al.

3.5 Bibliography

[1] Yang, M.; Ko, Y.-H.; Bang, J.; Kim, T.-S.; Lee, C.-W.; Li, M. "Effects of Ag addition on solid–state interfacial reactions between Sn–Ag–Cu solder and Cu substrate" Mater. Charact. 124 (2017) 250–259.

[2] K. Maslinda, A. S. Anasyida, M. S. Nurulakmal "Effect of Al addition to bulk microstructure, IMC formation, wetting and mechanical properties of low-Ag SAC solder" J Mater Sci: Mater Electron (2016) 27:489–502.

[3] Yee Mei Leong and A.S.M.A. Haseeb "Soldering Characteristics and Mechanical Properties of

Sn-1.0Ag-0.5Cu Solder with Minor Aluminum Addition" Materials 9 (2016) 522.

[4] Dhafer Abdulameer Shnawah, Mohd Faizul Mohd Sabri, Suhana Binti Mohd Said, Iswadi Jauhari, Mohammad Hossein Mahdavifard, Mohamed Bashir Ali Bashir, Mohamed Hamid Elsheikh "Interfacial reactions between Cu substrate and Sn–1Ag–0.5Cu solder containing 0.1 wt% Al by dipping method" J Mater Sci: Mater Electron 26 (2015) 8229–8239.

[5] Nur Nadhirah M.K., Maslinda K.b, Nurulakmal M.S., Anasyida A.S. "Isothermal Aging of Low-Ag SAC with Al addition" Procedia Chemistry 19 (2016) 492 – 497.

[6] Glenn Ross, Vesa Vuorinen, Mervi Paulasto-Krockel "Void formation and its impact on CueSn intermetallic compound formation" Journal of Alloys and Compounds, 677 (2016) 127–138.

[7] Chun Yu, Dongye Wang, Jieshi Chen, JijinXu, Junmei Chen, Hao Lu "Study of Cu6Sn5 and Cu3Sn growth behaviors by considering trace Zn" Materials Letters, 121 (2014) 166–169.

[8] Yousra Bettahi, Caroline Richard "Evolution of microstructure of Lead free cu/Sn solders and copper oxide phase precipitation in Cu3Sn intermetallic during thermal cycling" Microelectronics Reliability, 92 (2019) 20–26.

[9] Y. Tang, Q.W. Guo, S.M. Luo, Z.H. Li, G.Y. Li, C.J. Hou, Z.Y. Zhong, J.J. Zhuang "Formation and growth of interfacial intermetallics in Sn-0.3Ag-0.7Cu xCeO_2/Cu solder joints during the reflow process" Journal of Alloys and Compounds, 778 (2019) 741–755.

[10] K. Zeng, R. Stierman, T.C. Chiu, D. Edwards, K. Ano, K.N. Tu, "Kirkendall void formation in eutectic SnPb solder joints on bare Cu and its effect on joint reliability" J. Appl. Phys. 97 (2005), 024508.

[11] Hee Yul Lee, Ashutosh Sharma, Se Ho Kee, Young Woo Lee, Jung Tak Moon, and Jae Pil Jung "Effect of Aluminium Additions on Wettability and Intermetallic Compound (IMC) Growth of Lead Free Sn (2 wt. % Ag, 5 wt. % Bi) Soldered Joints" Electron. Mater. Lett., 10 (2014) 997–1004.

[12] Yajun Wang, Lorenz T. Biegler, Mukund Patel, John Wassick "Parameters estimation and model discrimination for solid-liquid reactions in batch processes" Chemical Engineering Science 187 (2018) 455–469.

[13] O. Yu Liashenko, F. Hodaj "Differences in the interfacial reaction between Cu substrate and

metastable supercooled liquid Sn–Cu solder or solid Sn–Cu solder at 222℃: Experimental results versus theoretical model calculations" Acta Materialia 99 (2015) 106–118.

[14] X. Huang "Investigation and analysis on the solder ball shear strength of plastic ball grid array, chip scale, and flip chip packages with eutectic Pb-Sn and Pb-free solders" Thesis (Ph.D.) Hong Kong University of Science and Technology, (2003).

[15] Asit Kumar Gain, Y.C. Chan, Winco K.C. Yung "Microstructure, thermal analysis and hardness of a Sn–Ag–Cu–1 wt% nano-TiO2 composite solder on flexible ball grid array substrates" Microelectronics Reliability 51 (2011) 975–984.

[16] Jahyun Koo, Changsoo Lee, Sung Jea Hong, Keun-Soo Kim, Hyuck Mo Lee "Microstructural discovery of Al addition on Sne0.5Cu-based Pb-free solder design" Journal of Alloys and Compounds 650 (2015) 106–115.

Chapter 4

Interfacial reactions and mechanical properties of SC-Cr/Cu solder joint

4.1 Introduction

Recently, several research groups have focused on developing composite electronic interconnect materials doped with metallic [1–7] and ceramic [7–9] particles to control their interfacial microstructure and mechanical properties. For example, a trace amount of Cr in lead-free Sn-Zn solder could repress the atomic diffusion and therefore reduce the interfacial IMC growth [5,6]. However, the effect of Cr addition in the Sn-Cu/Cu joint has not been systemically evaluated in the literature.

In this chapter, to be better consistent with the practical application environment, the Sn-0.7Cu-0.2Cr solder was fabricated as BGA (ball grid array) solder balls and soldered on the prototype modules. After cycles of thermal shock testing, the microstructure evolution of the BGA solders was observed and the shear strength of the solder balls was measured. In addition, to evaluate the reliability of the Sn-0.7Cu-0.2Cr solder for the automobile electronics application, the microstructure and shear strength variation of the commercial SAC305 and SC07 solders under multi-reflow, thermal aging and shock conditions were evaluated for comparison.

4.2 Experimental procedures

4.2.1 Fabrication of solder joint sample

The solder joint samples were fabricated by reflow process with the solder balls. The substrate material of test module was FR4 PCB, and the metal pad was Cu with an organic solderability preservative (OSP) surface finish. Detailed information of experimental procedures on the reflow assembling process of Sn-Cu-Cr solder can be found in *Chapter 3.2.1.* The conditions of reflow process are shown in **Table 4.1.** The peak temperatures of the Sn-3.0Ag-0.5Cu, Sn-0.7Cu, and Sn-0.7Cu-0.2Cr solders were 250, 255, and 260.5 °C, respectively. After the reflow process, the test samples were cooled to room temperature in air. **Figure 4.1** shows the schematic graph of the reflow profile for the Sn-0.7Cu-0.2Cr solder. **Figure 4.2** shows the image of actual soldering sample after reflow process.

4.2.2 Multiple reflow processes

Because a solder joint is typically exposed to a multi-reflow process owing to the characteristics of the manufacturing of the electronic component module, the characteristics of the solder joint were evaluated by repeating the reflow process up to 10 times. Detailed information of experimental procedures on the multi-reflow method of Sn-Cu-Cr solder can be found in *Chapter 3.2.2.*

4.2.3 Analysis of interfacial reaction and IMC growth

The microstructure of the IMC was observed using scanning electron microscopy (SEM, Hitachi S-4700) and energy dispersive X-ray spectroscopy (EDX, EDAX Genesis XM2 60). For the cross-sectional observations, the reflowed samples were polished with SiC paper and an Al_2O_3 polishing solution and then etched with a solution of 95 % C_2H_5OH−3 % HNO_3−2 % HCl (in vol %). Detailed information of experimental procedures on the analysis method of interfacial IMC of Sn-Cu-Cr solder can be found in *Chapter 3.2.3.*

Table 4.1 Reflow conditions for each solder.

Solder	Pre-heating Time(s)	Duration time above melting temperature(s)	Peak reflow temperature(°C)
Sn-3.0Ag-0.5Cu	107	53	250
Sn-0.7Cu	73	47	255
Sn-0.7Cu-0.2Cr	73	47	260.5

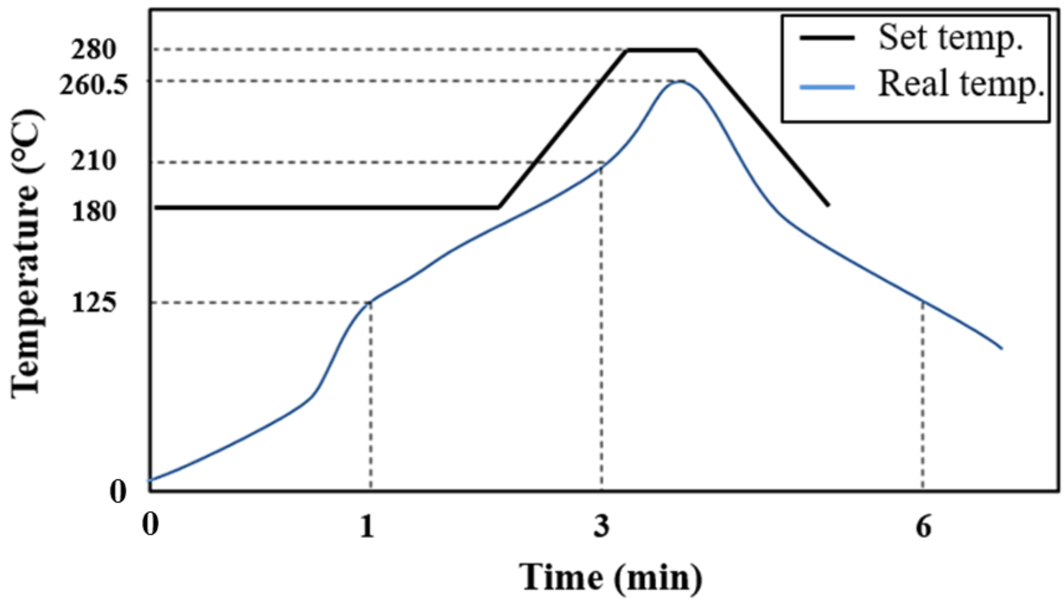

Figure 4.1 Reflow temperature profile for Sn-Cu-Cr solder.

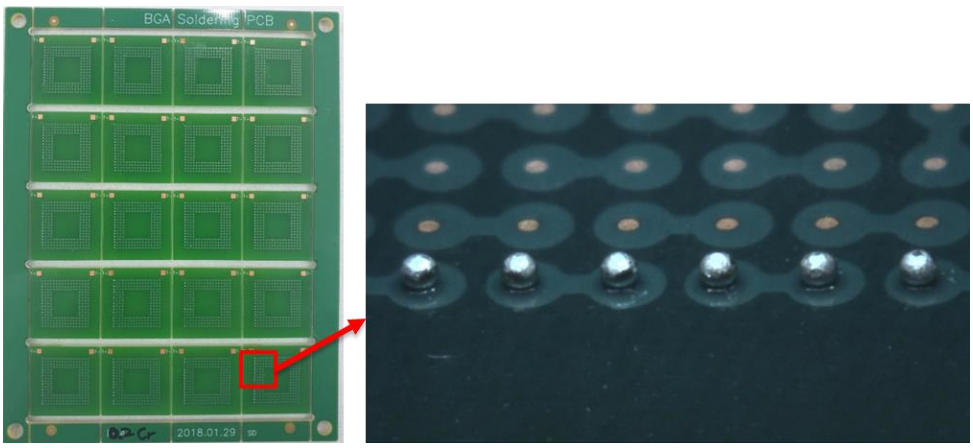

Figure 4.2 Images of actual sample for SC-0.2Cr solder after reflow process.

4.2.4 Isothermal aging and thermal shock

The aging temperatures were set to 100 °C, 125 °C, and 150 °C. The thermal shock conditions were set to -40 to 85 °C, -40 to 125 °C and -40 to 150 °C. The IMC growth and mechanical properties of the interface was observed after high-temperature shock. Furthermore, Solder joint samples were tested in a VT 7006 chamber (Votsch, Berlin, Germany) for 500 to 2,000 cycles with each shock lasting 20 min (JESD22-104; JEDEC, Arlington, VA, USA).

4.3 Results and discussion

4.3.1 IMC formation and growth under various thermal aging conditions

As previously reported, a typical Sn/Cu soldering system has two IMC phases, namely, Cu_6Sn_5 and Cu_3Sn phases [10–12]. **Figure 4.3** shows a phase diagram for Sn-Cu system. As the phase diagram shows, two intermetallic layers with Cu_6Sn_5 and Cu_3Sn phases are clearly observed at a soldering processing temperature of 350 °C or less, whereas other IMC phases such as Cu_{41}-Sn_{11} and $Cu_{10}Sn_3$ are observed at higher temperatures. The Cu_6Sn_5 IMC is generated by the reaction between the Sn atoms present in the solder and the Cu atoms in the substrate (4.1). Because Cu_6Sn_5 (η-phase) has the largest driving force for precipitation at the Cu/Sn interface [13]. In Cu-Sn soldering system, Cu_6Sn_5 (η-phase) precipitates firstly at the solder/Cu substrate interface followed by the precipitation of Cu_3Sn (ε-phase) at the Cu_6Sn_5/Cu substrate interface. The growth of the Cu_3Sn IMC layer during thermal aging is mostly controlled by the interdiffusion between Sn atoms diffused through the Cu_6Sn_5 IMC layer and Cu atoms from the Cu substrate (4.2). The growth of the Cu_3Sn IMC layer may also be contributed to by Cu atoms diffused through the Cu_3Sn to Cu_3Sn/Cu_6Sn_5 interface (4.3). Due to the reaction in equation (4.3), the amount of Cu atoms diffused from the Cu substrate to the Cu_6Sn_5/solder interface is significantly reduced as the Cu_3Sn layer thickens with aging time:

$$6Cu + 5Sn \rightarrow Cu_6Sn_5 \quad \cdots\cdots (4.1)$$

$$3Cu + Sn \rightarrow Cu_3Sn \quad \cdots\cdots (4.2)$$

$$Cu_6Sn_5 + 9Cu \rightarrow 5Cu_3Sn \quad (4.3)$$

Figures 4.4 – 4.6 show the cross-sectional microstructures of the IMC layers formed at the SAC305/Cu, SC07/Cu, and SC-0.2Cr/Cu interfaces during the thermal aging test. Overall, the interfacial IMCs became thicker and flatter as the thermal aging increased, and the higher the temperature, the greater the effect**.**

At all aging temperature conditions, the SAC305/Cu joint exhibited the thickest total IMC while the SC-0.2Cr/Cu joint was the thinnest. In the SC07/Cu joint, Cu_3Sn grew greatly with aging time, while the Cu_6Sn_5 thickness tended to decrease. However, in the SC-0.2Cr/Cu joint, Cu_3Sn showed barely any growth and Cu_6Sn_5 only slowly increased. In particular, in the SC-0.2Cr/Cu joint, the Cu_3Sn layer grown at 100 °C and 125 °C could not be observed, and could only be observed after 500 hours at 150 °C. The Kirkendall voids that formed in the Cu_3Sn and Cu substrate interface were not observed at 100 °C, though they increased greatly in the SAC305/Cu and SC07/Cu joints above 125 °C. As a result, under isothermal aging, the SC-0.2Cr/Cu joint showed more effective inhibition of Cu_3Sn growth than the SAC305/Cu and SC07/Cu joint.

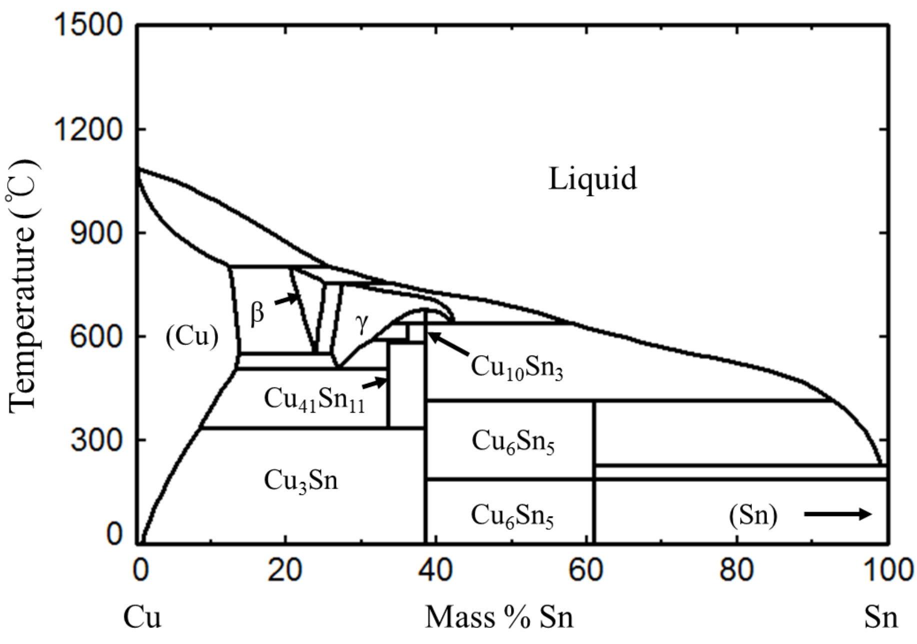

Figure 4.3 Sn-Cu Phase diagram.

Figures 4.7 – 4.9 show the changes in grain structures of Cu_6Sn_5 according to the thermal aging time. The results indicate that more smaller grain size is identified in the SC-0.2Cr/Cu joint than in the SAC305/Cu and SC07/Cu joints. The scallop-shaped Cu_6Sn_5 grains laterally grow until the Cu_6Sn_5 contacts with neighboring grains, and then they grows to vertical direction [14]. The reason of smaller grain size of Cu_6Sn_5 of SC-0.2Cr/Cu joint is seemed that addition of Cr leads to form more nucleation site during the solidification [15].

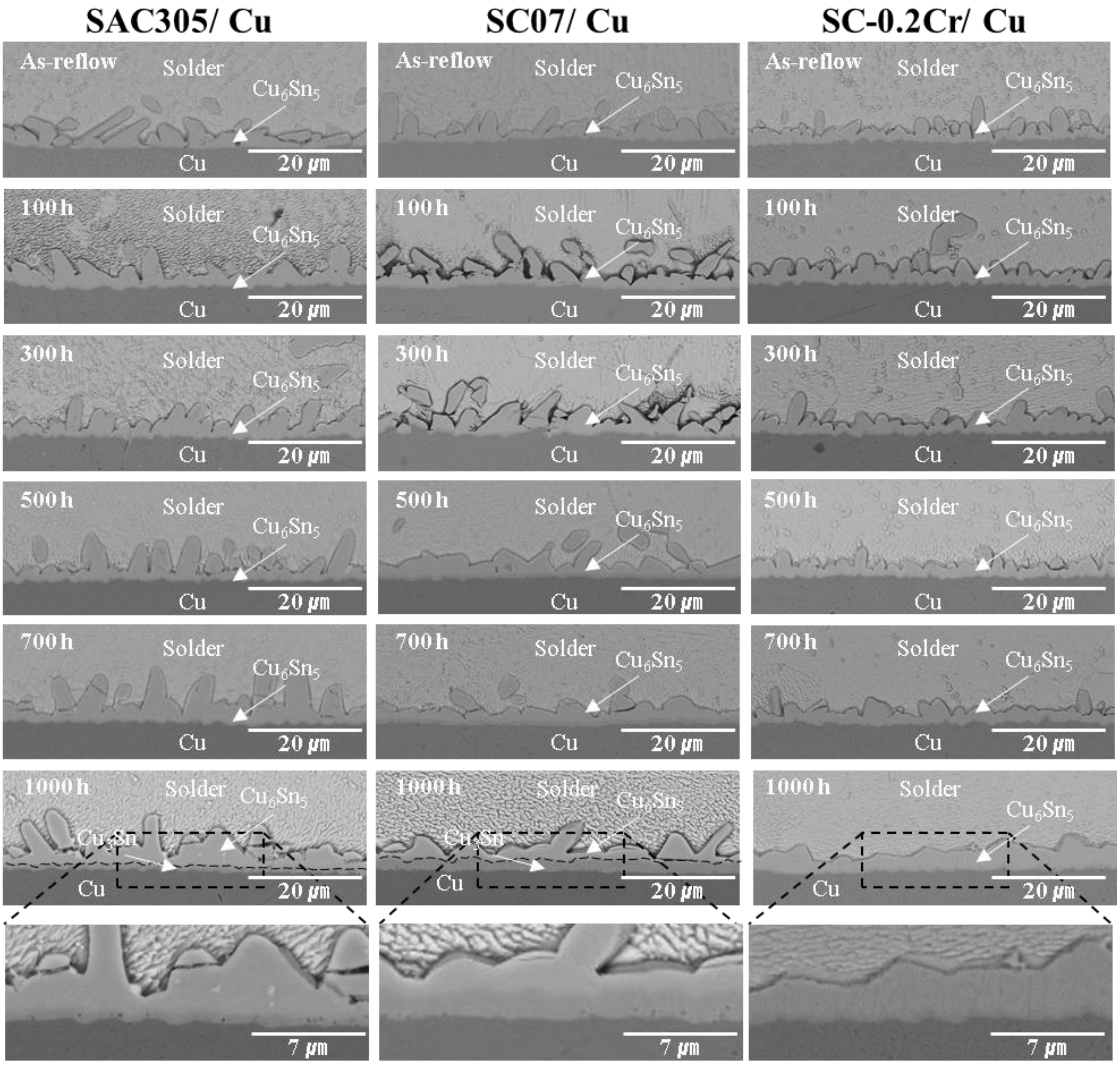

Figure 4.4 Cross-sectional microstructures of solder joints during isothermal aging at 100 °C.

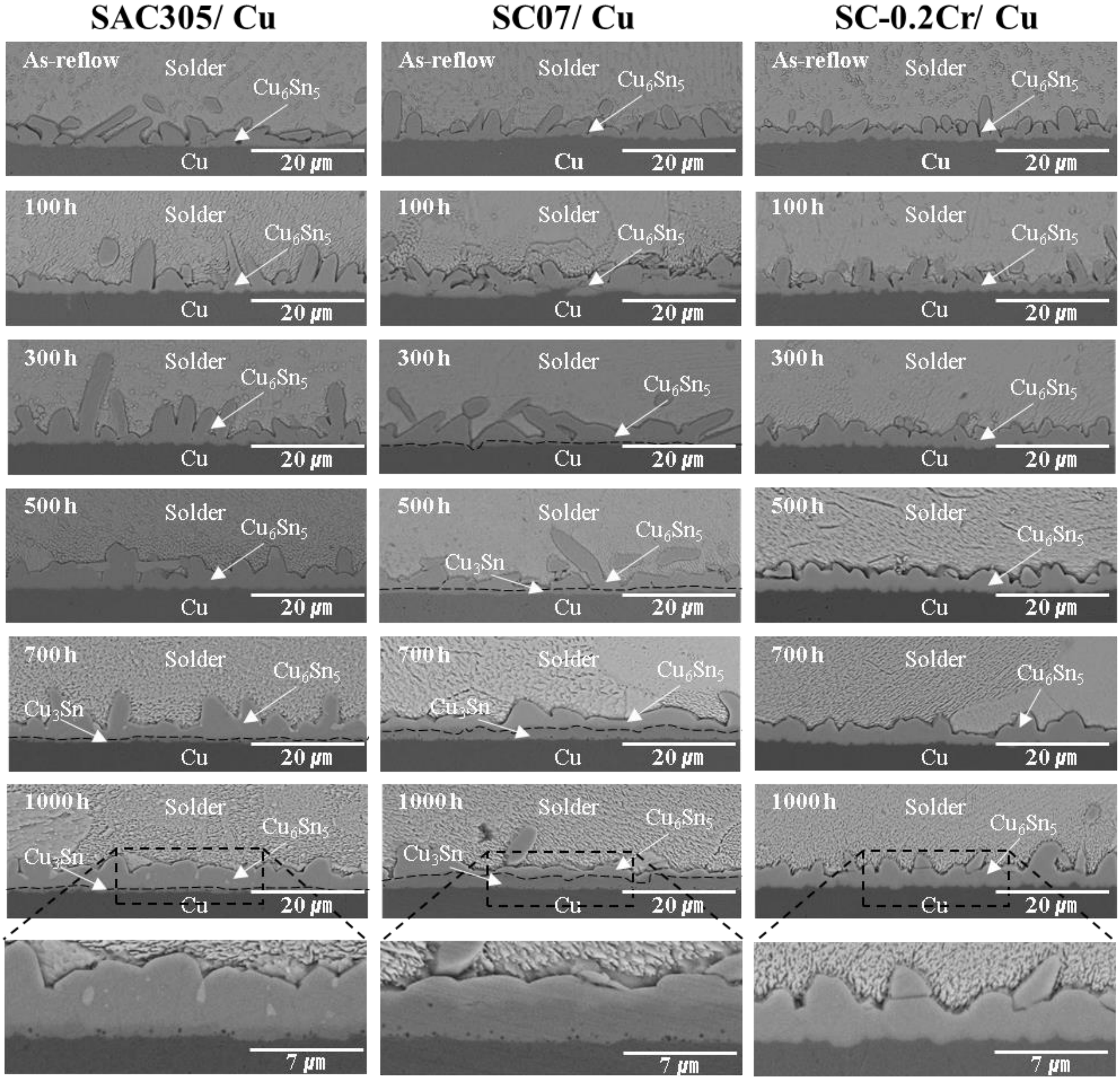

Figure 4.5 Cross-sectional microstructures of solder joints during isothermal aging at 125 °C.

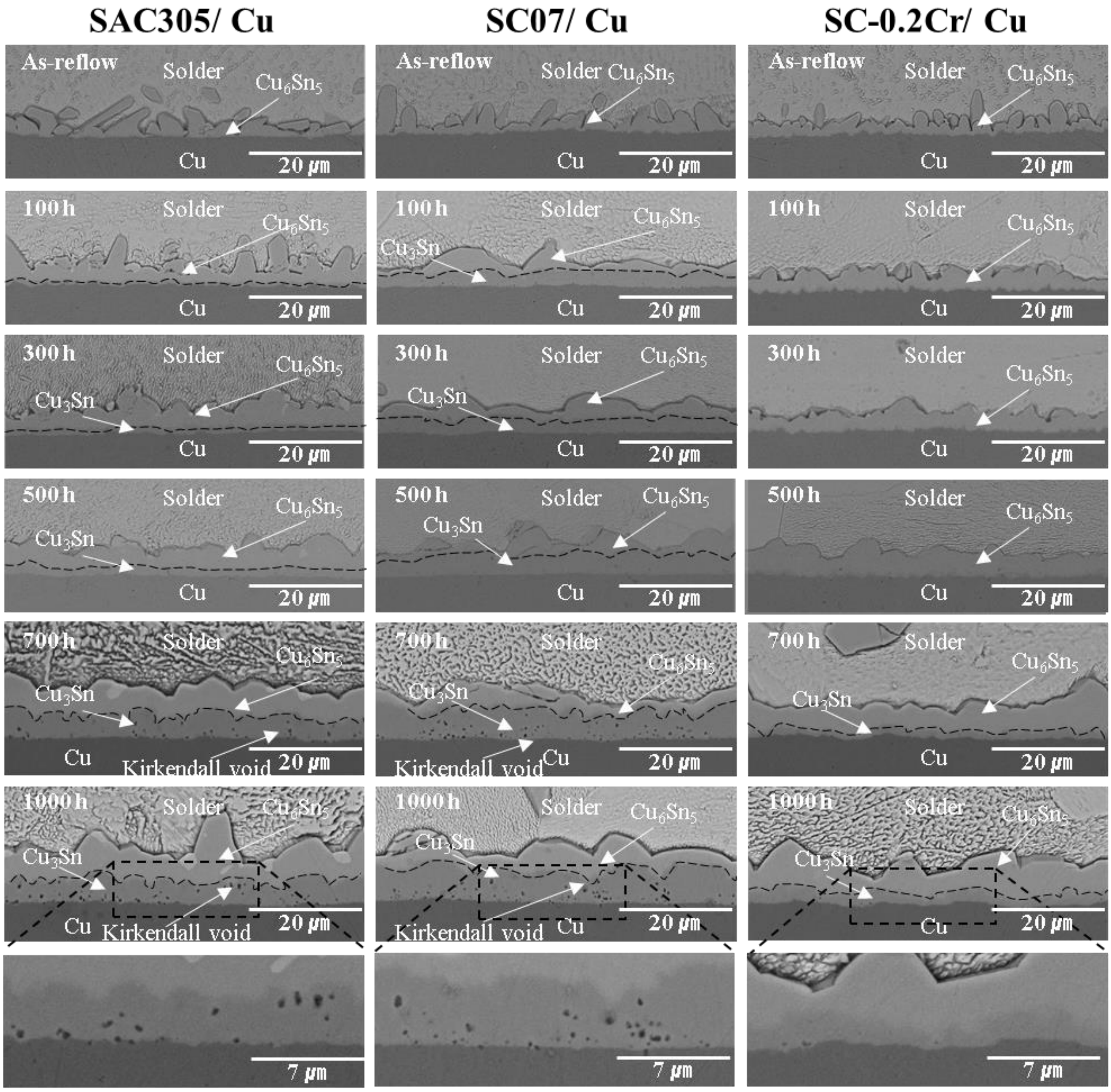

Figure 4.6 Cross-sectional microstructures of solder joints during isothermal aging at 150 °C.

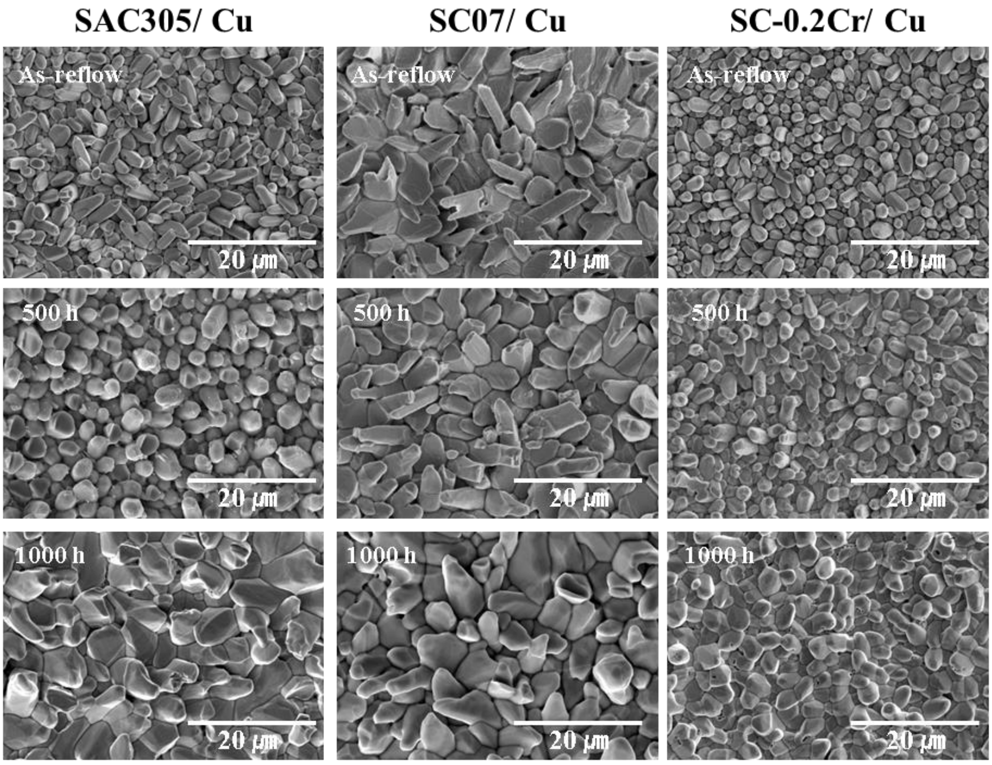

Figure 4.7 Top views of Cu_6Sn_5 IMC during isothermal aging at 100 °C.

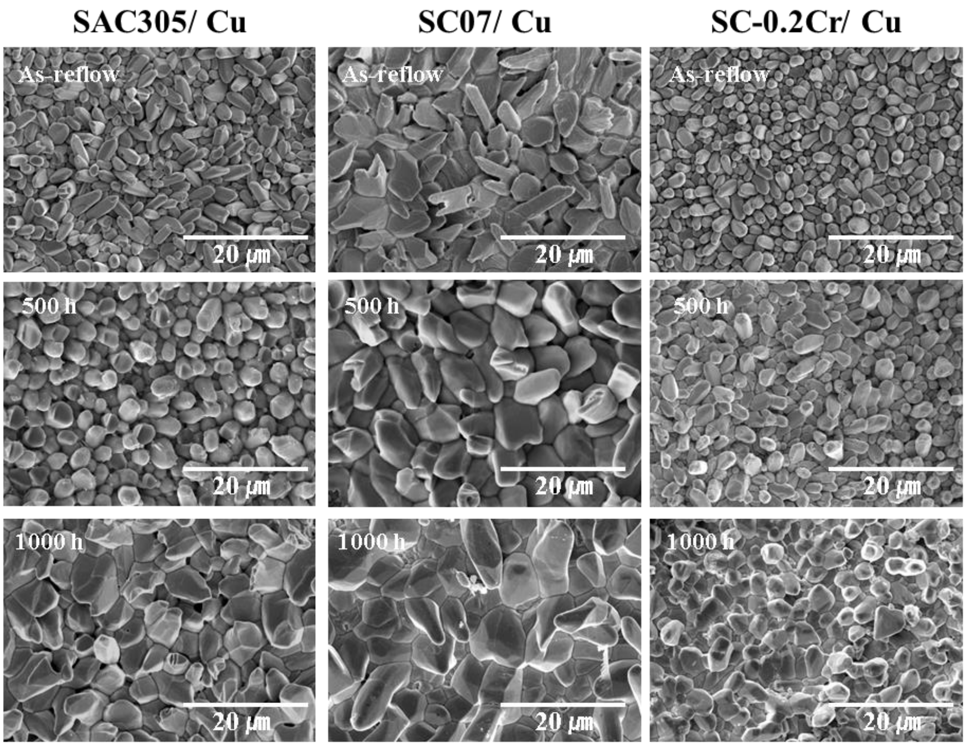

Figure 4.8 Top views of Cu_6Sn_5 IMC during isothermal aging at 125 °C.

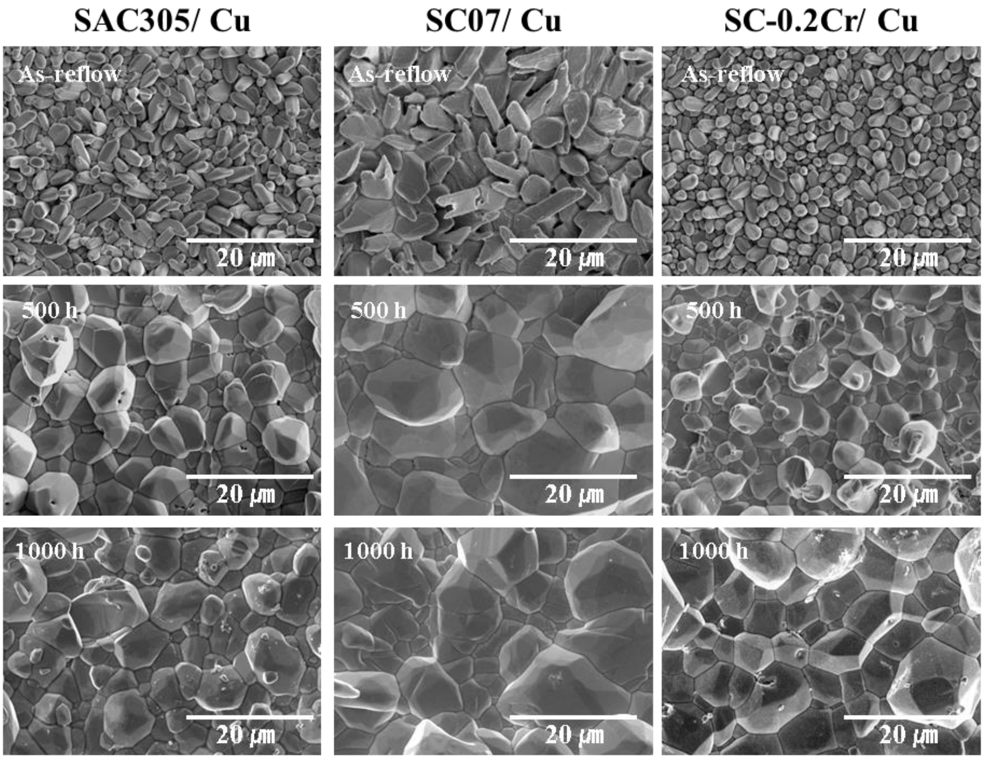

Figure 4.9 Top views of Cu_6Sn_5 IMC during isothermal aging at 150 °C.

4.3.2 IMC formation and growth under various thermal shock cycles

Figures 4.10, 4.11 and **4.12** shows the cross-sectional microstructures of the IMC layers formed at SAC305/Cu, SC07/Cu and SC-0.2Cr/Cu interfaces during thermal shock testing. Generally, the interfacial IMC became thicker and flatter with increasing thermal shocks. At -40 to 85 °C, neither Cu_6Sn_5 nor Cu_3Sn showed a large increase. However, at -40 to 125 °C and -40 to 150 °C in all three systems, the total IMC thickness tended to increase due to the rapid growth of Cu_3Sn. In the SC-0.2Cr/Cu joint, despite the increase in thermal shock cycle, though the Cu_6Sn_5 thickness tended to remain steady, the Cu_6Sn_5 thickness decreased in the SC07/Cu joint and Cu_3Sn greatly increased, leading the growth of the total IMC. Conversely, the SC-0.2Cr/Cu joint more dramatically inhibited Cu_3Sn growth than the SC07/Cu joint. Compared with the interfacial IMC formed in the three reaction systems, the addition of Cr effectively inhibited interfacial IMC growth, especially the Cu_3Sn IMC growth. Specifically, very few Cu_3Sn IMC and Kirkendall voids were detected at the SC-0.2Cr/Cu interface, even after 2,000 cycles of thermal shock testing, whereas the Cu_3Sn and

Kirkendall voids were significant at the SAC305/Cu and SC07/Cu interfaces after 1,000 cycles.

Fundamentally, the formation and growth of the interfacial IMC growth is caused by the Cu and Sn diffusion through the interface. To figure out how Cr inhibits the interfacial IMC growth, its effects on the Cu and Sn diffusion must be clarified. Next, the amounts of Cu and Sn atoms in the interfacial IMC layers were separately calculated for comparison as follows [16].

$$M_{Cu} = T_{Cu_6Sn_5} \cdot \rho_{Cu_6Sn_5} \cdot \upsilon_{Cu/Cu_6Sn_5} + T_{Cu_3Sn} \cdot \rho_{Cu_3Sn} \cdot \upsilon_{Cu/Cu_3Sn} \cdots \quad (4.4)$$

$$M_{Sn} = T_{Cu_6Sn_5} \cdot \rho_{Cu_6Sn_5} \cdot \upsilon_{Sn/Cu_6Sn_5} + T_{Cu_3Sn} \cdot \rho_{Cu_3Sn} \cdot \upsilon_{Sn/Cu_3Sn} \cdots \quad (4.5)$$

In which *M* is the total weight of the Cu or Sn element per unit area, *T* is the thickness of the Cu_6Sn_5 or Cu_3Sn layers, *v* is the weight fraction of Cu or Sn in the Cu_6Sn_5 or Cu_3Sn molecule and ρ is the density of the Cu_6Sn_5 or Cu_3Sn IMC, which is 8.45 or 8.97 $g \cdot cm^3$, respectively [17,18]. The calculated diffusion rates of Sn and Cu were summarized in **Figure 4.13**. The Sn diffusion rate are 0.38, 0.14 and 1.49 $\mu g \cdot mm^{-2}/K \cdot$cycles in SAC305/Cu, SC07/Cu and SC-0.2Cr/Cu reactions, respectively. Correspondingly, the Cu diffusion rates are 3.13, 5.36 and 0.96 $\mu g \cdot mm^{-2}/K \cdot$cycles in SAC305/Cu, SC0.7/Cu and SC-0.2Cr/Cu reaction systems, respectively. The addition of Cr slightly increased Sn diffusion but significantly repressed the Cu diffusion under thermal shock test. From these results, we believe that Cr inhibited the solid-state interfacial IMC growth primarily through slowing down the Cu diffusion through the interface. Detailed discussion of this mechanism is showed in *chapter 4.3.5*.

It is well known that only the Cu_3Sn and Cu_6Sn_5 phases are formed at the SAC305/Cu interface. Therefore, under similar Sn diffusion conditions, a lower Cu diffusion flux leads to repression of the Cu_3Sn layer growth and the Kirkendall void formation at the interface in the SC-0.2Cr/Cu reaction system, as shown in **Figures 4.11** and **4.12**. Generally, many Kirkendall voids would be formed in the interfacial IMC layers, especially in the Cu_3Sn layer, with prolonged thermal treatment. This is because Cu is the dominant diffusing species in the reaction and the competition in growth between Cu_6Sn_5 and Cu_3Sn tends to favor the latter when the ratio of Cu to Sn is large in the sample [19]. The transformation of 1 molecule of Cu_6Sn_5 into 2 molecules of Cu_3Sn will leave behind 3 Sn atoms, which will attract 9 atoms of Cu to form 3 more molecules of Cu_3Sn. The vacancy flux needed to transport the Cu atoms will accumulate at the Cu_3Sn and Cu/Cu_3Sn interface to form Kirkendall voids, which are undesirable in device applications [19]. Combined with the brittle nature of the IMC, such void defects could further deteriorate the interfacial connection of the solder joint under mechanical stress. In this regard, control of Cu_3Sn IMC formed at the interface is important. Therefore, the inhibition of Cu_3Sn IMC growth and the Kirkendall formation in the SC-0.2Cr/Cu reaction system is expected to improve the joint reliability, which will be discussed in the following section.

Additionally, the Tendency of IMC growth after aging and thermal shock was discussed. First, the total IMC of the SC-0.2Cr/Cu joint grew to approximately 1.3 μm after aging at 100 °C and 125 ℃ for 1,000 hours. However, at 150 ℃, the thickness greatly increased to approximately 4.5 μm. In contrast, under thermal shock, the thickness increased by 0.2 μm and 0.5 μm after 2,000 cycles at -40 to 85 ℃ and -40 to 125 °C, respectively, and by approximately 2 μm at -40 to 150 ℃. As a result, the effect obtained after 2,000 cycles in thermal shock at temperatures of -40 to 150 ℃ was the same to that obtained after 500 hours of aging at 150 ℃.

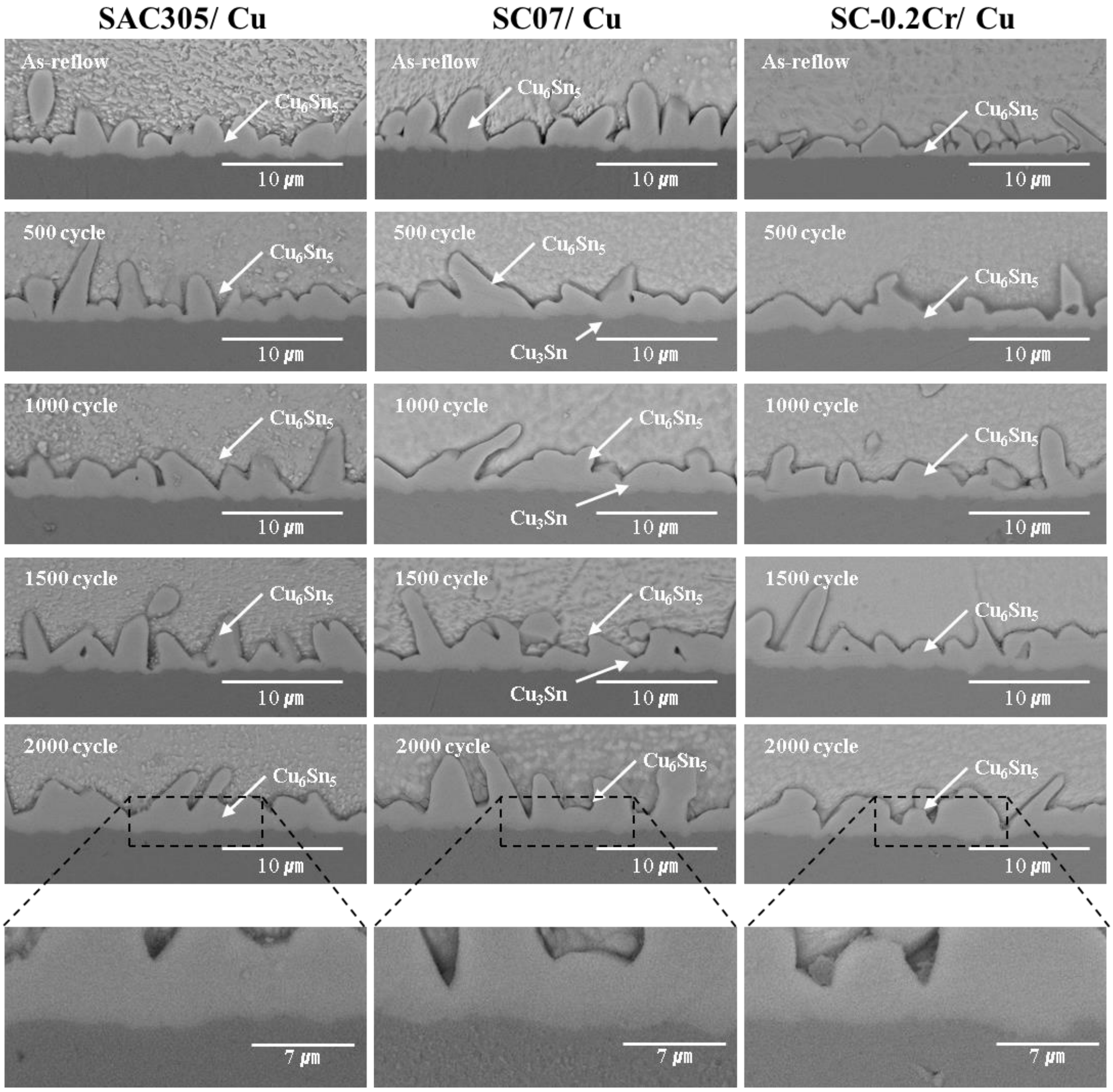

Figure 4.10 Cross-sectional microstructures of solder joints during thermal shock at -40 to 85 ℃.

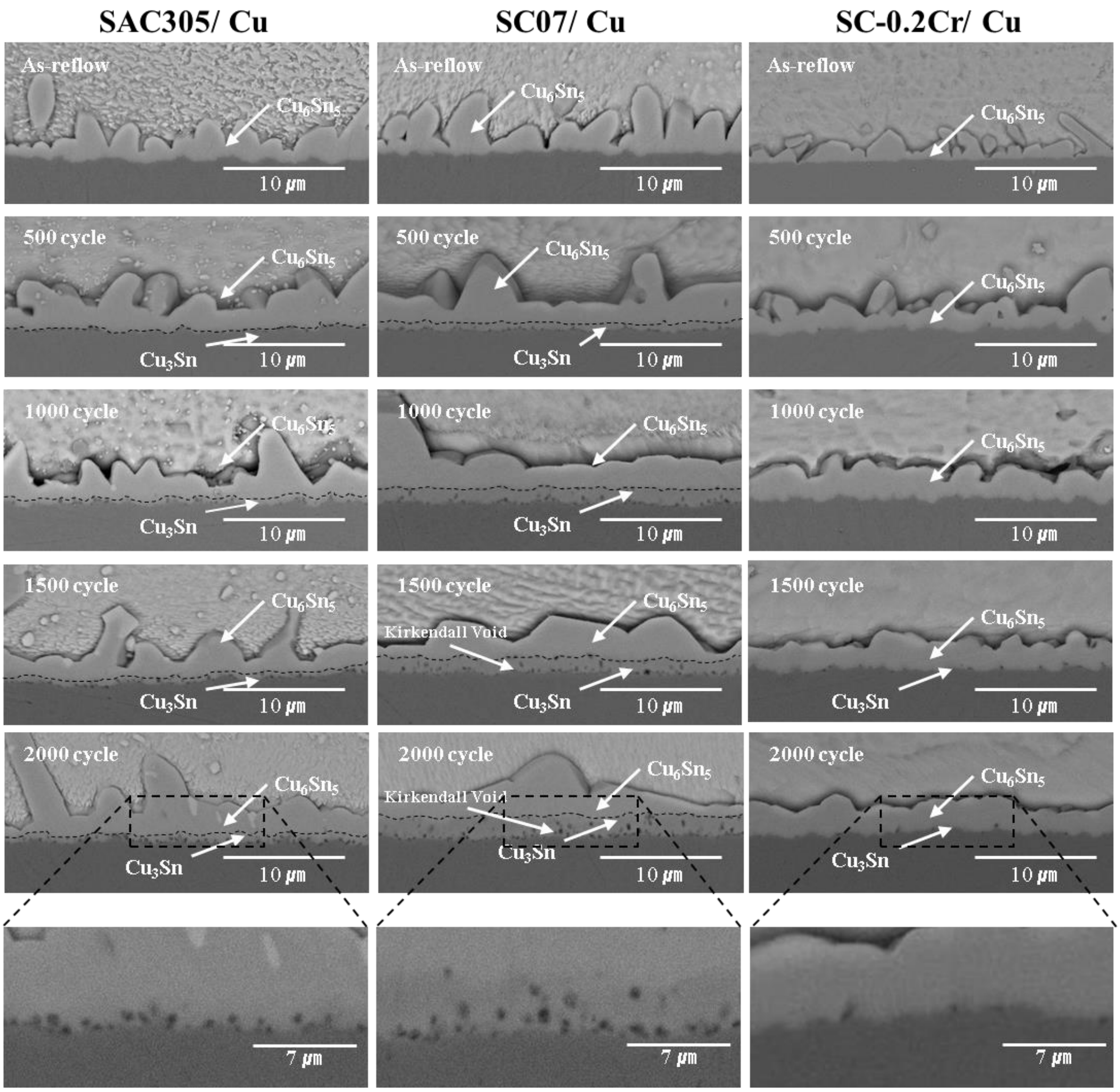

Figure 4.11 Cross-sectional microstructures of solder joints during thermal shock at -40 to 125 ℃.

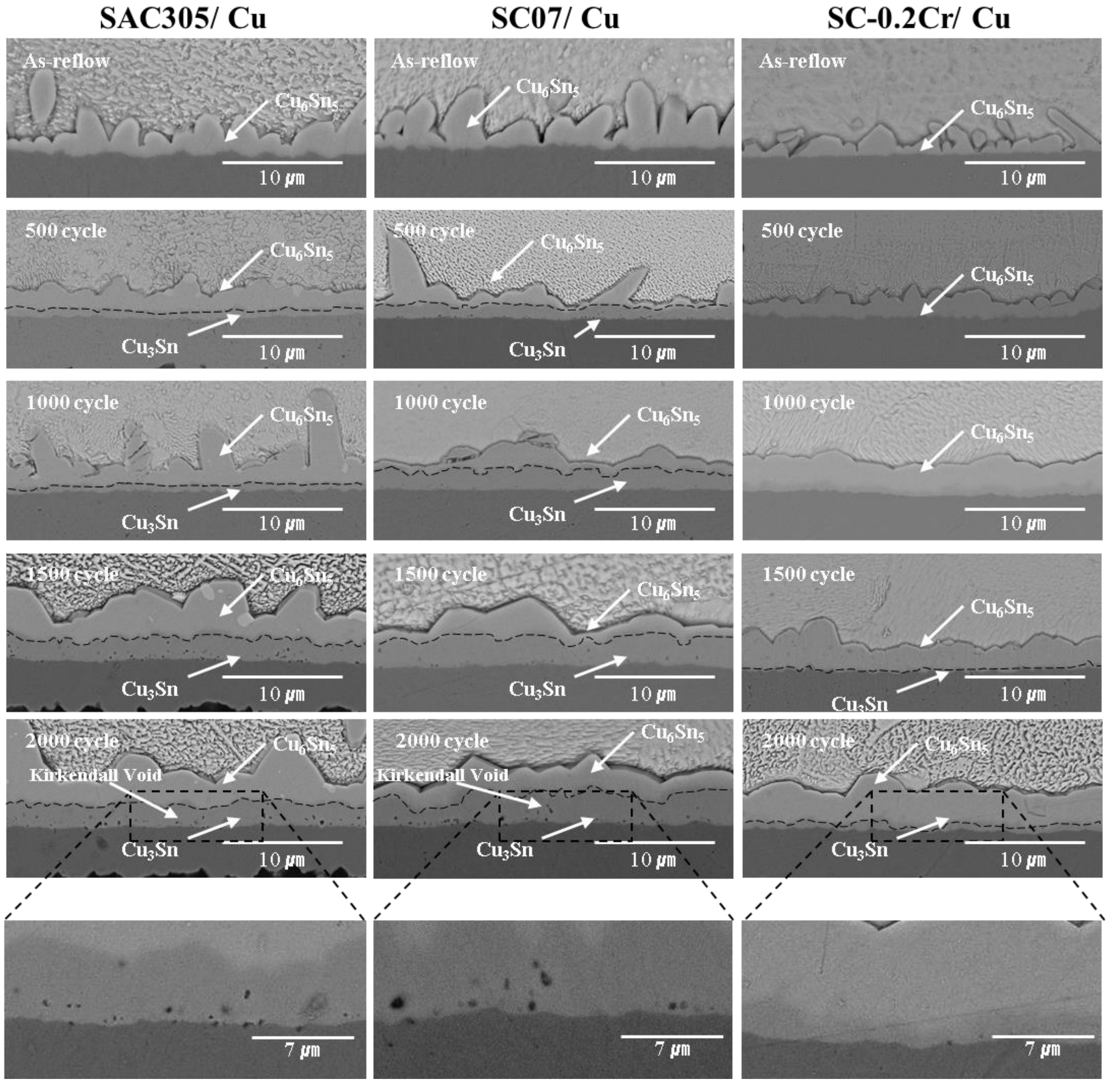

Figure 4.12 Cross-sectional microstructures of solder joints during thermal shock at -40 to 150 ℃.

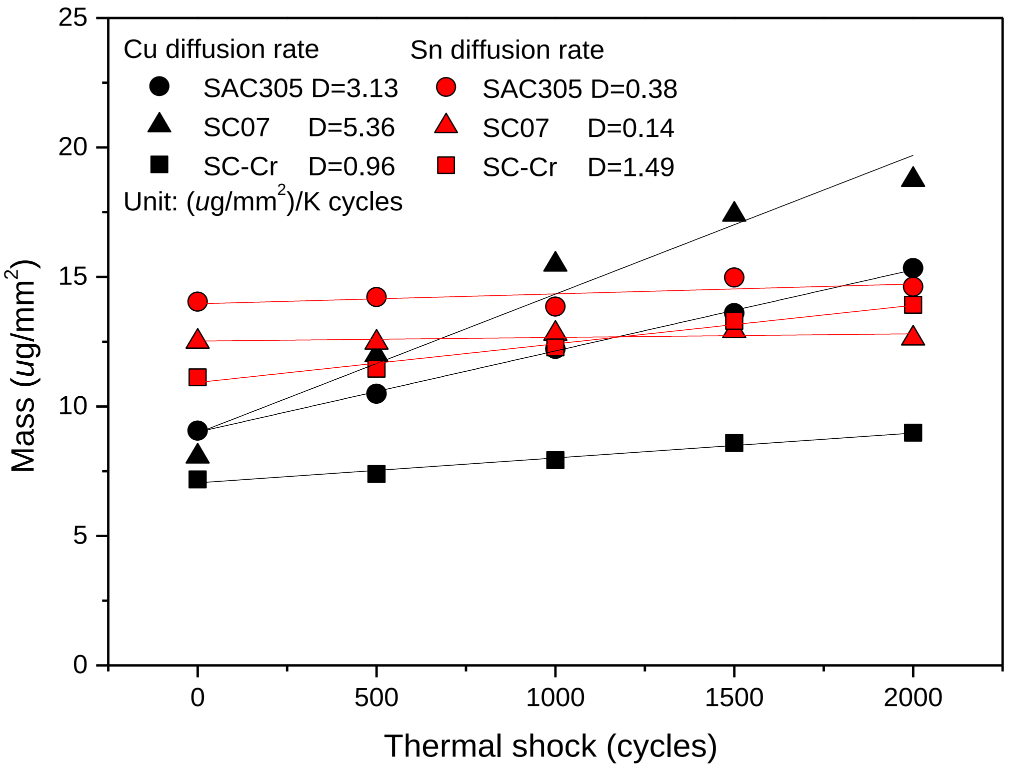

Figure 4.13 Plot of diffusivities of Cu and Sn versus thermal shock cycles.

4.3.3 IMC formation and growth under multi-reflow conditions

Figures 4.14 and **4.15** shows the change in IMC at the interface according to the number of reflows. During the reflow, Cu quickly dissolve into the molten solder because of its high solubility. So, layer by layer type Cu_6Sn_5 and Cu_3Sn are formed in Interface [20–22]. Typically, a temperature profile of reflow consists of preheating, ramping, soaking and cooling zones. At the preheating stage, the solder is not fully liquefied, thus the diffusion of Sn atoms from the solder to the Cu substrate is slower. As the concentration of Cu atoms is locally higher than Sn atoms in the surface of Cu substrate, a very thin ε-Cu_3Sn (few nm scale) IMC layer is formed at the Cu interface. Cu_3Sn could not be observed by scanning electron microscopy due to short soldering time in reflow process. At the ramping, the liquid–solid state diffusion between the Sn of the molten solder and the Cu substrate will started at this time. More Sn atoms will be supplied to the Cu substrate and form a thick η-Cu_6Sn_5 IMC layer on the thin ε-Cu_3Sn IMC layer. At the soaking zone (above T_m of solder), IMC grains will continue to grow during this period of time. At the cooling zone, the Cu atoms are precipitated locally on top of the existing η-Cu_6Sn_5 IMC interface due to the lower energy state condition [13].

In all diffusion systems, the volume of Cu_6Sn_5 grains was increased with a reflow cycle increase [23]. In comparison between the interfacial IMCs formed in the three reaction systems, the addition of Cr was shown to effectively suppress the interfacial IMC growth, particularly the growth of Cu_3Sn IMC.

As mentioned in *Chapter 3.3.2*, diffusion through Cu_6Sn_5 grain boundaries is known to be much faster in liquid solder/solid copper reactions than in solid solder/solid copper reactions Therefore, the IMC growth rates should be compared in different reaction systems. First, the total IMC of the SC-0.2Cr/Cu joint grew by approximately 4.5 μm after 1,000 hours of aging at 150 °C, and approximately 2 μm after 2,000 cycles in thermal shock at temperatures of -40 to 150 ℃. Furthermore, the thickness grew by approximately 1.5 μm after 10 multi-reflow cycles. These results are similar to the total IMC thickness grown after 2,000 cycles at -40 to 125 ℃ and then 400 hours of aging at 150 ℃. Therefore, the effect of 10 multi-reflow cycles can be considered equivalent to that obtained after 2,000 cycles in thermal shock at -40 to 125 ℃ and then 400 hours of aging at 150 ℃. Ten reflow cycles corresponds to approximately 1 hour. As a result, multi-reflow (liquid/solid reaction) demonstrated a much faster diffusion rate than isothermal aging and thermal shock (solid/solid reaction).

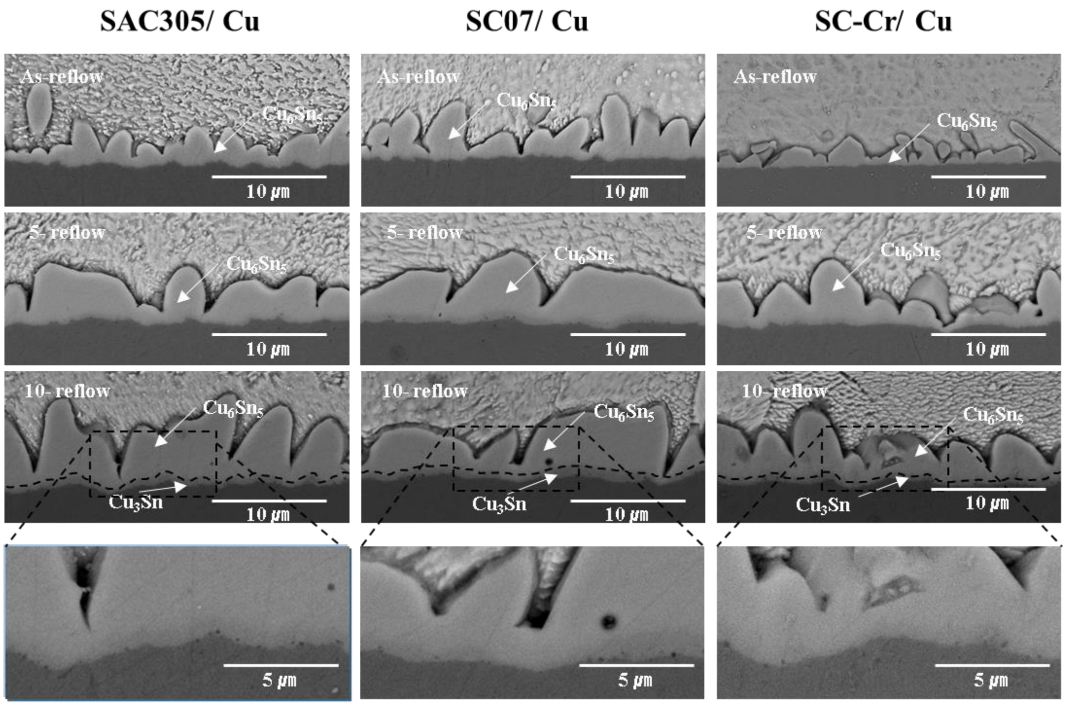

Figure 4.14 Cross-sectional images at the interface during multi-reflow process.

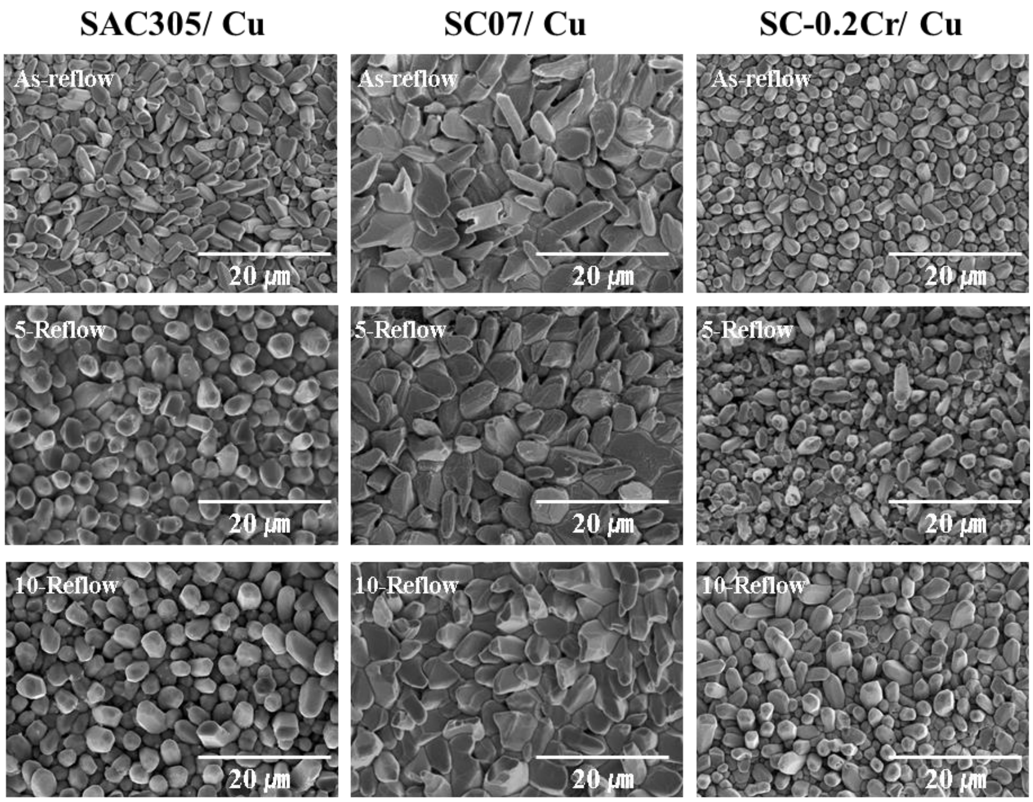

Figure 4.15 Top view images of Cu_6Sn_5 IMC during multi-reflows.

4.3.4 Effect of Cr addition on interfacial IMC

As shown in **Figure 4.16**, Cr compounds can be confirmed near the Sn/Cu_6Sn_5 interface in EPMA mapping. The Cr K signal is detected with Sn L signal together, thus it seems Cr-Sn compounds. There are no intermetallic phases in an equilibrium phase diagram of Cr-Sn binary system [24]. However, some reports have suggested meta-stable intermetallic compounds between Cr and Sn, such as $CrSn_2$ [25] and Cr_2Sn_3 [26]. Koo et al. [27] also presented the presence of $CrSn_2$ intermetallic compounds phase near the interface in the minor Cr and Ca adopted Sn-0.7Cu solder using an EPMA analysis.

In my cases, the size of Cr compounds exhibits approximately under 0.5 μm, which is smaller than a spatial resolution of SEM based spectroscopy analysis. For more precise analysis on this Cr compound, we utilized a TEM technique, which can offer a spectroscopic data with the very fine spatial resolution as well as a diffraction pattern on the same position. An *in-situ* lift-out method using a focused ion beam (FIB, JIB-4500, JEOL) was employed in order to prepare a specific-sited TEM lamellar sample including Cr compounds, where marked with a dotted box in BSE image of **Figure 4.16**. A carbon layer with the thickness of 2 μm was deposited on the surface of cross-section sample prior to FIB milling, and the exact position of Cr was marked by FIB line milling, as shown in **Figure 4.16**. The direction of TEM lamellar sample was denoted as that "A" is a solder side and "B" is a Cu pad side in EPMA (Figure 4.17), FIB (Figure 4.17) and TEM (Figure 4.18) images.

Figure 4.17 shows a scanning TEM (STEM) bright field (BF) image and EDS mapping results on the Sn L, Cu K and Cr L. Cr compounds located at the interface of Cu_6Sn_5/solder and near the interface of it. We can infer that these compound is a $CrSn_2$ intermetallic compound through the EDS spot analysis on these compounds (Sn: 69.3 %, Cr: 29.1 % and Cu 1.6 % in atomic percent). A selected area electron diffraction (SAED) pattern of Cr-Sn compound, obtained from denoted area with dotted circle in **Figure 4.17**, shows good agreement with the reported crystal structure of an orthorhombic $CrSn_2$ (space group: Fddd; proto type: Mg_2Cu; a=541.7 pm, b=944.0 pm and c=1839.6 pm) intermetallic compound [25]. Thus, it can be identified as $CrSn_2$ with the combination of EDS point analysis and SAED pattern.

In addition, solder dipping tests were conducted for evaluate the Cu_6Sn_5 nucleation behavior of Cr added solder. **Figure 4.18** shows the Cu_6Sn_5 IMC grain images observed after dipping the Cu coupon into the SC07/Cu and SC-0.2Cr/Cu joints under various melting temperature conditions for one second. The Cu_6Sn_5 IMC grain exhibited the smallest grain size at 260 °C for both solders, and the grain size increased as the temperature increased to 280 °C and 300 °C. Under all reaction temperatures, the Cu_6Sn_5 IMC grains of the SC-0.2Cr/Cu joint were smaller in size than those of the SC07/Cu joint. **Figure 4.19** shows the Cu_6Sn_5 IMC grain images observed after dipping the Cu coupon into the SC07/Cu and SC-0.2Cr/Cu joints under various temperature conditions for three seconds. For three-second dipping, the size of Cu_6Sn_5 IMC increased in both solders compared to one-second dipping.

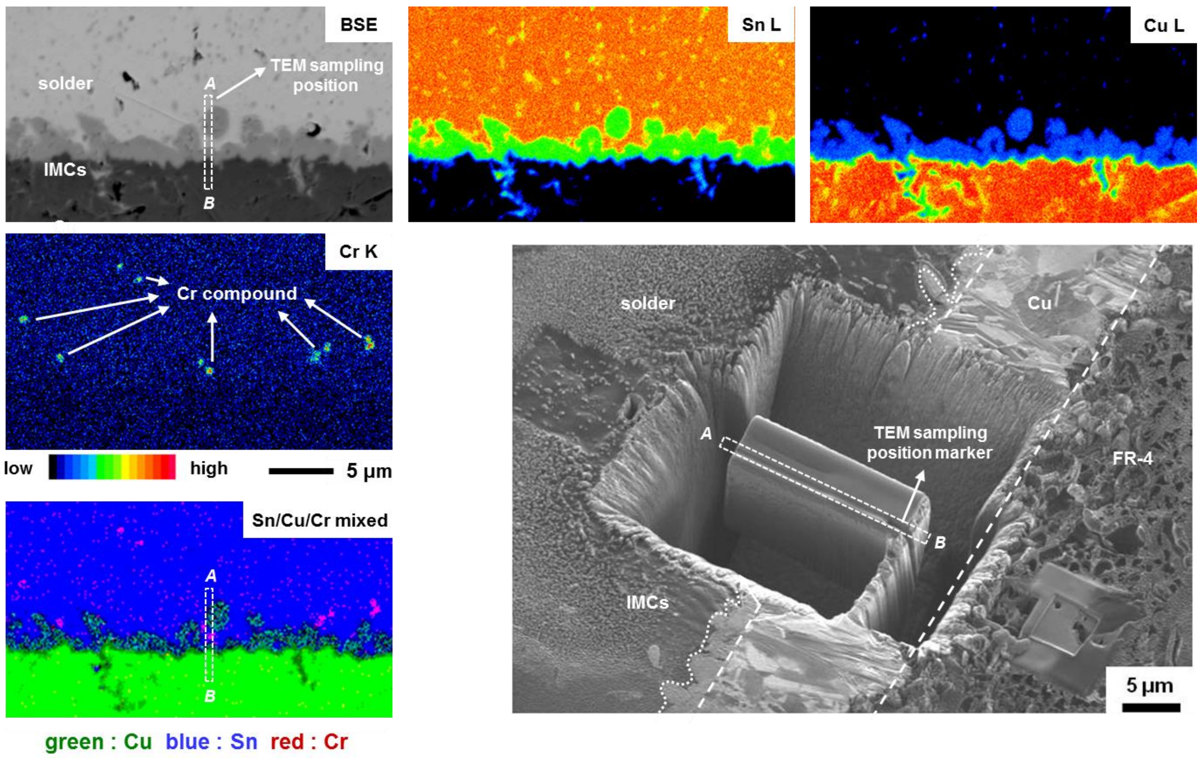

Figure 4.16 EPMA mapping results and FIB sampling position image.

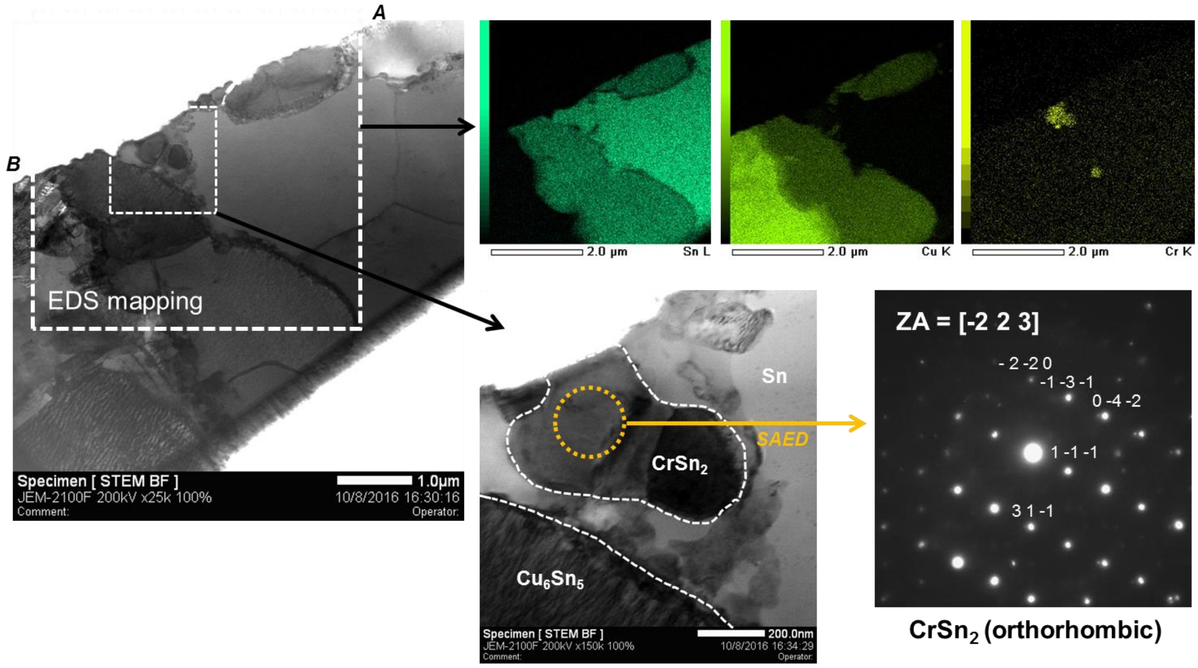

Figure 4.17 EDS mapping result and SAED pattern analysis result.

This is in good agreement with the result of the existing literature that the Cu_6Sn_5 grain size increased under the same temperature as the time increased [27]. The grain size change according to the temperature showed a tendency similar to that of one-second dipping. The Cu_6Sn_5 IMC grain size was smallest at 260 °C for both solders, and the size increased as the temperature increased. Moreover, the SC-0.2Cr/Cu joint exhibited the smaller Cu_6Sn_5 IMC grain size than the SC07/Cu even when the dipping time increased. This shows a similar tendency to the result of the existing literature that the Cr addition to solder suppressed the growth of Cu_6Sn_5 IMC at the interface [28].

Figure 4.20 shows the number of Cu_6Sn_5 IMC grains per um^2 at various reaction temperatures. At 260 °C, both solders exhibited the highest number of the grains per um^2. When dipping into the SC07/Cu joint was performed for one and three seconds, 3.028 and 1.944 per um^2 were observed, respectively. Moreover, when dipping into the SC-0.2Cr/Cu joint was performed for one and three seconds, 3.306 and 2.361 per um^2 were observed, respectively. For both solders, the reaction temperature that produced the smallest number of the grains per um^2 was 300 °C. When dipping into the SC07/Cu joint was performed for one and three seconds, 1.222 and 0.611 per um^2

were observed. Moreover, when dipping into the SC-0.2Cr/Cu joint was performed for one and three seconds, 1.601 and 0.833 per um^2 were observed. In **Figure 4.20**, the number of the grains per um^2 decreased as the dipping time increased. The figure clearly shows that the SC07/Cu joint exhibited the smaller number of the grains per um^2 than the SC-0.2Cr/Cu joint. The "inverted C" shapes of the curves are in good agreement with the results of the existing nucleation theory [29].

Figure 4.21 shows the average size of the Cu_6Sn_5 IMC grains formed at various reaction temperatures. The average grain size was inversely proportional to the results of **Figure 4.20.** At 260 °C, the average grain size was the smallest for both solders. When dipping into the SC07/Cu joint was performed for one and three seconds, 0.433 and 0.545 um were measured, respectively. When dipping into the SC-0.2Cr/Cu joint was performed for one and three seconds, 0.387 and 0.475 um were observed, respectively. For both solders, the reaction temperature that led to the largest average grain size was 300 °C. When dipping into the SC07/Cu joint was performed for one and three seconds, 0.669 and 0.97 um were observed. Moreover, when dipping into the SC-0.2Cr/Cu was performed for one and three seconds, 0.613 and 0.833 um were observed. Overall, the grain size of the SC07/Cu was approximately 12 % larger than that of the SC-0.2Cr/Cu joint.

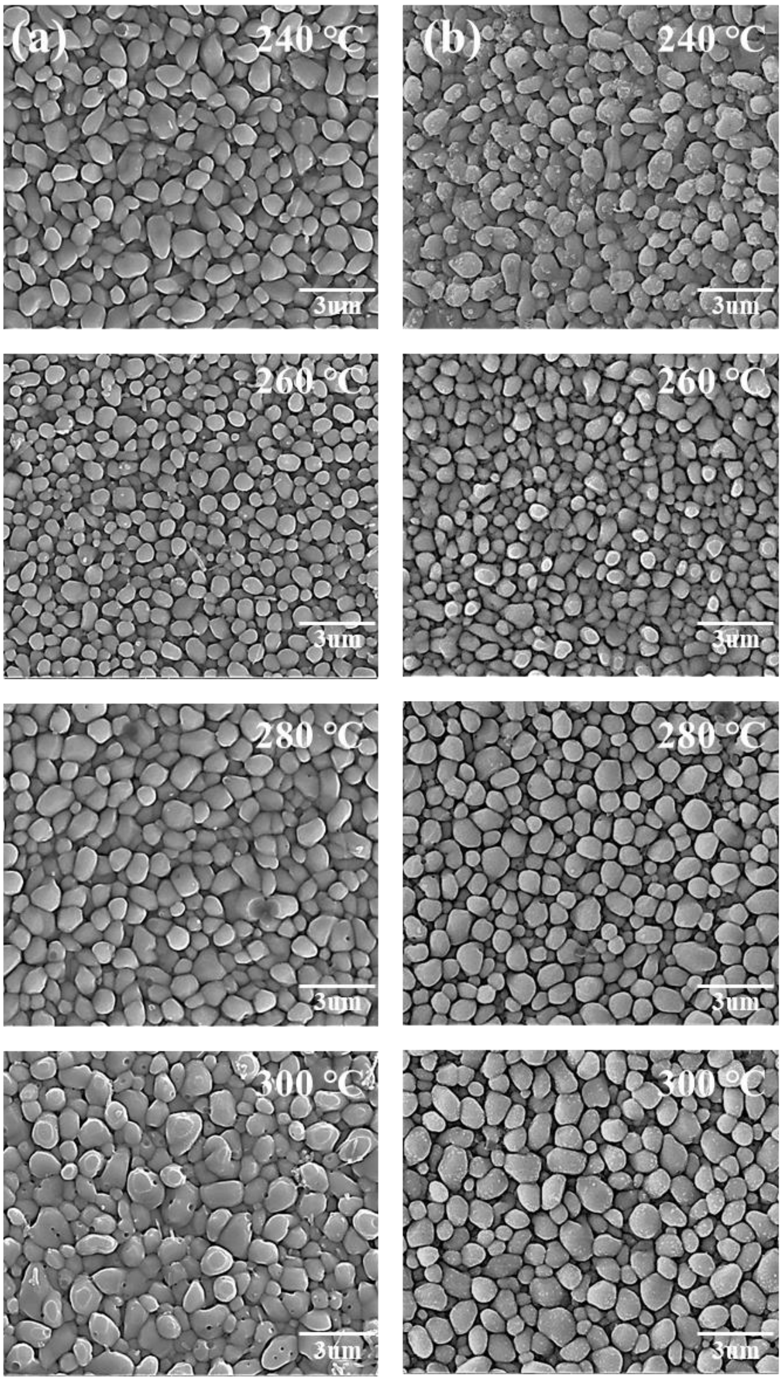

Figure 4.18 Top views image of Cu_6Sn_5 IMCs for 1(s) dipping at various reaction temperature at the (a) SC07/Cu (b) SC-0.2Cr/Cu joint.

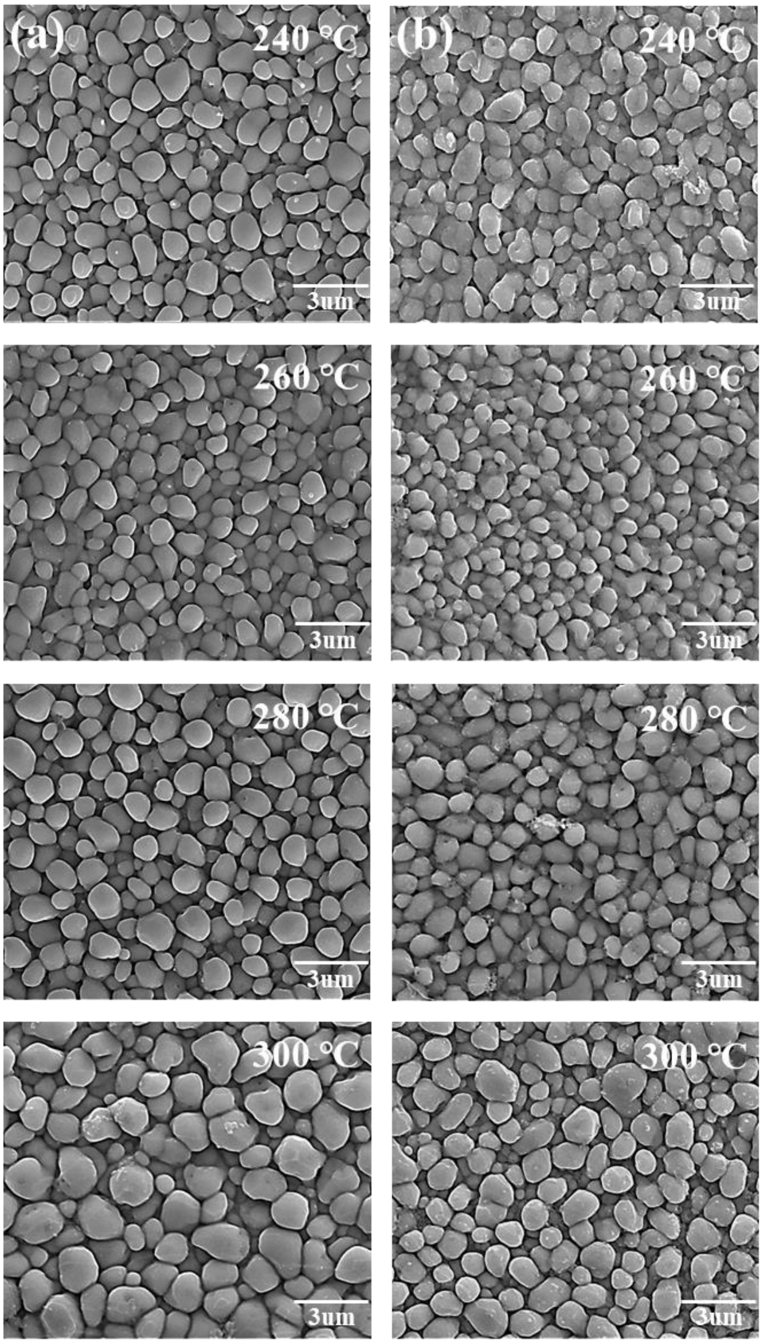

Figure 4.19 Top views image of Cu_6Sn_5 IMCs for 3(s) dipping at various reaction temperature at the (a) SC07/Cu (b) SC-0.2Cr/Cu joint.

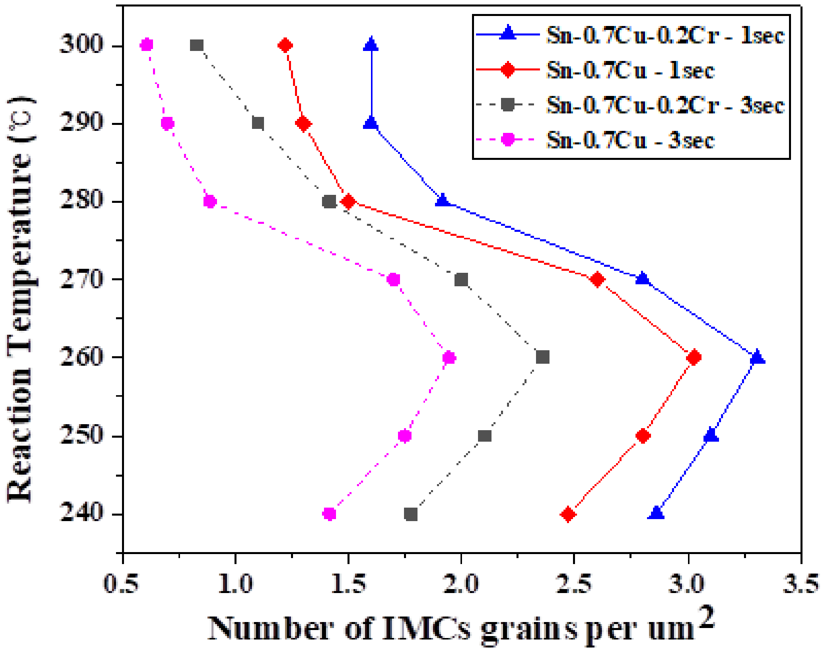

Figure 4.20 Number of Cu_6Sn_5 IMC grain per um^2 at various reaction temperature.

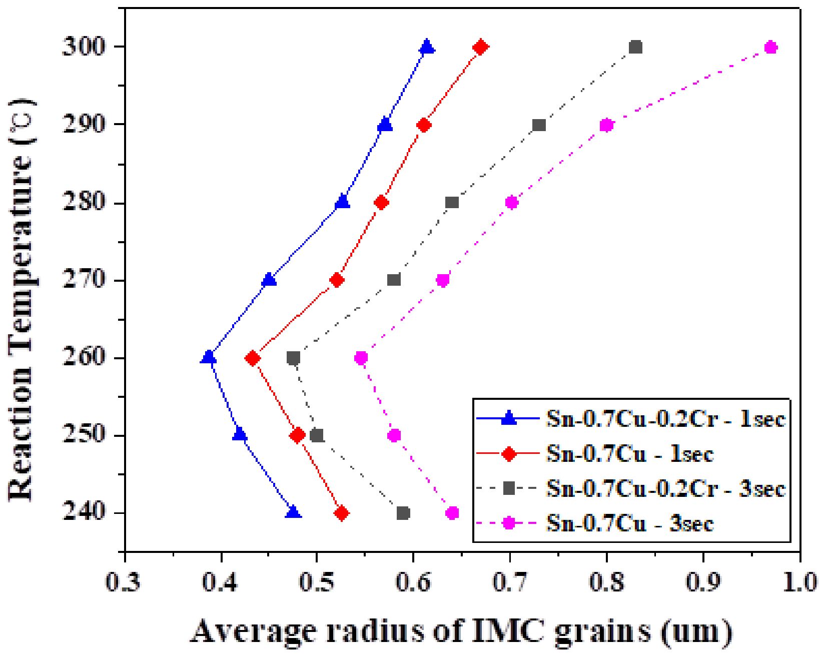

Figure 4.21 Average radius of Cu_6Sn_5 IMC grain at various reaction temperature.

4.4 Conclusion

This chapter evaluated the IMC growth behavior and mechanical properties of the SC-0.2Cr/Cu joint interface under high temperatures. In the as-reflow condition, the SC-0.2Cr/Cu joint showed very fine Cu_6Sn_5 compared to the SAC305/Cu and SC07/Cu joints. The addition of Cr likely reduced the undercooling or free energy required for nuclear formation and the critical nucleus size required for solidification. Thermal aging, thermal shock, and multiple reflow were used for the heat treatment of the solder joint sample. In each heat treatment process, the SC-0.2Cr/Cu joint inhibited IMC growth more effectively than the SAC305/Cu and SC07/Cu joints. In particular, the growth of Cu_3Sn was greatly reduced, and the formation of the Kirkendall void between Cu_3Sn and Cu substrate was greatly suppressed. STEM and EPMA were used to observe the dispersed $CrSn_2$ near Cu_6Sn_5. $CrSn_2$ present at the interface likely interfered with the interdiffusion of Sn and Cu, thereby effectively suppressing the growth rate of IMC.

4.5 Bibliography

[1] Gain, A.K.; Zhang, L. "Microstructure, thermal analysis and damping properties of Ag and Ni nano-particles doped Sn–8Zn–3Bi solder on OSP-Cu substrate" J. Alloy. Compd. 617 (2014) 779–786.

[2] Zhang, S.; Yang, M.; Wu, Y.; Du, J.; Lin, T.; Peng, H.; Huang, M.; Paik, K.W. "A study on the optimization of anisotropic conductive films for Sn-3Ag-0.5Cu-Based flex-on-board application at a 250 ℃ bonding temperature" IEEE Trans. Comp. Pack. Manuf. 8 (2018) 1–9.

[3] Fouzder, T.; Li, Q.; Chan, Y.; Chan, D. "Interfacial microstructure and hardness of nickel (Ni) nanoparticle-doped tin-silver-copper (Sn-Ag-Cu) solders on immersion silver (Ag)-plated copper (Cu) substrates" J. Mater. Sci. Mater. Electron. 25 (2014) 4012–4023.

[4] Chen, X.; Zhou, J.; Xue, F.; Bai, J.; Yao, Y. "Microstructures and mechanical properties of Sn-0.1Ag-0.7Cu-(Co, Ni, and Nd) lead-free solders" J. Electron. Mater. 44 (2015) 725–732.

[5] Chen, X.; Hu, A.; Li, M.; Mao, D. "Effect of a trace of Cr on intermetallic compound layer for tin–zinc lead-free solder joint during aging" J. Alloy. Compd. 470 (2009) 429–433.

[6] Bi, J.; Hu, A.; Hu, J.; Luo, T.; Li, M.; Mao, D. "Effect of Cr additions on interfacial reaction between the Sn–Zn–Bi solder and Cu/electroplated Ni substrates" Microelectron. Reliab. 51 (2011) 636–641.

[7] Zhang, L.; Tu, K.N. "Structure and properties of lead-free solders bearing micro and nano particles" Mater. Sci. Eng. R Rep. 82 (2014) 1–32.

[8] Yakymovych, A.; Plevachuk, Y.; Švec, P., Sr.; Švec, P.; Janičkovič, D.; Šebo, P.; Janičkovič, D.; Šebo, P.; Beronská, N.; Roshanghias, A.; etc. "Morphology and shear strength of lead-free solder joints with $Sn_{3.0}Ag_{0.5}Cu$ solder paste reinforced with ceramic nanoparticles" J. Electron. Mater. 45 (2016) 6143–6149.

[9] Xing, W.Q.; Yu, X.Y.; Li, H.; Ma, L.; Zuo, W.; Dong, P.; Wang, W.X.; Ding, M. "Effect of nano Al_2O_3 additions on the interfacial behavior and mechanical properties of eutectic Sn-9Zn solder on low temperature wetting and soldering of 6061 aluminum alloys" J. Alloy. Compd. 695 (2017) 574–582.

[10] Yang, M.; Ko, Y.-H.; Bang, J.; Kim, T.-S.; Lee, C.-W.; Li, M. "Effects of Ag addition on solid–state interfacial reactions between Sn–Ag–Cu solder and Cu substrate" Mater. Charact. 124 (2017) 250–259.

[11] N, Mookam, P. Tunthawiroon, and K. Kanlayasiri, "Effects of copper content in Sn-based solder on the intermetallic phase formation and growth during soldering" ICMM 361 (2018) 012008.

[12] C. Yu, H. Lu, and S. Li, "Effect of Zn addition on the formation and growth of intermetallic compound at Sn–3.5 wt% Ag/Cu interface" J. of Alloys and Compd. 460 (2008) 594–598.

[13] Ai Ting Tan, Ai Wen Tan and Farazila Yusof "Influence of nanoparticle addition on the formation and growth of intermetallic compounds (IMCs) in Cu/Sn–Ag–Cu/Cu solder joint during different thermal conditions" Sci. Technol. Adv. Mater. 16 (2015) 033505.

[14] M.S. Park, R. Arroyave,"Formation and growth of intermetallic compound Cu6Sn5 at early stages in lead-free soldering" Journal of Electronic Materials, 39 (2010) 2574-2582.

[15] H.R Kotadia, O. Mokhtari, M.P. Clode, M.A Green, S.H Mannan, "Intermetallic compound growth suppression at high temperature in SAC solders with addition on Cu and Ni-P substrates" J. of

Alloys and Compd. 511 (2012) 176-188.

[16] Yang, M.; Cao, Y.; Joo, S.; Chen, H.; Ma, X.; Li, M. "Cu_6Sn_5 precipitation during Sn-based solder/Cu joint solidification and its effects on the growth of interfacial intermetallic compounds" J. Alloys Compd. 582 (2014) 688–695.

[17] Ghosh, G.; Asta, M. "Phase stability, phase transformations, and elastic properties of Cu_6Sn_5: Ab initio calculations and experimental results" J. Mater. Res. 20 (2005) 3102–3117.

[18] Nogita, K.; Gourlay, C.M.; Nishimura, T. "Cracking and phase stability in reaction layers between Sn-Cu-Ni solders and Cu substrates" JOM 61 (2009) 45–51.

[19] K.N. Tu (Ed.). "Solder Joint Technology: Materials, Properties, and Reliability" Springer, New York, (2007) 386.

[20] He Gao, Fuxiang Wei, Yanwei Sui, Jiqiu Qi, "Growth behaviors of intermetallic compounds on the Sn-0.7Cu-10BixCo/Co interface during multiple reflow" Materials and Design 174 (2019) 107794.

[21] T.L. Yang, J.J. Yu, W.L. Shih, C.H. Hsueh, C.R. Kao, "Effects of silver addition on Cu–Sn microjoints for chip-stacking applications" J. Alloys Compd. 605 (2014) 193–198.

[22] A.K. Gain, L. Zhang, Y.C. Chan, "Microstructure, elastic modulus and shear strength of alumina (Al_2O_3) nanoparticles-doped tin–silver–copper (Sn–Ag–Cu) solders on copper (Cu) and gold/nickel (Au/Ni)-plated Cu substrates, J. Mater. Sci. Mater. Electron" 26 (2015) 7039–7048.

[23] Haoran Ma, Anil Kunwar, Ru Huang, Jun Chen, Yunpeng Wang, Ning Zhao, Haitao Ma, " Size effect on IMC growth induced by Cu concentration gradient and pinning of Ag_3Sn particles during multiple reflows" Intermetallics 90 (2017) 90–96.

[24] M. Venkatraman, J.P. Neumann, "The Cr-Sn (chromium-tin) system" Bulletin of Alloy Phase Diagrams, 9 (1988) 159-162.

[25] T. Wölpl, W. Jeitschko, "Crystal structures of VSn2, NbSn2 and CrSn2 with Mg2Cu-type structure and NbSnSb with CuAl2-type structure" Journal of Alloys and Compounds, 210 (1994) 185-190.

[26] J.H. Koo, J.W. Chang, Y.W. Lee, S.J. Hong, K.S. Kim, H.M. Lee, "New Sn–0.7Cu-based solder alloys with minor alloying additions of Pd, Cr and Ca" J. Alloys Compd. 608 (2014) 126–132.

[27] Zhongbing Luo, Lai Wang, Qinqin Fu, Chongqian Cheng, and Jie Zhao, "Formation of interfacial g9-Cu6Sn5 in Sn–0.7Cu/Cu solder joints during isothermal aging" J. Mater. Res., 26 (2011) 1468.

[28] R.A. GAGLIANO, G. GHOSH, and M.E. FINE, "Nucleation Kinetics of Cu6Sn5 by Reaction of Molten Tin with a Copper Substrate" Journal of ELECTRONIC MATERIALS, 31 (2002) 1195–1202.

[29] M.S. Park a, R. Arro´yave "Concurrent nucleation, formation and growth of two intermetallic compounds (Cu6Sn5 and Cu3Sn) during the early stages of lead-free soldering" Acta Materialia 60 (2012) 923–934.

Chapter 5

Calculation of activation energy and life prediction of SC-Cr/Cu solder joint

5.1 Introduction

A thick IMC growth on the interface typically results in negative consequences [1–3]. The brittle nature of the IMC and its mismatching physical properties, such as thermal expansion coefficient and elastic modulus, lead to a weak bonding characteristic. Furthermore, if the IMC is too thick, the ductility and the strength of the solder can weaken [4]. Researchers have recently developed composite solders that offer better characteristics over the existing conventional solders [5–8]. There are studies that discuss and analyze the microstructure, mechanical properties, and interfacial properties of Sn-based solders with trace elements added [8–10]. However, studies on Sn-Cu based solders with added Cr are currently very limited. This chapter focuses on IMC growth kinetics during solid-state aging of Cr-added Sn-Cu interfaces. The activation energy of IMC growth is calculated by the square root of IMC layer growth rates at various temperatures [11].

Initially, the fatigue model of a solder joint was developed using data from temperature cycling experiments. Most models that assess the fatigue of a solder joint require stress-strain data.

Table 5.1 Summary of solder joint fatigue models.

	Fatigue model	Equation nos.	Model class	Applicable packages	Required parameters	Coverage	Constants
1	Coffin-Manson	2	Plastic strain	All	Plastic strain	Low cycle fatigue	c = constant, ε_f' = fatigue ductility coefficient
2	Total strain (Coffin-Manson-Basquin)	3	Plastic strain + elastic strain	All	Strain range	High and low cycle fatigue	b = fatigue strength exponent c = fatigue ductility exponent σ_f' = fatigue strength coefficient ε_f' = fatigue ductility coefficient
3	Solomon	4	Plastic shear strain	All	Plastic shear strain,	Low cycle fatigue	α = constant θ = inverse fatigue ductility coefficient
4	Engelmaier	5	Total shear strain	Leaded and leadless, TSOP	Total shear strain	Low cycle fatigue	$c = -0.442 - 6e - 4T_s + 1.74e - 2\ln(1 + f\ )$ T_s = mean cyclic solder joint temp (°C) f = cyclic frequency (cycles/day), $2\varepsilon_f' = 0.65$
5	Miner	6, 7	Superposition (plastic and creep)	PQFP, FCOB w/ fill	Plastic failure and creep failure	Plastic shear and matrix creep	N_p = plastic failure, N_c = creep failure
6	Knecht and Fox	8	Matrix creep	All	Matrix creep shear strain	Matrix creep only	$c = 890\%$
7	Syed	9	Accumulation of creep strain energy	PBGA, SMD, NSMD	gbs energy and mc energy	Implies full coverage	E_{gbs} = accumulated equivalent creep strain/cycle E_{mc} = accumulated equivalent matrix creep/cycle
8	Dasgupta	10	Total strain energy	LLCC, TSOP	Energy	Joint geometry accounted for	ΔW_{total} = total strain energy density $W_0 = 0.1573$, $k = -0.6342$
9	Liang	11	Stress/strain energy density based	BGA and leadless joints	Energy	Constants from isothermal low cycle fatigue tests	C and m = temperature dependent material constants W_{ss} = stress strain hysteresis energy
10	Heinrich	12, 13	Energy density based	BGA	Energy	Hysteresis curve	ΔW = viscoplastic strain energy/cycle
11	Darveaux	14	Energy density based	Leadless, PBGA	Damage + energy	Hysteresis curve	a = total possible crack length da/dN = crack growth, N_o = crack initiation
12	Pan	17	Strain energy density	LCCC	Strain energy density and plastic energy density	Hysteresis curve	C = strain energy density E_p = plastic strain creep energy density/cycle E_c = creep strain energy density/cycle
13	Stolkarts	18	Damage accumulation	All	Damage	Hysteresis curve and damage evolution	$d = 0.5$ for solder (damage parameter) k = material constant
14	Norris and Landzberg	19	Temperature and frequency	All	Temperature frequency	Test condition versus use conditions	u-use t-test f-frequency T = temperature Φ_u/Φ_t = isothermal fatigue life ratio

These data were collected using strain gauges [12]. **Table 5.1** shows the fatigue models of solder joints [12]. Usually, a solder joint fatigue model utilizes the Norris and Landzberg model, which was developed by improving the Coffin-manson low cycle fatigue model of a metal [13].

5.2 Experimental procedures

5.2.1 Isothermal aging and thermal shock

The aging temperatures were set to 100 ℃, 125 ℃, and 150 ℃. And the thermal shock conditions were set to -40 to 85 ℃, -40 to 100 ℃ and -40 to 150 ℃.

Detailed information of experimental procedures on the thermal aging and thermal shock method can be found in *Chapter 3.2.5.*

5.2.2 Measuring of IMC thickness

The microstructure of the IMC was observed using scanning electron microscopy (SEM, Hitachi S-4700) and energy dispersive X-ray spectroscopy (EDX, EDAX Genesis XM2 60). To further observe the thermal stress, the thickness and microstructure of the IMC were measured using cross-sectional images according to the following procedure [14]: (1) an SEM image of each sample was obtained at the appropriate magnification, (2) the grayscale SEM image was enhanced using Adobe Photoshop to identify the interfaces between the different layers, and (3) the mean thickness (H_{IMC}) of the individual layers was calculated using the following equation:

$$H_{IMC}=H_{SEM}\times N_{IMC}/N_{SEM} \quad (5.1)$$

where H_{SEM} is the actual height of the SEM image, and N_{IMC} and N_{SEM} are the numbers of pixels in the IMC layers and the entire image, respectively.

5.3 Results and discussion

5.3.1 Calculation of activation energy

Typically, the thickness of the reaction layer for a diffusion couple can be represented using a simple parabolic equation [15–17].

$$W = kt^{n} \quad (5.2)$$

Where W refers to the thickness of an IMC layer, k refers to the increasing rate constant, t refers to the reaction time, and n refers to the time index. **Figure 5.1** shows the thickness of the IMC layer as a function of the square root of each thermal aging time. In this case, when the reaction is mainly controlled by a diffusion mechanism, the value of n is empirically determined to be 0.5 [15]. The average thickness of the interfacial IMC layer was found to increase linearly with the square root of the thermal aging time, and the increasing rate of the thickness became higher at higher temperatures. However, the SC-0.2Cr/Cu joint shows a significantly lower increase in total thickness compared with the other two systems.

The Arrhenius relationship is used to calculate the activation energy for the growth of all IMCs and the Cu_3Sn layer [15–19].

$$k^2 = k_0^2 \exp\left(-\frac{Q}{RT}\right) \quad (5.3)$$

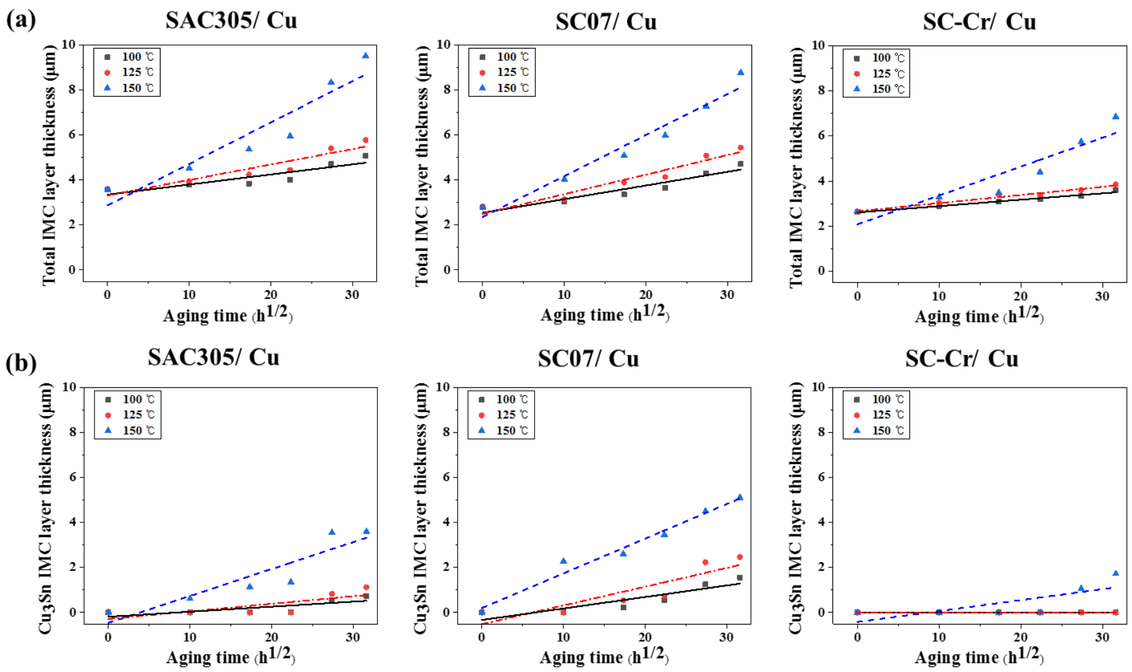

Figure 5.1 Average thickness of IMC: (a) total IMC and (b) Cu_3Sn at different temperatures.

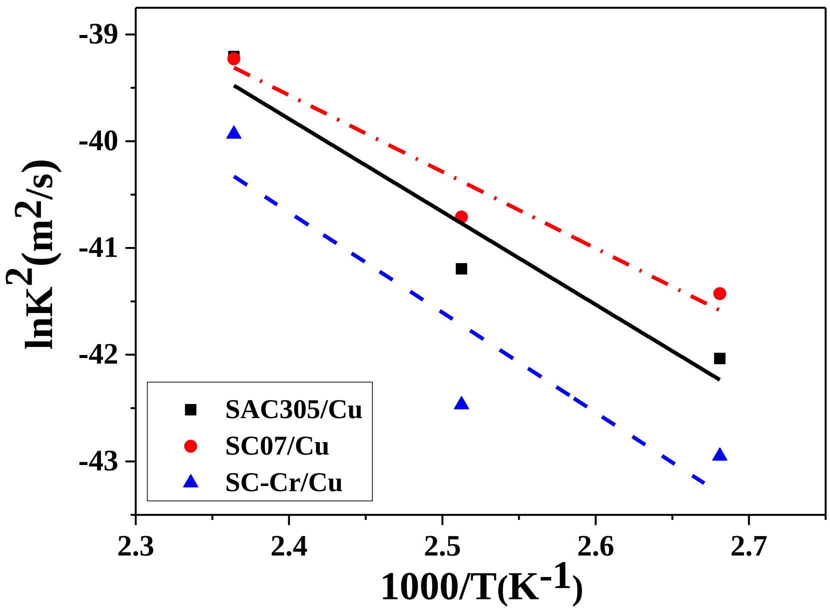

Figure 5.2 Arrhenius plot of total IMC layer growth.

Table 5.2 Calculated values of the activation energy (Q) for the growth of the IMCs layers.

Solder/substrate	Temperature range (℃)	Reaction time (h)	Intermetallics	Activation energy (kJ/mol)	Diffusion couple method	Reference
SAC305/Cu	100 – 150	1,000	$Cu_6Sn_5 + Cu_3Sn$	73.52	Reflow	This work
SC07/Cu	100 – 150	1,000	$Cu_6Sn_5 + Cu_3Sn$	57.31	Reflow	This work
SC-Cr/Cu	100 – 150	1,000	$Cu_6Sn_5 + Cu_3Sn$	77.96	Reflow	This work

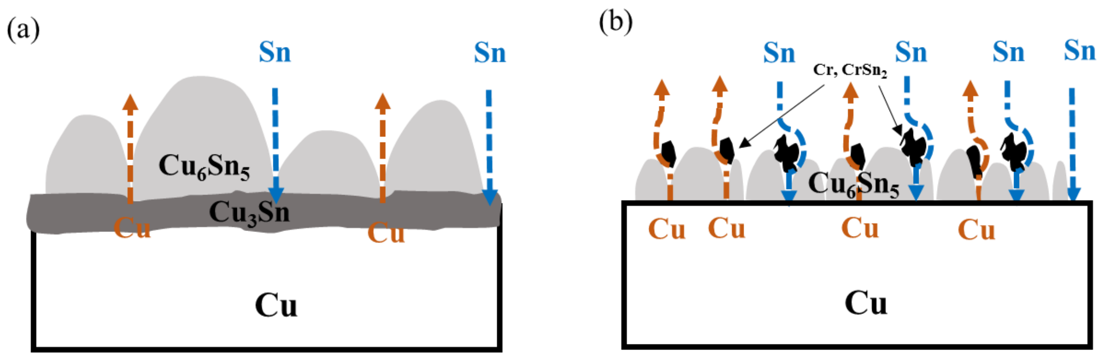

Figure 5.3 Schematics of Cu and Sn interdiffusion in (a) SC07/Cu and (b) SC-0.2Cr/Cu joints.

Where k^2 refers to the square of the reaction constant, k_0^2 refers to the frequency factor, Q refers to the activation energy, R refers to the gas constant (8.314 J/mol K), and T refers to the thermal aging temperature. The activation energy was calculated from the Arrhenius plot based on a linear model. **Figure 5.2** shows the Arrhenius plot of the activation energies of all IMCs and Cu_3Sn, as calculated for each diffusion system. As shown in **Table 5.2**, the activation energies were 73.52 kJ mol for the SAC305/Cu, 57.31 kJ/mol for the SC07/Cu, and 77.96 kJ/mol for the SC-0.2Cr/Cu joint. These results are similar to those of Yoon et al. and Abdelhadi et al. [15,18]. The activation energy of IMC growth during isothermal aging is an energy barrier for the interdiffusion and reaction between Cu and Sn at the interface. Therefore, the higher activation energy indicates more difficult IMC growth. In conclusion, Cu diffuses into Sn and forms a Cu-Sn compound at the interface. At this time, the addition of Cr does not reduce the kinetic energy of Cu directly. However, IMC growth in the solid state reaction was inhibited by precipitation of CrSn2 at the boundary of Cu6Sn5 (main diffusion path of Cu), and the result was calculated as the activation energy of the interfacial IMC as a factor.

Fig. 5.3 shows the diffusion behavior of Cu and Sn according to the precipitation of $CrSn_2$ in the SC-0.2Cr/Cu joint. The migration of Cu and Sn occurs through the fast diffusion channels, such as grain boundary and dislocation in elevated temperature. When Cr was added to the Sn-0.7Cu alloy, Cr reacted with Sn to form $CrSn_2$, and $CrSn_2$ precipitated near the Cu_6Sn_5 interface, which act as a barrier to the diffusion of Cu into Sn. As a result, interfacial IMC growth in solid state diffusion was depressed. As previous studies have indicated, $CrSn_2$ produced during the alloy fabrication process is precipitated near the IMC layers and dispersed, and some products are observed at the Cu_6Sn_5 grain boundary [20]. These results indicate that the addition of Cr in Sn-Cu solder is effective for the suppression of the increase in thickness of all IMCs, including Cu_3Sn. In addition, It was reported that the adding minor elements precipitated near the grain boundary effectively inhibited the growth of IMC by blocking the diffusion path [21,22].

5.3.2 Calculation of acceleration factor(AF)

Figure 5.4 shows Weibull plot for chip joint failure according to a thermal shock test at -40 °C to 150 °C. The thermal shock test was performed up to 3,000 cycles, and a resistance increase by 20 % or more was determined as failure after measuring the resistance every 500 cycles. Here, the scale parameters show a reliability life of 63.2 %, and the values of scale parameters are listed in **Table 5.3**. The scale parameters of SAC305/Cu, SC07/Cu and SC-0.2Cr/Cu joints were determined as approximately 3,899 cycles, 5,491 cycles, and 6,223 cycles, respectively. The scale parameter of an SC-0.2Cr/Cu was approximately 11 % higher than that of an SC07/Cu joint, and approximately 37 % higher than that of an SAC305/Cu joint.

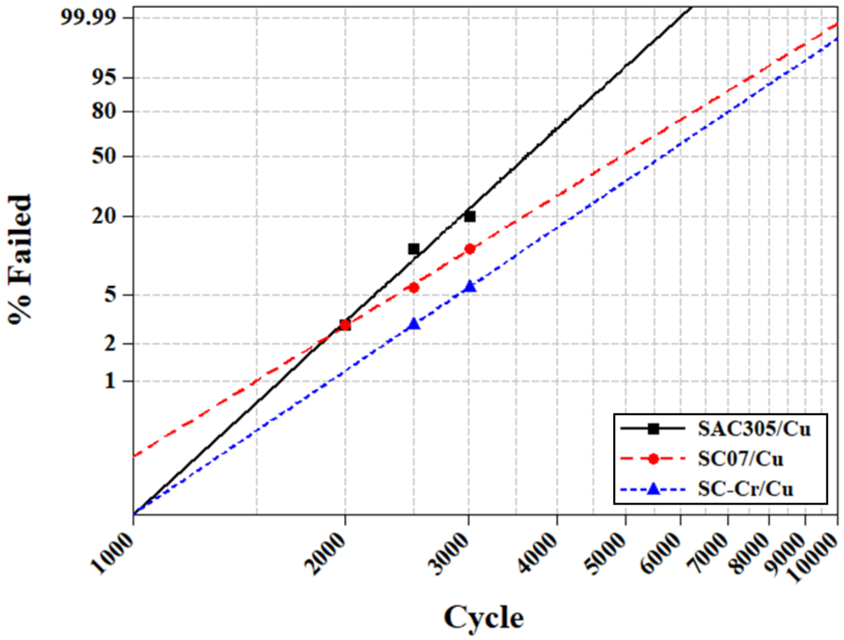

Figure 5.4 Weibull plot of joint failure by thermal shock test.

Table 5.3 Scale parameter of SAC305/Cu, SC07/Cu and SC-0.2Cr/Cu joints.

Diffusion couple	scale parameter (cycle)
SAC305/Cu	3,889
SC07/Cu	5,491
SC-Cr/0.2Cu	**6,223**

After the thermal shock test, the Norris and Landzberg equation was applied to determine the acceleration factor (AF) corresponding to the use conditions of the automotive module, as follows [23]:

$$\mathrm{AF} = \left(\frac{\Delta T_{test}}{\Delta T_{field}}\right)^{-b} \times \left(\frac{f_{field}}{f_{test}}\right)^{-a} exp\left[\frac{Ea}{k}\left(\frac{1}{T_{max,field}} - \frac{1}{T_{max,test}}\right)\right] \quad (5.4)$$

where

AF = Acceleration factor

ΔT_{test} = The temperature range during a cycle at test condition

ΔT_{field} = The temperature range during a cycle at field condition

f_{test} = The cycling frequency at test condition

f_{field} = The cycling frequency at field condition

a = Cycling frequency exponent

b = Temperature range exponent

K = Boltzman's constant 8.623 x 10-5 eV/K

Ea = Activation Energy

According to a previous study that determined the AF using Pb-free solders, the *a* value and the *b* value were set as 1.662 and 1/3, respectively [24]. Thus, assuming that the solders used in this study are similar to the Pb-free solders in the previous study, the *a* value and the *b* value were set as 1.662 and 1/3, respectively. Furthermore, the activation energy (*Ea*) was determined through an aging test. **Table 5.4** shows test and field conditions, and the field conditions were selected in reference to the specifications of an automobile manufacturer.

5.3.3 Life prediction of solder joint using fatigue models

To derive the AF, the test conditions were set as -40 °C to 150 °C, which are harsher than the field conditions. As a result, the AFs were determined as 1.823, 1.327, and 1.987 for the SAC305/Cu, SC07/Cu and SC-0.2Cr/Cu joints, respectively. The life prediction cycle for the use conditions of actual automotive electronics was calculated suing the following equation:

$$N_{test\ cycle} = \frac{N_{field\ cycle}}{AF} \quad (5.5)$$

Based on the previously determined AF for each solder, **Table 5.5** shows the predicted field cycles according to test conditions. The field cycles of the SAC305/Cu, SC07/Cu and SC-0.2Cr/Cu joints were determined as approximately 7,090, 7,287 and 12,366 cycles, respectively.

On the assumption that the field warranty life is 10 years, the predicted field life cycle is calculated as 7,300 cycles. Thus, the SC-0.2Cr/Cu joint met the required field warranty life of 10 years, whereas the SAC305 and SC07 solders did not satisfy this requirement.

Table 5.4 Thermal shock test and field condition for automotive module.

	T_{min} (°C)	T_{max} (°C)	△T (°C)	Frequency of Usage (cycles per day)
Test condition	-40	150	190	48
Field condition	-40	125	165	2

Table 5.5 Predicted field cycle of SAC305/Cu, SC07/Cu and SC-0.2Cr/Cu joints.

Diffusion couple	$N_{field\ cycle}$ (cycle)
SAC305/Cu	7,090
SC07/Cu	7,287
SC-Cr/0.2Cu	**12,366**

5.4 Conclusion

The growth behavior of IMC was evaluated after aging at 100℃, 125℃ and 150℃ respectively to calculate to the activation energy of SC-0.2Cr/Cu joint. The activation energies were 73.52 kJ mol for the SAC305/Cu, 57.31 kJ/mol for the SC07/Cu, and 77.96 kJ/mol for the SC-0.2Cr/Cu joint. These results are similar to those of Yoon et al. and Abdelhadi et al. The activation energy of IMC growth during isothermal aging is an energy barrier for the interdiffusion and reaction between Cu and Sn at the interface. Therefore, the higher activation energy indicates more difficult IMC growth.

To calculation of AF, the thermal shock test condition was set as -40 °C to 150 °C, which are harsher than the field conditions. As a result, the AFs were determined as 1.823, 1.327, and 1.987 for the SAC305/Cu, SC07/Cu and SC-0.2Cr/Cu joints, respectively. Based on the previously determined AF for each solder, the predicted field life cycles of the SAC305/Cu, SC07/Cu and SC-0.2Cr/Cu joints were determined as approximately 7,090, 7,287 and 12,366 cycles, respectively.

5.5 Bibliography

[1] Yu-Yun Shiue, Tung-Han Chuang "Effect of La addition on the interfacial intermetallics and bonding strengths of Sn–58Bi solder joints with Au/Ni/Cu pads" Journal of Alloys and Compounds 491 (2010) 610–617.

[2] G. GHOSH "INTERFACIAL MICROSTRUCTURE AND THE KINETICS OF INTERFACIAL REACTION IN DIFFUSION COUPLES BETWEEN Sn–Pb SOLDER AND Cu/Ni/Pd METALLIZATION" Acta mater. 48 (2000) 3719–3738.

[3] Xin Ma, Fengjiang Wang, Yiyu Qian, Fusahito Yoshida "Development of Cu–Sn intermetallic compound at Pb-free solder/Cu joint interface" Materials Letters 57 (2003) 3361– 3365.

[4] WENGE YANG, LAWRENCE E. FELTON, and ROBERT W. MESSLER, JR. "The Effect of Soldering Process Variables on the Microstructure and Mechanical Properties of Eutectic Sn-Ag/Cu Solder Joints" Journal of Electronic Materials, 24 (1995).

[5] T. H. Chuang, M. W. Wu, S. Y. Chang, S. F. Ping, L. C. Tsao "Strengthening mechanism of nano-Al2O3 particles reinforced Sn3.5Ag0.5Cu lead-free solder" J Mater Sci: Mater Electron (2011) 22:1021–1027.

[6] Asit Kumar Gain, Tama Fouzder, Y.C. Chan, A. Sharif , N.B. Wong, Winco K.C. Yungd "The influence of addition of Al nano-particles on the microstructure and shear strength of eutectic Sn–Ag–Cu solder on Au/Ni metallized Cu pads" Journal of Alloys and Compounds 506 (2010) 216–223.

[7] He Gao, Fuxiang Wei, Yanwei Sui, Jiqiu Qi "Growth behaviors of intermetallic compounds on the Sn-0.7Cu-10BixCo/Co interface during multiple reflow" Materials and Design 174 (2019) 107794.

[8] L.C. Tsao, S.Y. Chang, C.I. Lee, W.H. Sun, C.H. Huang "Effects of nano-Al2O3 additions on microstructure development and hardness of Sn3.5Ag0.5Cu solder" Materials and Design 31 (2010) 4831–4835.

[9] L.C. Tsao, C.P. Chu, S.F. Peng "Study of interfacial reactions between Sn3.5Ag0.5Cu composite alloys and Cu substrate" Microelectronic Engineering 88 (2011) 2964–2969.

[10] J. Shen, Y.C. Liu, Y.J. Han, Y.M. Tian, H.X. Gao "Erratum to Strengthening effects of ZrO2 nanoparticles on the microstructure and microhardness of Sn–3.5Ag lead-free solder" Materials

Science and Engineering A 476 (2008) 378.

[11] L.C. Tsao "Suppressing effect of 0.5 wt.% nano-TiO2 addition into Sn–3.5Ag–0.5Cu solder alloy on the intermetallic growth with Cu substrate during isothermal aging" Journal of Alloys and Compounds 509 (2011) 8441– 8448.

[12] W.W. Lee, L.T. Nguyen, G.S. Selvaduray "Solder joint fatigue models: review and applicability to chip scale packages" Microelectronics Reliability 40 (2000) 231–244.

[13] Rajendra D. Pendse, Peng Zhou "Methodology for predicting solder joint reliability in semiconductor packages" Microelectronics Reliability 42 (2002) 301–305.

[14] M. Yang, H. Ji, S. Wang, Y.H. Ko, C.W. Lee, J. Wu, M. Li "Effects of Ag content on the interfacial reactions between liquid Sn–Ag–Cu solders and Cu substrates during soldering" J. Alloys Compd. 679 (2016) 18–25.

[15] J.W. Yoon, Y.H. Lee, D.G. Kim, H.B. Kang, S.J. Suh, C.W. Yang, C.B. Lee, J.M. Jung, C.S. Yoo, S.B. Jung "Intermetallic compound layer growth at the interface between Sn–Cu–Ni solder and Cu substrate" J. of Alloys and Compd. 381 (2004) 151–157.

[16] J.W. Yoon, B.I. Noha, B.K. Kim, C.C. Shur, S.B. Jung "Wettability and interfacial reactions of Sn–Ag–Cu/Cu and Sn–Ag–Ni/Cu solder joints" J. of Alloys and Compd. 486 (2009) 142–147.

[17] N. Dariavach, P. Callahan, J. Liang, and R. Fournelle "Intermetallic growth kinetics for Sn-Ag, Sn-Cu, and Sn-Ag-Cu lead-free solders on Cu, Ni, and Fe-42Ni substrates" Journal of Electronic Materials, 35 (2006) 1581–1592.

[18] O.M. Abdelhadi, L. Ladani "IMC growth of Sn-3.5Ag/Cu system: Combined chemical reaction and diffusion mechanisms" J. of Alloys and Compd. 437 (2012) 87–99.

[19] L.C. Tsao "Suppressing effect of 0.5 wt.% nano-TiO2 addition into Sn–3.5Ag–0.5Cu solder alloy on the intermetallic growth with Cu substrate during isothermal aging" J. of Alloys and Compd. 509 (2011) 8441–8448.

[20] J.H. Bang, D.Y. Yu, Y.H. Ko, M.S. Kim, H. Nishikawa, C.W. Lee "Intermetallic compound formation and mechanical property of Sn-Cu-xCr/Cu lead-free solder joint" J. Alloys Compd. 728 (2017) 992–1001.

[21] L. Xu, L. Wang, H. Jing, X. Liu, J. Wei and Y. Han "Effects of graphene nanosheets on interfacial reaction of Sn-Ag-Cu solder joints" Journal of Alloys and Compounds 650 (2015) 475-481.

[22] D. Ma, P. Wu "Improved microstructure and mechanical properties for Sn58Bi0.7Zn solder joint by addition of graphene nanosheets" Journal of Alloys and Compounds 671 (2016) 127-136.

[23] Norris KC, Landzberg AH. "Reliability of controlled collapse interconnections" IBM J Res Dev (1969) 266–271.

[24] Salmela Olli "Acceleration factors for lead free solder materials" IEEE Trans Component Package Technol. (2007) 700–706.

Chapter 6

Mechanical property and fracture mode of SC-0.2Cr/Cu joint

6.1 Introduction

The shear strength of the solder joints depends on the microstructure of the solder matrix and the interfacial connection. Generally, the shear strength of the solder joints decreased with thermal shock test [1–13]. According to Kim's simulation results of shear tests at different shear speeds [14,15], the shear force increased with increasing shear speed. At a low shear speed, the stress could be released though the deformation of the soft solder matrix, indicating that the shear strength should be more closely related to the strength of solder matrix; whereas at a high shear speed, due to the rapid deformation in solder matrix, a great stress would accumulate at the interface, indicating that the shear strength should be more related to the interfacial connection. Therefore, shear testing at shear speeds from 0.01 m/s to 1 m/s was conducted to examine the effects of solder microstructure and the interfacial IMCs on the joint reliability.

6.2 Experimental procedures

6.2.1 Evaluation of mechanical properties

To evaluate the mechanical properties of solder joints after thermal storage, thermal shock and multiple reflows, ball shear tests were conducted at the various shear speeds. Detailed information of experimental procedures on the evaluation method of mechanical properties of Sn-Cu-Cr solder can be found in *Chapter 3.2.4.*

6.3 Results and discussion

6.3.1 Shear strength of solder joint

Figures 6.1 – 6.3 shows the shear strength based on the shear speed after isothermal aging. Typically, all solders show a tendency to decrease their shear strength under thermal treatment [16–20]. At high speeds (1 m/s), the SC-0.2Cr/Cu joint showed a tendency in which the shear strength was maintained in comparison to the SAC305/Cu and SC07/Cu joints, despite no significant change in the shear strength at low speeds (0.01 and 0.1 m/s). **Table 6.1** show the degradation rate of shear strength after isothermal aging. Overall, the degradation rate of shear strength tended to increase as the aging temperature and shear speed increased. In particular, the SC-0.2Cr/Cu joint showed a 22.3 % decrease at 150 °C and 1 m/s, while the SAC305/Cu and SC07/Cu joints showed a 30 % and 35.7 % decrease, respectively. To determine the causes of the difference, the failure mechanism based on the shear rate must be derived.

Table 6.1 Degradation rate of shear strength after isothermal aging.

Solder/ Temp.	SAC305/Cu			SC07/Cu			SC-0.2Cr/Cu		
Shear speed	100℃	125℃	150℃	100℃	125℃	150℃	100℃	125℃	150℃
0.01(m/s)	18.6%	19.8%	24.8%	24.2%	24.8%	32.3%	12.8%	13.2%	11.6%
0.1(m/s)	13.7%	17.9%	20.6%	22.1%	25.5%	27.0%	10.3%	13.5%	15.3%
1(m/s)	20.1%	22.6%	30.0%	26.1%	26.7%	35.7%	9.3%	16.7%	22.3%

(a)

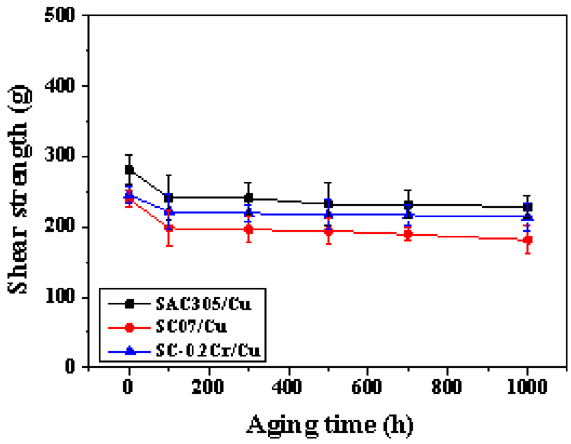

(b)

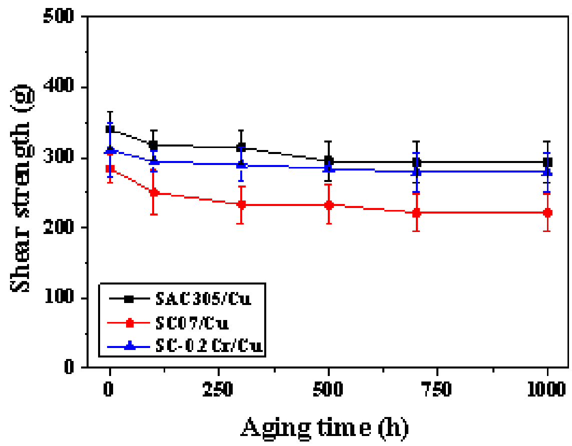

(c)

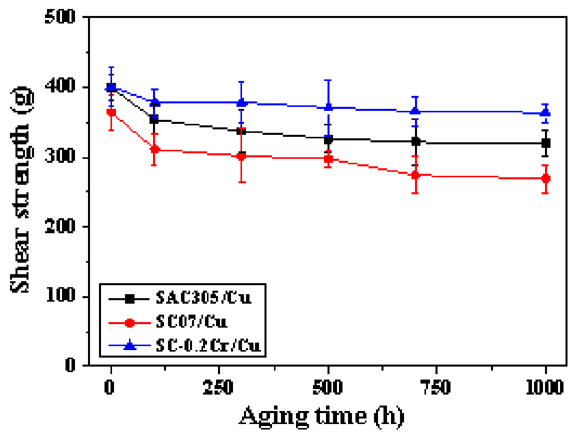

Figure 6.1 Shear strength of solder joints during isothermal aging at 100 ℃ under (a)0.01 m/s, (b)0.1 m/s and (c)1 m/s shear speed.

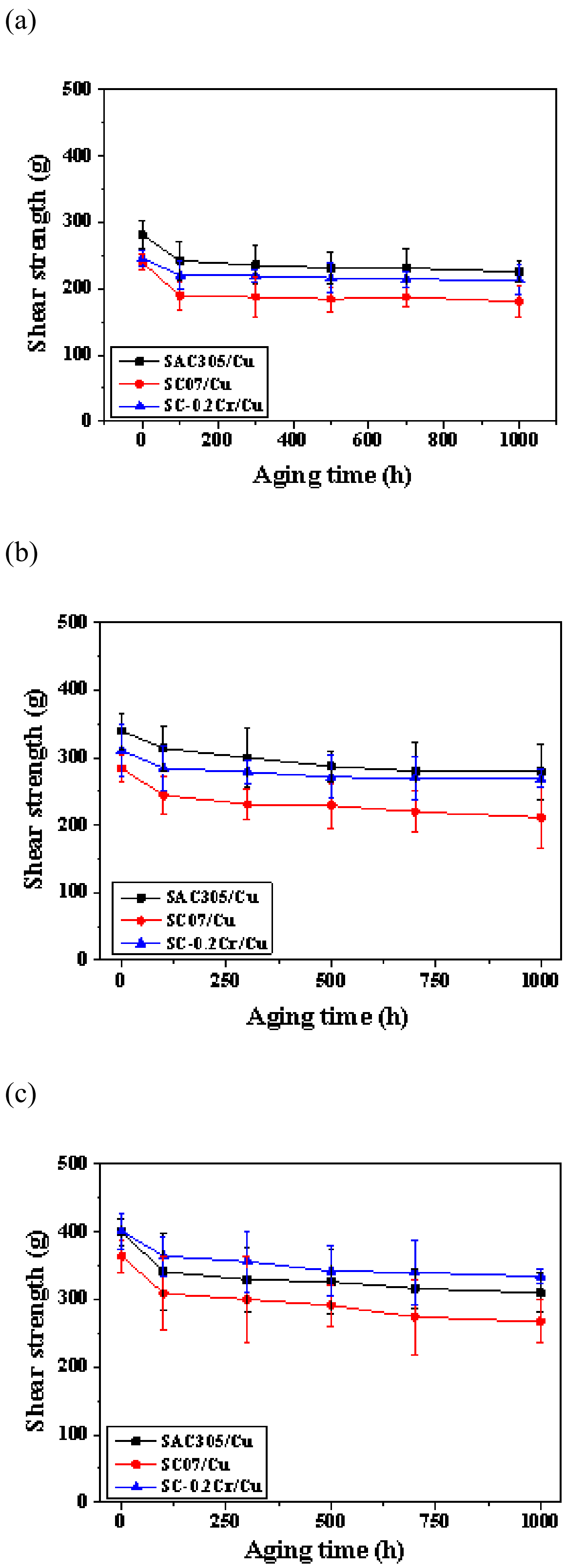

Figure 6.2 Shear strength of solder joints during isothermal aging at 125 ℃ under (a)0.01 m/s, (b)0.1 m/s and (c)1 m/s shear speed.

(a)

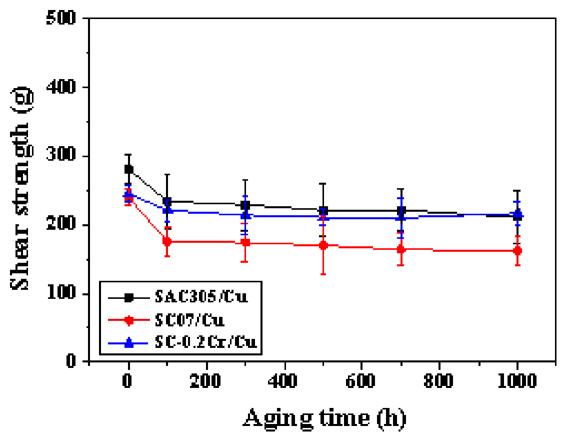

(b)

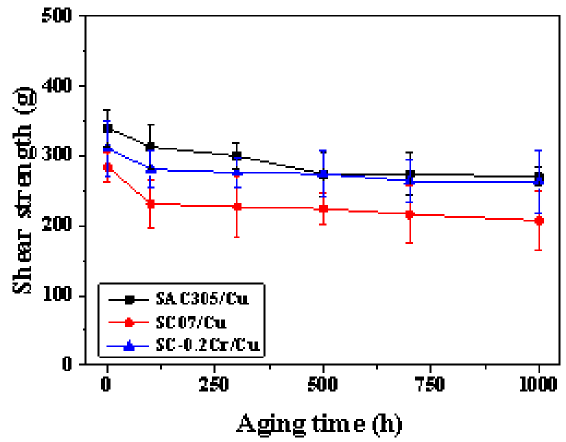

(c)

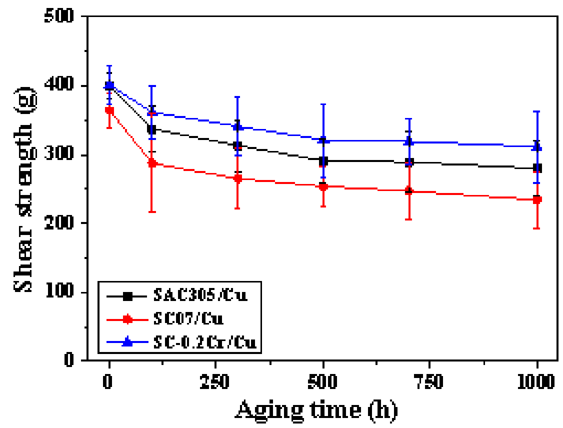

Figure 6.3 Shear strength of solder joints during isothermal aging at 150 ℃ under (a)0.01 m/s, (b)0.1 m/s and (c)1 m/s shear speed.

Table 6.2 Degradation rate of shear strength after thermal shock.

Solder/ Temp.	SAC305/Cu			SC07/Cu			SC-0.2Cr/Cu		
Shear speed	-40~85℃	-40~125℃	-40~150℃	-40~85℃	-40~125℃	-40~150℃	-40~85℃	-40~125℃	-40~150℃
0.01(m/s)	14.0%	22.6%	29.7%	16.5%	20.2%	37.2%	17.1%	17.6%	27.5%
0.1(m/s)	19.0%	27.9%	29.7%	21.9%	33.6%	39.8%	10.4%	18.3%	26.3%
1(m/s)	22.4%	30.5%	36.8%	34.4%	48.8%	53.3%	6.7%	14.7%	28.2%

Figures 6.4 – 6.6 shows the shear strength based on the shear speed after thermal shock. First, the initial shear strength of the SAC305/Cu joint was approximately 280 g under a shear rate of 0.01 m/s and the temperature range between -40℃ to 85℃. It was increased to approximately 320 g at a shear rate of 1 m/s. This result was similar to that of SC07/Cu. In the case of the SC-0.2Cr/Cu joint, however, the initial shear strength of 250 g was significantly increased to 380 g. Moreover, while the shear strengths of SAC305/Cu and SC07/Cu were continuously reduced, that of the SC-0.2Cr/Cu joint showed a tendency to be maintained from 500 cycles to 2,000 cycles. These results verify that the added Cr affected the initial shear strength of the solder joint and the effect became larger after the thermal shock cycles.

Table 6.2 shows the shear strength reduction rate after the thermal shock. While the shear strength reduction rates of SAC305/Cu and SC07/Cu increased as the temperature and the shear rate increased, that of the SC-0.2Cr/Cu joint showed a tendency to be maintained or rather reduced. In particular, under the temperature range between -40℃ and 85℃, it was observed that the degradation rate of shear strength significantly decreased as the shear rate increased. As a result, the SC-0.2Cr/Cu joint could effectively maintain its shear strength even under high shear rates at which the shear stress was concentrated on the interface because it significantly suppressed the interfacial IMC growth and Kirkendall void formation after the thermal shock.

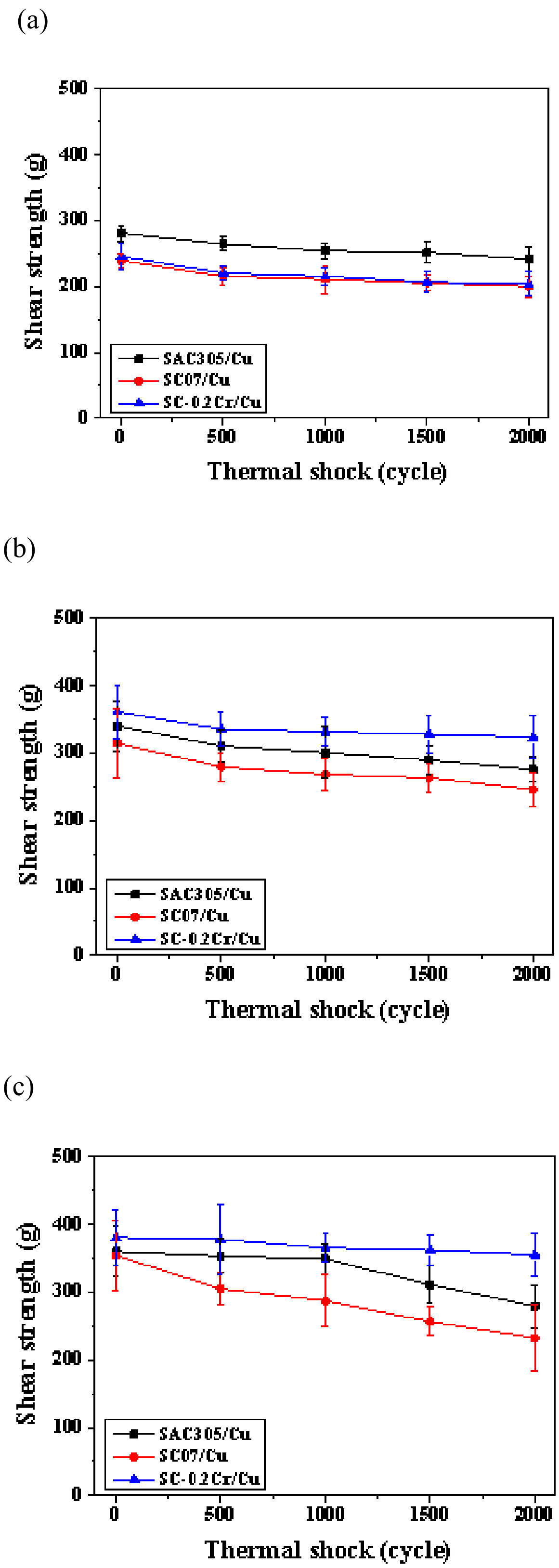

Figure 6.4 Shear strength of solder joints during thermal shock at -40~85 ℃ under (a)0.01 m/s, (b)0.1 m/s and (c)1 m/s shear speed.

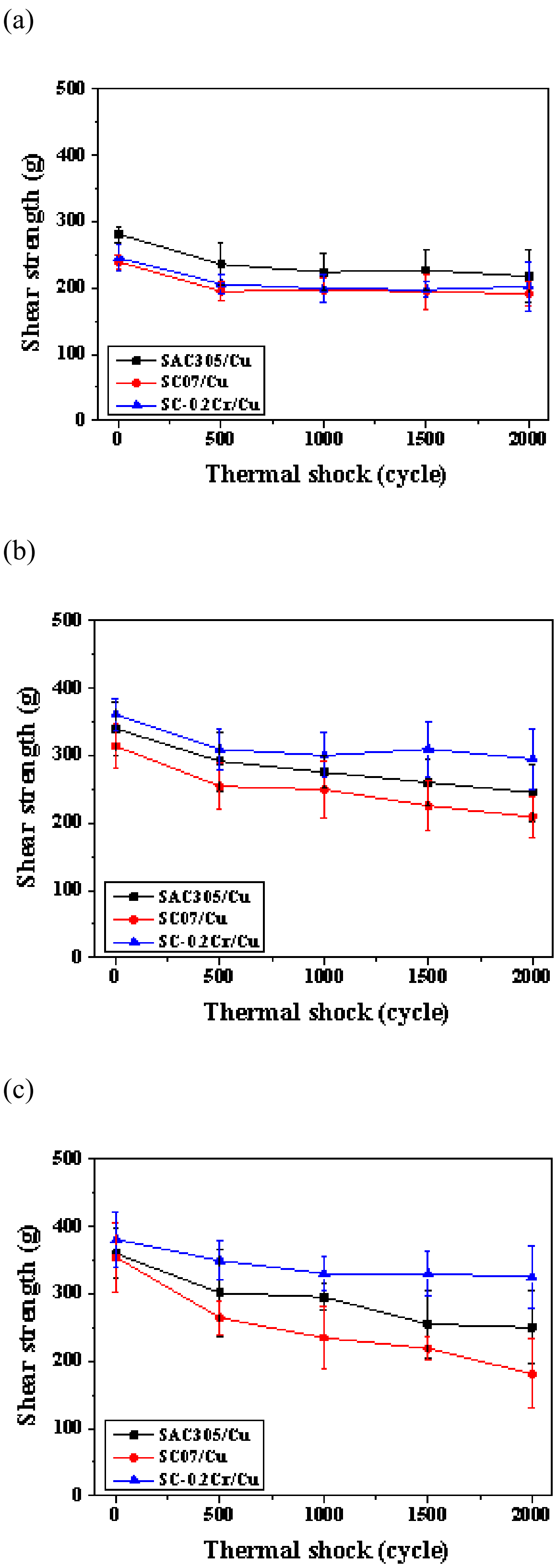

Figure 6.5 Shear strength of solder joints during thermal shock at -40~125 ℃ under (a)0.01 m/s, (b)0.1 m/s and (c)1 m/s shear speed.

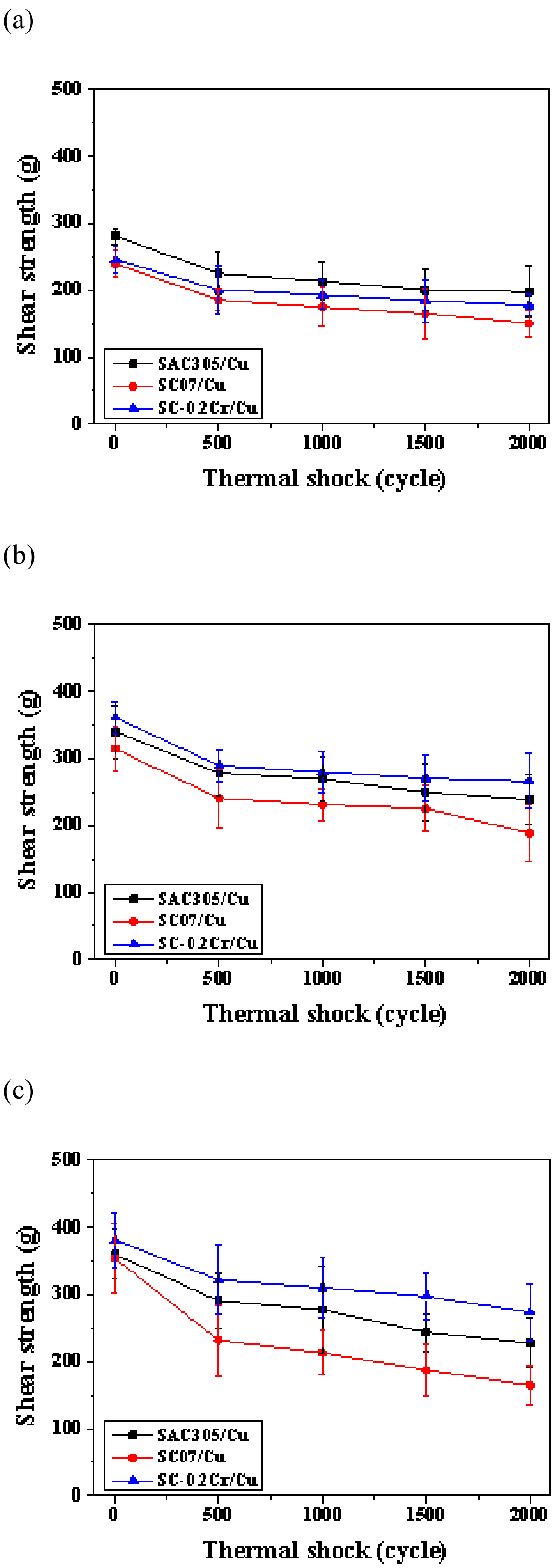

Figure 6.6 Shear strength of solder joints during thermal shock at -40~150 ℃ under (a)0.01 m/s, (b)0.1 m/s and (c)1 m/s shear speed.

Table 6.3 Degradation rate of shear strength after multi-reflow.

Solder joint / Shear speed	SAC305/Cu	SC07/Cu	SC-0.2Cr/Cu
0.01(m/s)	17.5%	19.7%	10.9%
0.1(m/s)	15.5%	18.2%	13.2%
1(m/s)	14.6%	16.1%	6.4%

Figure 6.7 shows the shear strength according to the multi-reflow. When the shear rate was 0.1 m/s or less, the shear strength was affected by the strength of the solder matrix. Owing to the dispersion effect of Ag_3Sn, the SAC305/Cu joint exhibited the highest initial shear strength. SC07/Cu showed the lowest initial shear strength and shear strength after the multi-reflow compared to SAC305/Cu and SC-Cr/Cu joints. **Table 6.3** shows the degradation rate of shear strength according to the multi-reflow. For all of the three systems, the degradation rate of shear strength showed a tendency to decrease as the shear rate increased. The SC-0.2Cr/Cu joint showed the largest difference. The SC-0.2Cr/Cu joint exhibited the highest shear strength under all shear rate conditions because it significantly suppressed the interfacial IMC growth and Kirkendall void formation in multiple reflows, which were liquid/solid reaction conditions. In particular, it showed higher performance at a strain rate of 1 m/s at which the shear stress was concentrated on the interface.

(a)

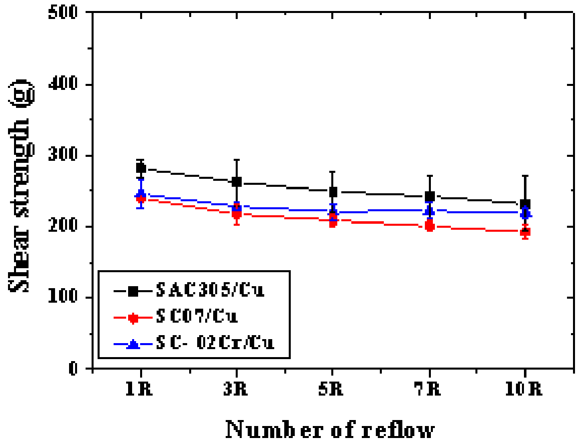

(b)

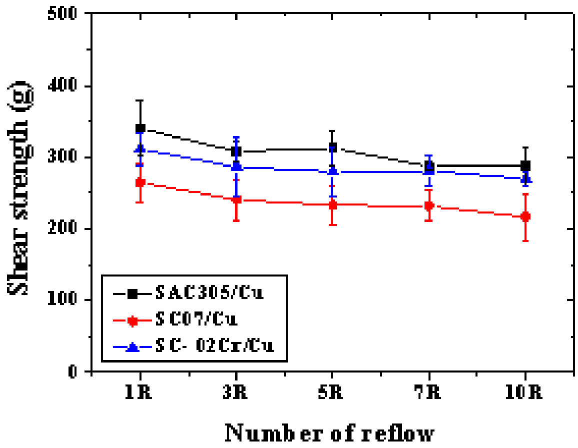

(c)

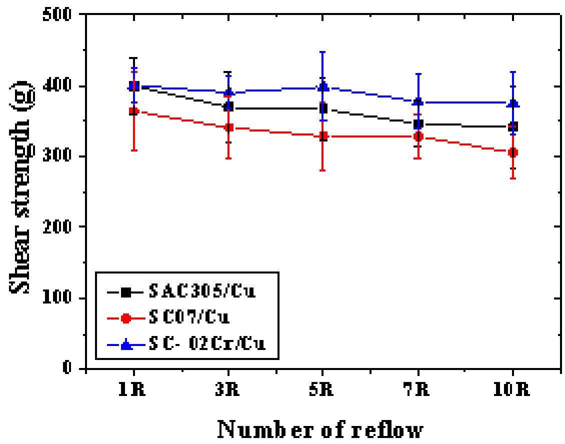

Figure 6.7 Shear strength of solder joints during multiple reflow under (a)0.01 m/s, (b)0.1 m/s and (c)1 m/s shear speed.

6.3.2 Analysis of fracture mode after shear test

Figures 6.8 – 6.10 show the fracture mode according to the isothermal aging temperature. The change from ductile fracture to brittle fracture was accelerated as the temperature and time increased. At a shear rate of 0.01 m/s, ductile fracture represented more than 80 % for all the joint systems. As the shear rate exceeded 0.1 m/s, however, the conversion into brittle fracture was accelerated. The SC-0.2Cr/Cu joint exhibited a perfect ductile fracture mode at 0.01 m/s and 100 ℃ while both complex fracture and brittle fracture were observed at temperatures higher than 125 ℃. Brittle fracture was not observed at the SC-0.2Cr/Cu joint even at 125 ℃ and 1 m/s. The SAC305/Cu and SC07/Cu joints, however, exhibited significantly increased brittle fracture at 125 ℃ and 0.1 m/s. In particular, at 150 ℃ and 1 m/s, brittle fracture accounted for over 50%. This appears to be because of the influence of IMC that grew rapidly after aging and the Kirkendall void formed on the interface. For the SC-0.2Cr/Cu joint, the brittle fracture rate was 10 % or less at 150 ℃ and 1 m/s. As a result, it appears that more ductile fracture occurred to the SC-0.2Cr/Cu joint than to the SAC305/Cu and SC07/Cu joints because the addition of Cr suppressed Cu_3Sn growth and Kirkendall void formation and thus the shear stress was concentrated on the solder matrix rather than on the interface.

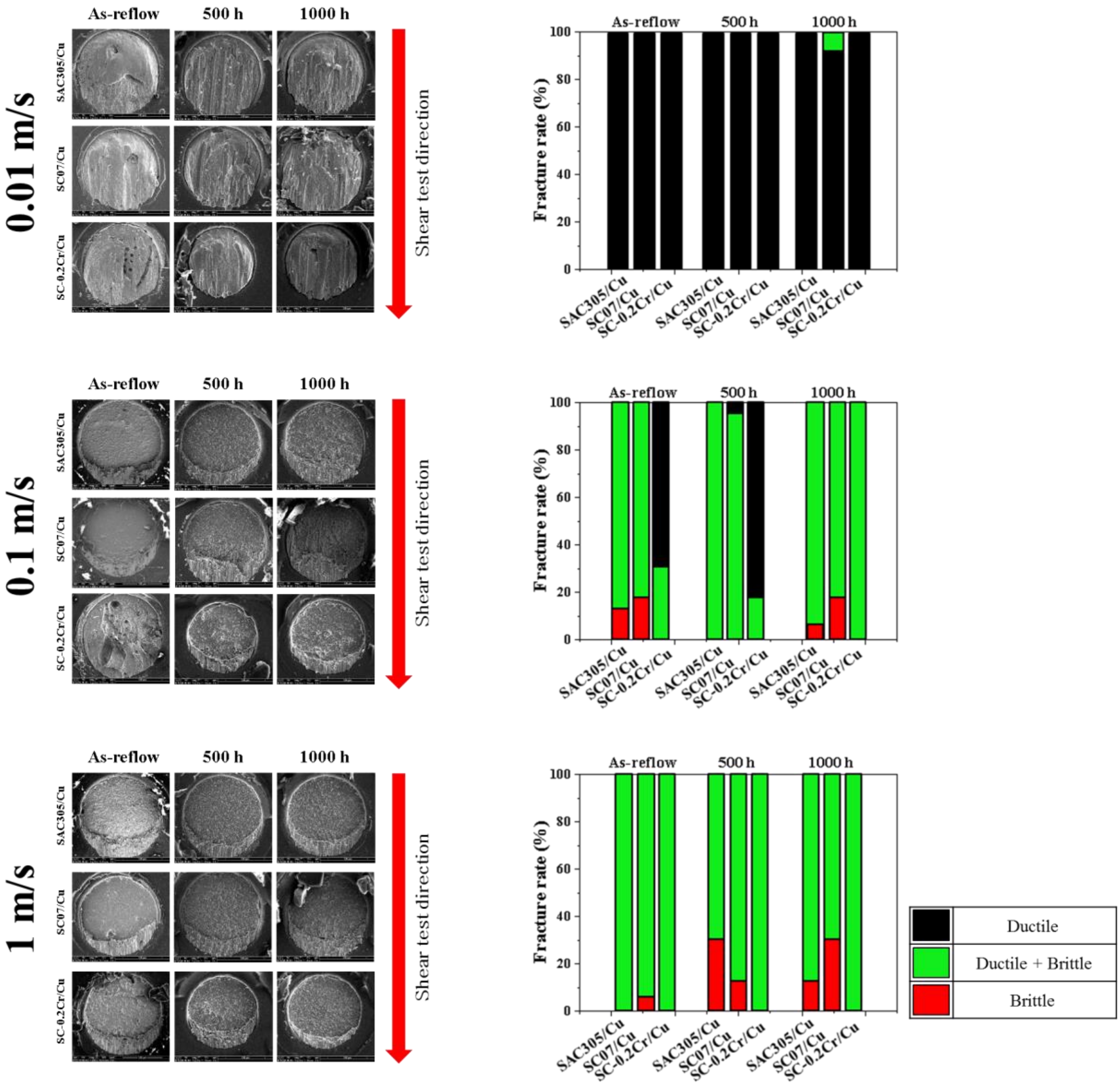

Figure 6.8 Fracture behavior of the solder joints under various shear speeds during aging at 100 ℃.

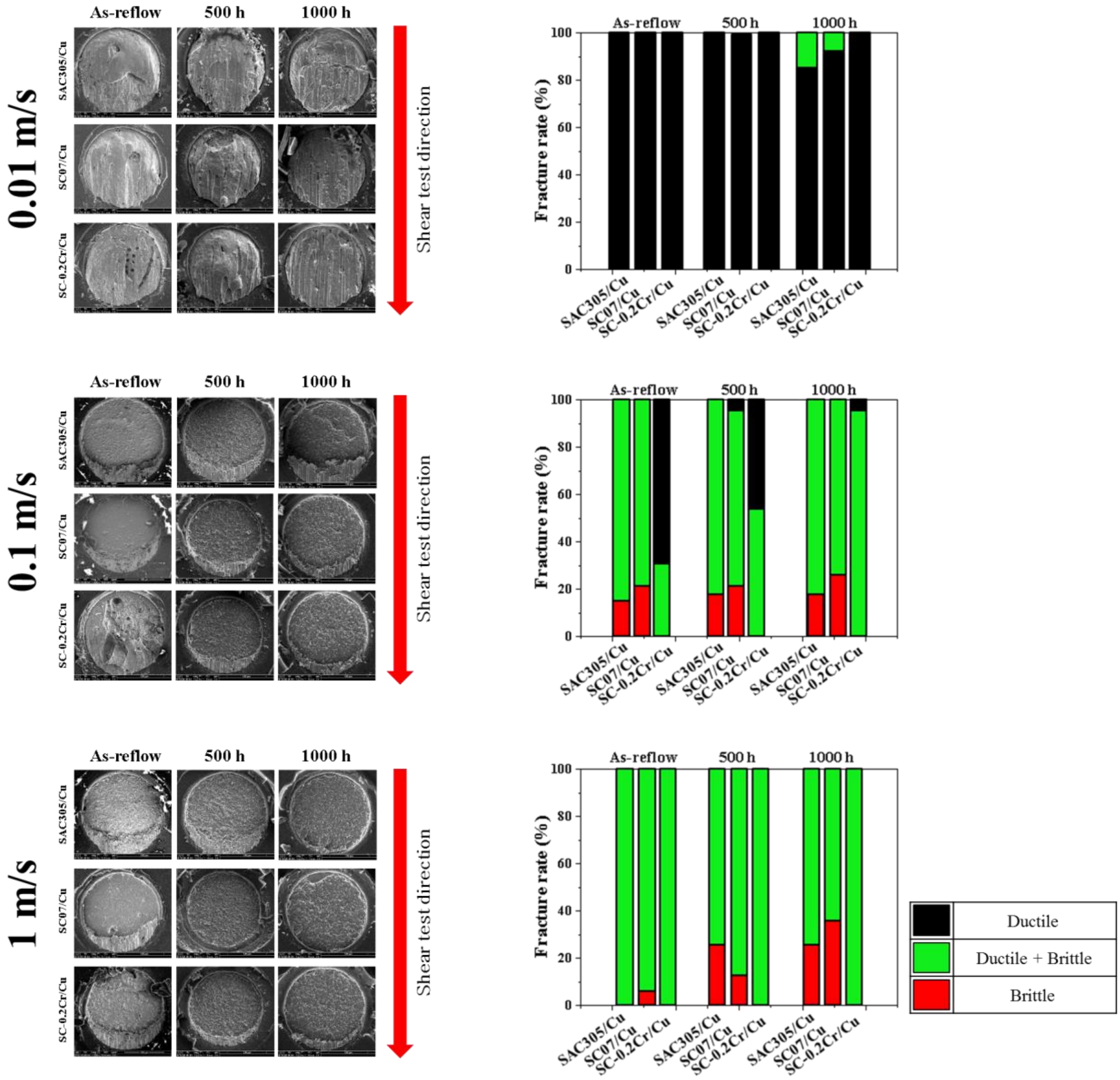

Figure 6.9 Fracture surfaces of the solder joints under various shear speeds during aging at 125 ℃.

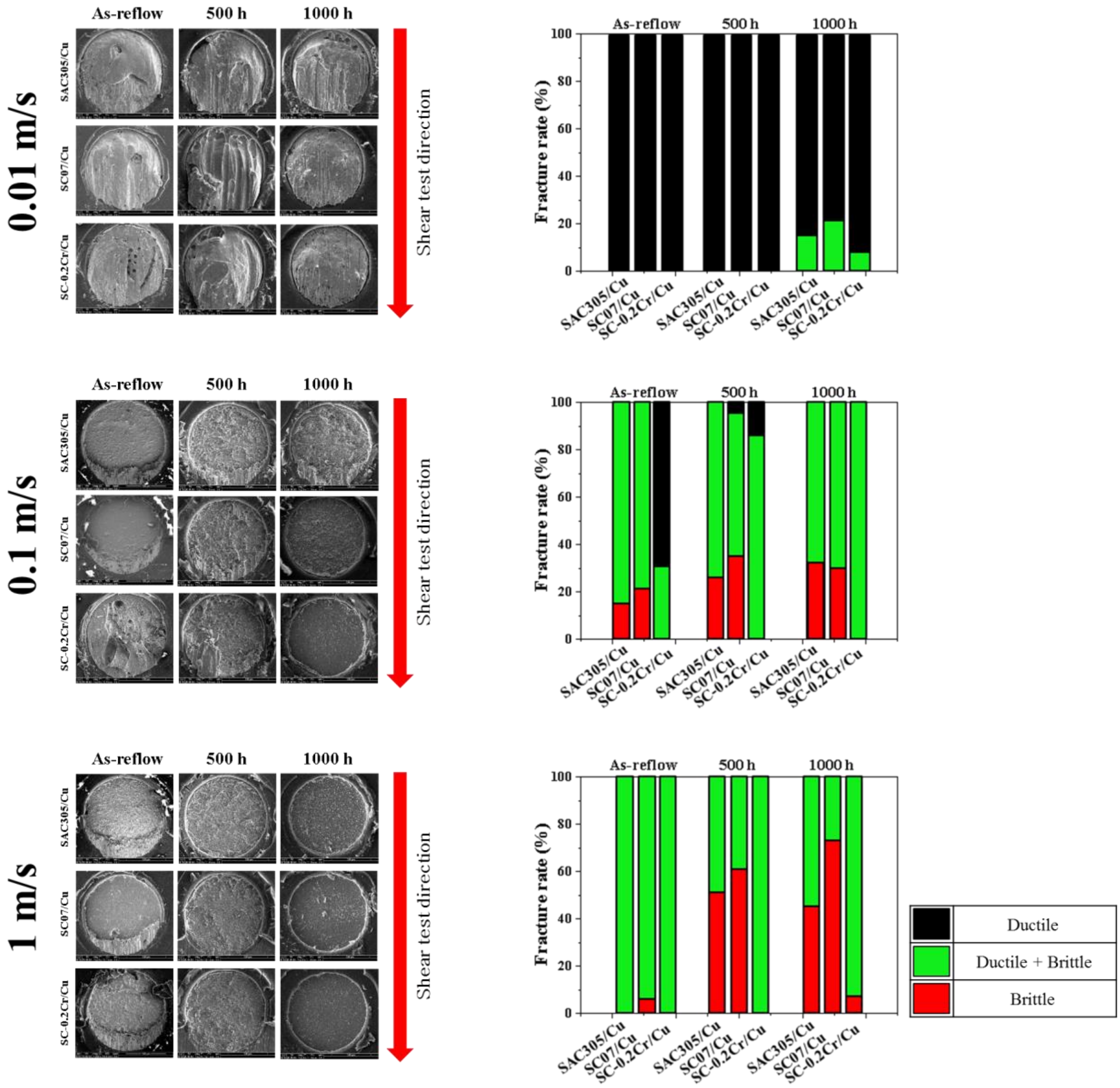

Figure 6.10 Fracture surfaces of the solder joints under various shear speeds during aging at 150 ℃.

Figures 6.11 – 6.13 show the fracture mode according to the thermal shock condition. The change from ductile fracture to brittle fracture was accelerated as the thermal shock temperature range increased and the number of cycles increased. While ductile fracture accounted for more than 90 % for all the systems at 0.01 m/s, the conversion into brittle fracture was accelerated as the shear rate exceeded 0.1 m/s. These results are very similar to the isothermal results. The SC-0.2Cr/Cu joint exhibited a perfect ductile fracture mode at a shear rate of 0.01 m/s regardless of the thermal shock temperature range. Moreover, the SC-0.2Cr/Cu joint exhibited only complex fracture even after 2,000 cycles under the temperature range between -40 °C to 150 °C. For the SAC305/Cu and SC07/Cu joints, however, brittle fracture rapidly increased under the thermal shock condition ranging from -40 °C to 125 °C and accounted for approximately 50 % after 200 cycles. The tendency of the fracture mode was very similar to the isothermal results, and the mechanisms were also considered identical.

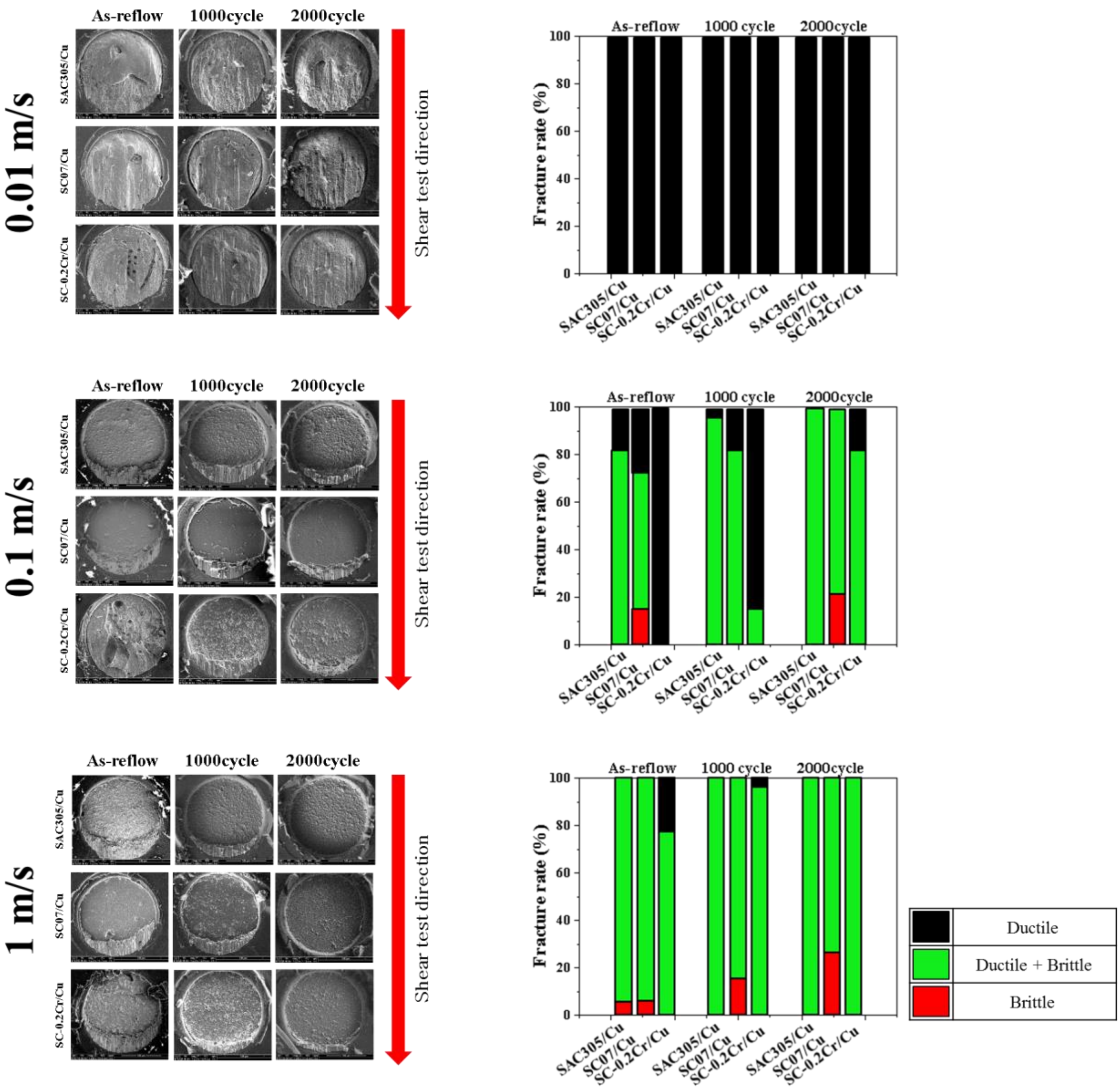

Figure 6.11 Fracture surfaces of the solder joints under various shear speeds during thermal shock at -40 ~ 85 ℃.

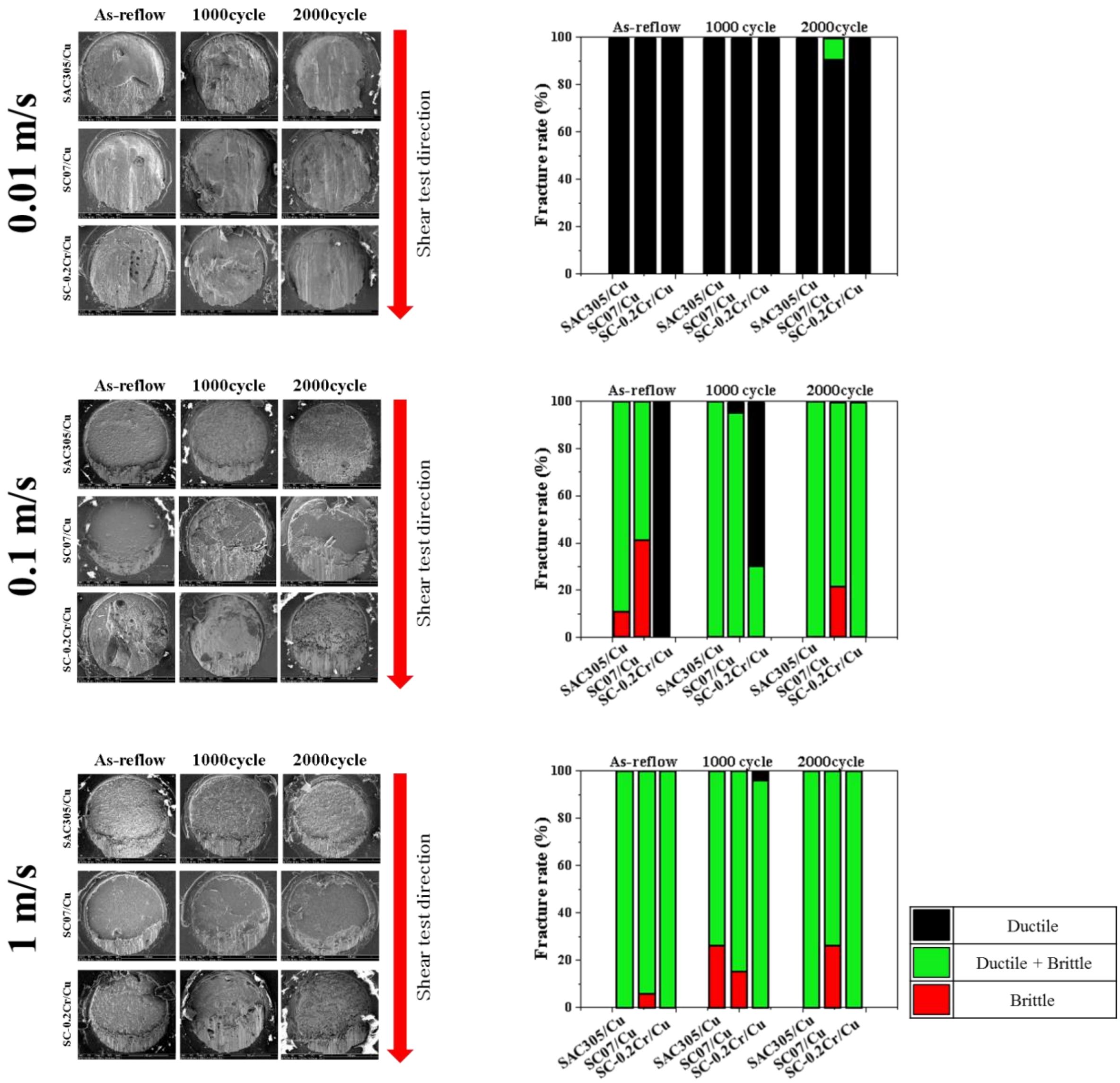

Figure 6.12 Fracture surfaces of the solder joints under various shear speeds during thermal shock at -40 ~ 125 ℃.

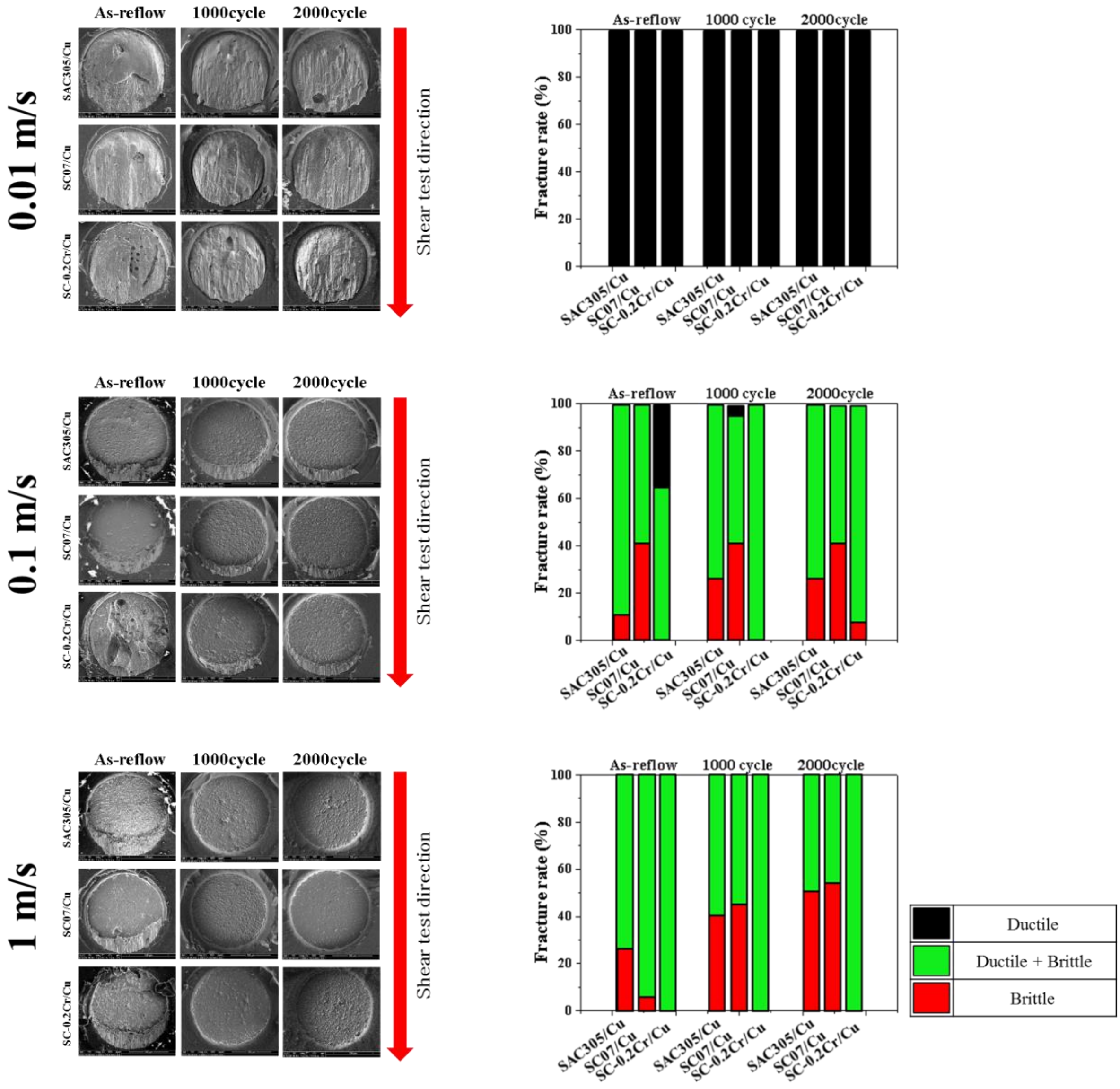

Figure 6.13 Fracture surfaces of the solder joints under various shear speeds during thermal shock at -40 ~ 150 ℃.

Figure 6.14 shows the fracture mode according to the multi-reflow. As can be seen from a shear rate of 1 m/s, the change from ductile fracture to brittle fracture was faster as the number of reflows increased. For the SC-0.2Cr/Cu joint, brittle fracture was not observed and only complex fracture was observed after ten reflows at all shear rates. For SAC305/Cu and SC07/Cu, on the other hand, brittle fracture accounted for almost 20 %. As a result, it can be said that the results of the multi-reflow were only different in fracture rate but showed a tendency similar to those of isothermal aging and thermal shock.

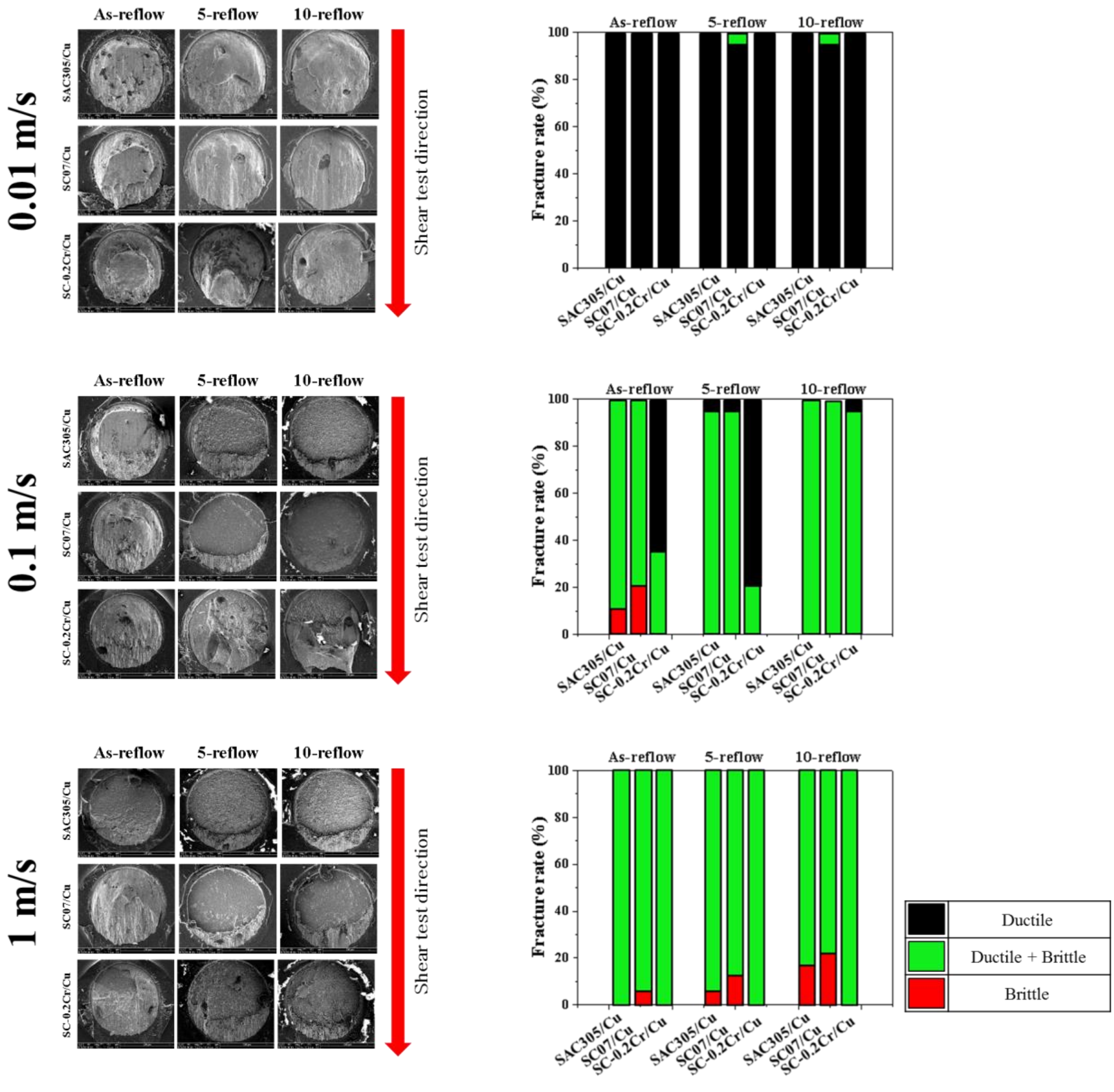

Figure 6.14 Fracture surfaces of the solder joints under various shear speeds during multi-reflow.

6.4 Conclusion

All cracks showed ductile behavior at low shear rates, and the brittle failure was dominant when the shear rates exceeded 0.1 m/s. These results suggest that when the shear rate is low, the shear strength of the solder joint is determined based on the shear strength of the solder matrix, and when the shear rate is high, the shear strength of the solder joint is dependent more on the interfacial connection. The degradation of the shear strength was shown to be similar for both thermal aging and multi-reflows, and was higher under thermal aging, particularly at higher temperatures. When the shear rate is high, a considerable amount of stress is transferred to the interface owing to the large deformation occurring in the solder matrix. Typically, owing to the fragile nature of IMCs, the thicker the IMCs become, the more fragile they are as the brittle areas increase [14,15]. Furthermore, if internal defects such as Kirkendall voids abound, a thicker interfacial IMC layer becomes more vulnerable to fracturing. The addition of Cr after comparing SAC305/Cu and SC07/Cu solder joints was shown to effectively suppress the growth of interfacial IMC and prevent the formation of Kirkendall voids. Thus, the SC-0.2Cr/Cu solder joints maintained a significantly higher shear strength in high-speed shear tests than the other two solder joints.

6.5 Bibliography

[1] Gain, A.K.; Zhang, L. "Harsh service environment effects on the microstructure and mechanical properties of Sn-Ag-Cu-1 wt % nano-Al solder alloy" J. Mater. Sci. Mater. Electron. 27 (2016) 11273–11283.

[2] Gain, A.K.; Zhang, L.; Quadir, M.Z. "Thermal aging effects on microstructures and mechanical properties of an environmentally friendly eutectic tin-copper solder alloy" Mater. Des. 110 (2016) 275–283.

[3] Pratt, R. E., Stromswold, E. and Quesnel, D. J. "Effect of solid-state intermetallic growth on the fracture toughness of Cu/63Sn-37Pb solder joints" *Components, Packaging, and Manufacturing Technology, Part A, IEEE Transactions on*, 19 (1996) 134–141.

[4] Song, F. and Lee, S. R. "Investigation of IMC thickness effect on the lead-free solder ball attachment strength: comparison between ball shear test and cold bump pull test results" *Electronic Components and Technology Conference, 2006. Proceedings. 56th*, (2006) 1196–1203.

[5] So, A. C. and Chan, Y. C. "Reliability studies of surface mount solder joints-effect of Cu-Sn intermetallic compounds" *Components, Packaging, and Manufacturing Technology, Part B: Advanced Packaging, IEEE Transactions on*, 19 (1996) 661–668.

[6] Chen, W.-Y., Yu, C.-Y. and Duh, J.-G. (2012). "Suppressing the growth of interfacial Cu–Sn intermetallic compounds in the Sn–3.0Ag–0.5Cu–0.1Ni/Cu–15Zn solder joint during thermal aging." *Journal of Materials Science*, 47, pp. 4012-4018.

[7] Tseng, C.-F., Wang, K.-J. and Duh, J.-G. (2010). "Interfacial reactions of Sn-3.0Ag-0.5Cu solder with Cu-Mn UBM during aging." *Journal of electronic materials*, 39, pp. 2522-2527.

[8] Sundelin, J. J., Nurmi, S. T., Lepistö, T. K. and Ristolainen, E. O. (2005). "Effect of PCB surface finish on creep properties of lead-free solder joints." *Soldering & surface mount technology*, 17, pp. 3-9.

[9] Nurmi, S. T., Sundelin, J. J., Ristolainen, E. O. and Lepistö, T. K. (2005). "The effect of PCB surface finish on lead-free solder joints." *Soldering & surface mount technology*, 17, pp. 13-23.

[10] Tu, P., Chan, Y. C. and Lai, J. "Effect of intermetallic compounds on the thermal fatigue of surface mount solder joints" *Components, Packaging, and Manufacturing Technology, Part B: Advanced Packaging, IEEE Transactions on*, 20 (1997) 87–93.

[11] Chan, Y., Tu, P., So, A. C. and Lai, J. "Effect of intermetallic compounds on the shear fatigue of Cu/63Sn-37Pb solder joints" *Components, Packaging, and Manufacturing Technology, Part B: Advanced Packaging, IEEE Transactions on*, 20 (1997) 463–469.

[12] Kang, S., Choi, W., Yim, M. and Shih, D. "Studies of the mechanical and electrical properties of lead-free solder joints" *Journal of electronic materials*, 31 (2002) 1292–1303.

[13] Yoon, J.-W., Kim, S.-W., Koo, J.-M., Kim, D.-G. and Jung, S.-B. "Reliability investigation and interfacial reaction of ball-grid-array packages using the lead-free Sn–Cu solder" *Journal of electronic materials*, 33 (2004) 1190–1199.

[14] Kim, J.W.; Kim, D.G.; Jung, S.B. "Mechanical strength test method for solder ball joint in BGA package" Met. Mater. Int. 11 (2005) 121–129.

[15] Kim, J.W.; Jang, J.K.; Ha, S.O.; Ha, S.S.; Kim, D.G.; Jung, S.B. "Effect of high-speed loading conditions on the fracture mode of the BGA solder joint" Microelectron. Reliab. 48 (2008) 1882–1889.

[16] K.N. Tu (Ed.). "Solder Joint Technology: Materials, Properties, and Reliability" Springer, New York, (2007) 386.

[17] K. Zeng, K.N. Tu, "Six cases of reliability study of Pb-free solder joints in electronic packaging technology" Mater. Sci. Eng. R. 49 (2005) 55–105.

[18] Q.K. Zhang, W.M. Long, Z.F. Zhang "Growth behavior of intermetallic compounds at Sn–Ag/Cu joint interfaces revealed by 3D imaging" J. Alloys Compd. 646 (2015) 405–411.

[19] T. Hurtony, A.S.L. Almasy, A. Len, B. Kugler, A. Bonyar, P. Gordon "Characterization of the microstructure of tin-silver lead free solder" J. Alloys Compd. 672 (2016) 13–19.

[20] R.W. Johnson, J.L. Evans, P. Jacobsen, J.R. Thompson, M. Christopher "The changing automotive environment: high-temperature electronics" IEEE Trans. Electron. Pack. Manuf. 27 (2004) 164–176.

Chapter 7
Summary

7.1 Summary

In this dissertation, new approaches using adding some elements to Pb-free solder were proposed and analyzed for improving characteristics of solder joint in electronic packaging of automotive electronics under harsh environments.

In Chapter 2, fabrication process and basic properties of the Sn-Cu solder containing Cr and Al(Si) to improve the property of the Sn-Cu solder for applying to automotive electronics were reported. When Cr and Al(Si) were doped in the Sn-Cu solder, the melting temperature was approximately 3 °C higher than the Sn-Cu solder. The wettability characteristics of Cr and Al(Si)-added solder were similar to that of the Sn-Cu solder. In the case of spreadability, Al(Si)-added solder was slightly higher than Cr-added solder. Furthermore, the addition of Cr and Al(Si) could effectively disperse the β-Sn + Cu-Sn IMC networks in solder matrix.

In Chapter 3, interfacial characteristics such as the IMC growth behavior and mechanical properties of the interfaces between Al(Si)-added Sn-Cu (SC-Al(Si)) solder and Cu substrate were studied compared to SC07. When Al(Si) was doped, the IMC growth of SC-Al(Si)/Cu joint was effectively suppressed compared with that of SC07/Cu joint during reflow because of Cu-Al phase solidification. IMC growth rates of SC-Al(Si)/Cu and Sn07/Cu joints were similar to each other during thermal aging while the IMC growth rate of SC-Al(Si)/Cu joint was slower than that of SC07/Cu joint under multi-reflow. Moreover, shear strength of solder joint in SC-Al(Si)/Cu joint was higher than that in SC07/Cu joint due to suppress IMC growth. Furthermore, Cu-Al, such as Al_2Cu and Sn-Cu-Al, and Cu_6Sn_5 were observed in solder matrix using EPMA mapping.

In Chapter 4, the IMC formation and growth behavior of interfaces between Cr-added Sn-Cu (SC-Cr) solder and Cu substrate were researched compared to Sn-3.0Ag-0.5Cu (SAC305) and Sn-0.7Cu (SC07) solder alloys. The addition of Cr reduced undercooling or free energy for nuclear formation and critical nucleus size and showed very fine Cu_6Sn_5. Moreover, IMC growth in the SC-Cr/Cu joint was more effectively inhibited than the SAC305/Cu and SC07/Cu joints. In particular, during various heat-treatments such as thermal aging, thermal shock and multiple reflow, the growth of Cu_3Sn was greatly suppressed, which result in remarkably reducing the formation of the Kirkendall void between Cu_3Sn and Cu substrate due to suppress the interdiffusion by dispersed $CrSn_2$ near Cu_6Sn_5.

In Chapter 5, the IMC growth behavior in SC-Cr/Cu joint was evaluated using calculating the activation energy during isothermal aging with various temperature conditions in order to compare with SAC305/Cu and SC07/Cu joints. The activation energies were 73.52 kJ mol for the SAC305/Cu 57.31 kJ/mol for the SC07/Cu, and 77.96 kJ/mol for the SC-Cr/Cu joint, respectively. These results mean the IMC growth effectively can be suppressed by adding Cr. Meanwhile, the accelerated factors (AFs) were determined as 1.823, 1.327, and 1.987 for the SAC305, SC07 and SC-Cr solders, respectively after the thermal shock test with the range of -40 °C to 150 °C which are harsher than the field conditions. Using AFs, the predicted field life cycles of the SAC305, SC07 and SC-Cr solders were approximately 7,090, 7,287 and 12,366 cycles, respectively. Therefore, the addition of Cr can improve reliability of solder joint for automotive electronics.

In Chapter 6, the shear strength of SC-Cr/Cu joint was evaluated after thermal treatment. The degradation rate of shear strength was lowest in SC-Cr/Cu joint compared to SAC305/Cu and SC07/Cu joints. Meanwhile, result of analysis of fracture surface, SC-Cr/Cu joint shows more ductile areas by inhibiting growth of IMC and Kirkendall Void.

In this dissertation, these results finally show that the properties of solder joint and interfaces can be improved when the minor elements such as Cr and Al(Si) were minimally added to Sn-Cu solder alloy. Especially, the addition of 0.2 wt.% Cr can suppress the growth of IMC and Kirkendall void, which result in improving the mechanical properties of solder joint. Therefore, it will be expected that Sn-Cu-0.2Cr (0.2 wt.% Cr) will applied to fabrications of electronic modules under harsh environments as a high-reliability solder material.

Research achievements

List of SCI publications

1. Intermetallic compound formation and mechanical property of Sn–Cu–xCr/Cu lead–free solder joint. *Journal of Alloys and Compounds, 728 (2017) 992-1001.* Junghwan Bang, Dong-Yurl Yu, Yong-Ho Ko, Min-Su Kim, Hiroshi Nishikawa, Chang-Woo Lee

2. Improvement in Thermomechanical Reliability of Low Cost Sn–Based BGA Interconnects by Cr Addition. *Metals 2018, 8, 586.* Junghwan Bang, Dong-Yurl Yu, M. Yang, Yong-Ho Ko, Jeong-Won Yoon, Hiroshi Nishikawa Chang-Woo Lee

3. Intermetallic compound growth between Sn–Cu–Cr lead-free solder and Cu substrate. *(Accepted from Journal of Microelectronics Reliability, 2019/06).* Junghwan bang, Dong-Yurl Yu, Jun-Hyuk Son, Yong-Ho Ko, Chang-Woo Lee, Hiroshi Nishikawa

4. Interfacial reactions of fine-pitch Cu/Sn.3.5Ag pillar joints on Cu/Zn and Cu/Ni under bump metallurgies. *Journal of Alloys and Compounds, 616 (2014) 394-400.* Mi-Song Kim, Myoung-Seok Kang, Jung-Hwan Bang, Chang-Woo Lee, Mok-Soon Kim and Sehoon Yoo

5. Effect of Bath Life of Ni(P) on the Brittle-Fracture Behavior of Sn-3.0Ag-0.5Cu/ENIG. *Journal of Electronic Materials, 43 (2014) 4457-4463.* WONIL SEO, KYOUNG-HO KIM, JUNG-HWAN BANG, MOK-SOON KIM and SEHOON YOO

6. Interfacial reaction and intermetallic compound formation of Sn–1Ag/ENIG and Sn–1Ag/ENEPIG solder joints. *Journal of Alloys and Compounds, 627 (2015) 276-280.* Jeong-Won Yoon, Jung-Hwan Bang, Chang-Woo Lee, Seung-Boo Jung

7. Properties and Reliability of Solder Microbump Joints Between Si Chips and a Flexible Substrate. *Journal of Electronic Materials, 44 (2015) 2458-2466.* YONG-HO KO, MIN-SU KIM, JUNGHWAN BANG, TAEK-SOO KIM and CHANG-WOO LEE

8. Bonding copper ribbons on crystalline photovoltaic modules using various lead-free solders. *JOURNAL OF MATERIALS SCIENCE-MATERIALS IN ELECTRONICS, 26 (2015) 9721-9726.* Chulmin Oh, young Kim, Juhee Kim, Junghwan Bang, Jeongwon Ha, Won-Sik Hong

9. Growth inhibition of interfacial intermetallic compounds by pre-coating oriented Cu6Sn5 grains on Cu substrates. *Journal of Alloys and Compounds, 701 (2017) 553-541.* Ming Yang, Yong-Ho Ko, Junghwan Bang, Taek-Soo Kim, Chang-Woo Lee, Shuye Zhang, Mingyu Li

10. Interfacial reactions and mechanical strength of Sn-3.0Ag-0.5Cu/Ni/Cu and Au-20Sn/Ni/Cu solder joints for power electronics applications. *MICROELECTRONICS RELIABILITY, 71 (2017) 119-125.* Byung-Suk Lee, Yong-Ho Ko, Jung-Hwan Bang, Chang-Woo Lee, Sehoon Yoo, Jun-Ki Kim, Jeong-Won Yoon

11. Effects of Ag addition on solid–state interfacial reactions between Sn–Ag–Cu solder and Cu substrate. *MATERIALS CHARACTERIZATION, 124 (2017) 250-259.* Ming Yang, Yong-Ho Ko, Junghwan Bang, Taek-Soo Kim, Chang-Woo Lee, Mingyu Li

12. Joint reliability of various Pb-free solders under harsh vibration conditions for automotive electronics. *MICROELECTRONICS RELIABILITY, 86 (2018) 66-71.* Kyeonggon Choi, Dong-Youl Yu, Sungdo Ahn, Kyoung-Ho Kim, Jung-Hwan Bang,Yong-Ho Ko

13. Effects of graphene oxide on the electromigration lifetime of lead-free solder joints. *JOURNAL OF MATERIALS SCIENCE-MATERIALS IN ELECTRONICS, 30 (2019) 2334-2341*. Yong-Ho Ko, Kirak Son, Gahui Kim, Young-Bae Park, Dong-Yurl Yu, Junghwan Bang and Taek-Soo Kim

List of presentations

International conferences

1. Advanced Ceramics and Composites (ICACC 2014), Florida, USA, January 2014. “Joint Property of Sn-Cu-Cr(Ca) High Temperature Solder for High Reliability of Automobile ECU”

2. IIW Annual assembly & International conference (IIW 2014), Seoul, Korea, July 2014. “Joint Property of Sn-Cu-Cr(Ca) Middle Temperature Solder for High Reliability of Automobile ECU”

3. 3th International Symposium on Visualization in Joining & Welding Science through Advanced Measurements and Simulation (Visual-JW 2014), Osaka, Japan, Nov. 2014. "Advanced bonding technology with high accuracy of micro-bump on thin wafer"

4. 22nd International Symposium in Mathematical Programming, Seoul, Korea, July 2015. "A Study of Joint Properties of Sn-Cu-AlSi Solder for Automotive Electronics Modules"

5. Advanced Metallization Conference 2015(ADMETA plus 2015) Asian session, Seoul, Korea, Sep. 2015. "Joint Reliability of Sn-Cu-Cr for Automotive Electronics Modules"

6. TMS2016 145th Annual Meeting & Exhibition, San diego, USA. "Joint Properties of Sn-Cu-(X)Al(Si) for Automotive Electronics Modules"

7. International Conference on Electronic Materials and Nanotechnology for Green Environment (ENGE 2016) Jeju-Do, Korea, Nov. 2016. "Intermetallic compound formation and mechanical property of Sn-Cu-xCr lead-free solder"

8. 4th International Symposium on Visualization in Joining & Welding Science through Advanced Measurements and Simulation (Visual-JW 2016), Osaka, Japan, Oct. 2016. "Intermetallic compound formation and mechanical property of Sn-Cu-xCr lead-free solder joint"

9. International Welding/Joining Conference-Korea 2017 (IWJC), "A Study on the Thermal ageing Characteristics of Sn-xSb Solder for Automotive Power Module"

10. SMTA Pan Pacific Microelectronics Symposium 2018, Hawaii, USA, February 2018. "Intermetallic compound formation and mechanical property of Sn-Cu-xCr lead-free solder joint"

11. 2018 International Conference on Electronics Packaging and IMAPS All Asia Conference (ICEP-IAAC2018), Nagoya, Japan, April 2018. "Intermetallic compound formation and mechanical property of Sn-Cu-xCr lead-free solder joint"

12. TMS2019 148th Annual Meeting & Exhibition (TMS 2018), San antonio, USA. "Intermetallic compound formation and mechanical property of Sn-Cu-xCr lead-free solder joint"

Acknowledgments

Firstly, I would like to express my sincere gratitude to my supervisor, *Prof. Hiroshi Nishikawa*, for his continuous guidance and academic advice during my doctoral course. Besides my supervisor, I would like to appreciate my thesis committee: *Prof. Kirihara Soushyuu* and *Prof. Muta Hiroaki*, for their insightful comments and encouragement, but also for the hard question which incented me to widen my research from various perspectives.

I would like to thank the members of Prof. Nishikawa laboratory, *Mr. Sanghun Jin, Mr. Shiqi Zhou, Ms. Mai Morishita*, for their great help.

I would like to express the appreciation to member of Micro-joining center of Korea Institute of Industrial Technology, *Dr. Jung-Han Kim, Dr. Chang-Woo Lee, Dr. Jun-Ki Kim, Dr. Cheolhee-Kim, Dr. Sehoon Yoo, Dr. Yong-ho Ko, Dr. Jeong-Won Yoon, Dr. Min-Su Kim, Mr. Dong-Yurl Yu, Mr. Jun-Hyuk Son*, for their useful advice and support on my doctoral course. Without they precious support it would not be possible to conduct this research.

I would like to express the appreciation to *Dr. Won-Sik Hong, Prof. Nam-Hyun Kang, and Dr. Cheol-Min Oh*, for their useful advice on my doctoral course.

Last but not the least, I would like to thank my beloved family: my parents, my wife (*Bora*), my son (*Joowon*), brothers and sister, for their support and sincere concern.

Junghwan Bang
Division of Sustainable Energy and Environmental Engineering, Graduate School of Engineering
Manufacturing Process, Joining and Welding Research Institute
Osaka University